Design and Calibration of a RF Capacitance Probe for Non-Destructive Evaluation of Civil Structures

by

Jason Jon Yoho

Thesis submitted to the Faculty of the
Virginia Polytechnic Institute and State University
in partial fulfillment of the requirements for the degree of

Masters of Science
In
Electrical Engineering

Dr. Sedki M. Riad, Chair
Dr. Imad L. Al-Qadi
Dr. Ioannis M. Besieris

April 3, 1998
Blacksburg, Virginia

Keywords: Non-Destructive Evaluation, RF Measurements, Material Characterization
©Copyright 1998, Jason Jon Yoho

Design and Calibration of a RF Capacitance Probe for Non-Destructive Evaluation of Civil Structures

Jason Yoho

Chairman: Dr. Sedki M. Riad

The Bradley Department of Electrical and Computer Engineering

Abstract

Portland cement concrete (PCC) structures deteriorate with age and need to be maintained or replaced. Early detection of deterioration in PCC (e.g., alkali-silica reaction, freeze/thaw damage, or chloride presence) can lead to significant reductions in maintenance costs. However, it is often too late to perform low-cost preventative maintenance by the time deterioration becomes evident.

Non-destructive evaluation (NDE) methods are potentially among the most useful techniques developed for assessing constructed facilities. They are noninvasive and can be performed rapidly. Portland cement concrete can be nondestructively evaluated by electrically characterizing its complex dielectric constant. The real part of the dielectric constant depicts the velocity of electromagnetic waves in PCC. The imaginary part describes the conductivity of PCC and the attenuation of electromagnetic waves, and hence the losses within the PCC media.

Dielectric properties of PCC have been investigated in a laboratory setting using a parallel plate capacitor operating in the frequency range of 0.1MHz to about 40MHz. This capacitor set-up consists of two horizontal-parallel plates with an adjustable separation for insertion of a dielectric specimen (PCC). While useful in research, this approach is not practical for field implementation

In this research, a capacitance probe has been developed for field application. The probe consists of two planar conducting plates and is made of flexible materials for placement on exposed surfaces of the specimens to be tested.

The calibration method of both capacitive systems has been extensively studied to minimize systematic errors in the measurement process. These two measurement systems will be discussed and compared to one another on the basis of sensitivity and measurement repeatability.

Dedicated to my wonderful parents, Bud and Polly, my brothers, Aaron and Charley, and my best friend, Anne.

Acknowledgement

I would like to express my deepest gratitude to my friend and advisor, Dr. Sedki M. Riad, who has provided me with numerous opportunities to perform research in the area of high frequency measurement and calibration techniques. I am greatly indebted to him for the challenges he has placed upon me as well as his invaluable guidance throughout this research. His advise, encouragement, and support of my education will always be remembered and appreciated.

I would also like to thank my research associate, Brian Diefenderfer, for his effort and knowledge offered throughout our research period. He has increased my understanding and knowledge in materials used in civil structures as well as the concepts and advantages of non-destructive evaluation of these structures.

I would also like to express my appreciation to my committee members, Dr. Imad L. Al-Qadi and Dr. Ioannis M. Besieris, for their suggestions and advice throughout this research. I would also like to thank Dr. Imad L. Al-Qadi for the many opportunities he has provided me with throughout the duration of my research with him. Their suggestions and guidance helped enhance the quality of the study.

I would also like to thank my parents and my brothers for their support and care throughout college education. Their support has been invaluable and the reason I have succeeded to be where I am today as a person and a student.

I would also thank Anne, my best friend, and her family for their support and interest throughout my college education. I want to thank Anne for helping me make decisions regarding my education and for being so supportive of all of my goals.

I finally would like to thank my friends and research associates of the Time Domain Laboratory, Iman, Ahmed, Saad, Yaser, David, and Mr. Ahmed for their help and support anytime I needed it. Thanks everyone.

Table of Contents

List of Figures

List of Tables

Chapter 1
Introduction

Measurement techniques for the evaluation of the electrical properties of material have been devised based on electromagnetic wave interaction in a medium. These techniques investigate the electromagnetic behavior of a material under test from which the material properties can be extracted from the measured data by the application of devised algorithms. The material property that this thesis will deal with is the relative permittivity of the material under test. The relative permittivity, or complex dielectric constant, can be used to electrically characterize civil structures such a Portland cement concrete. The real portion of the dielectric constant is related to the velocity of the electromagnetic waves in structures. The imaginary portion is closely related to the conductivity of the structures and the electromagnetic waves' attenuation. Bussey [1] provides a survey of measurement to characterize for magnetic permeability and electric permittivity at radio and microwave frequencies. These measurements are based on shaping the material under test into a standard electromagnetic configuration such as a parallel plate capacitor. This thesis will focus on the parallel plate capacitor fixture as

well as a developed capacitor probe in which the conducting plates of the measurement fixture are contained in a single geometric plane. The goal of the capacitor probe is to reproduce the measurements of standard structures in a nondestructive method that can be implemented for field use.

The parallel plate measurement system for the characterization of civil structures has been investigated and implemented at Virginia Tech to study the electromagnetic properties of civil structures leading to non-destructive evaluation of these structures. This thesis will present a revised algorithm of ongoing research of the parallel plate measurement system as well as the design, construction, governing algorithms, and implementation of the capacitance probe. This thesis will present the characterization of civil structures using the previously mentioned measurement systems based in the frequency domain. Elaborate calibration schemes have been investigated in the frequency domain for both of the measurement systems. The parallel plate measurement system has been investigated in the frequency band of 100kHz to about 40MHz. The capacitor probe measurement system will be investigated in the lower half of this frequency band, 100kHz to 20MHz. The reason for the reduction in the frequency spectrum is that the majority of the relevant characterization data is found in the lower band. This band reduction will also decrease computational time dependence, which is desirable due to the higher complexity of the algorithms used in the capacitance probe measurement system. Sections 1.1 describe frequency domain measurement techniques. Section 1.2 describes non-destructive evaluation (NDE) concepts. Section 1.4 presents the organization of the thesis.

1.1 Frequency Domain Measurements

Frequency domain measurements imply continuous wave operation where a frequency sweep is used to cover the bandwidth of interest. For the measurement systems described in this thesis, a single port measurement technique will be used. Scattering parameters, or S-parameters, will be employed between the measurement device, such as a vector network analyzer, and the electromagnetic test fixture that will

contain the test specimen. Extensive calibration schemes will need to be employed using both of the measurement setups to ensure accuracy.

1.2 Non-Destructive Evaluation

Non-destructive evaluation is one branch of material characterization that is non-invasive in nature and does not disturb the test structure during the measurement process. This type of evaluation is an attractive feature in the assessment of existing building structures. Millions of dollars are spent each year in the United States to repair deteriorated civil engineering structures. Deterioration of concrete structures is mainly due to freeze-thaw damage, corrosion of reinforcing steel, and aggregate/matrix separation caused by chemical reactions. For the most part, these mechanisms are active under the surface and cannot be accurately assessed by visual observation. Therefore, a majority of the repair and rehabilitation funds are spent to fix conditions not discovered until the work is contracted and the repair begins, or until the deterioration is visible and thus has reached an advanced stage which may jeopardize the structural stability of the facility. Recognizing the potential damage before its occurrence will preserve the structures' strength and reduce life-cycle costs.

A number of direct contact measurements, such as chloride content, corrosion potentials, and corrosion currents, have been utilized to predict levels of corrosion in Portland cement concrete reinforcing bars. However, these techniques have not provided reliable and accurate assessments because of their inaccuracy (for corrosion potentials and currents) and limited representation of the entire structure. As a result of these limitations, maintenance and rehabilitation decisions have been based on experience and visual damage. Thus, resulting in inefficient and costly repair and rehabilitation processes.

Non-destructive evaluation methods are potentially one of the most useful techniques ever developed for assessing the load-bearing state of large concrete structures. Their importance results from the noninvasive nature of the techniques and the anticipated rapidity of the measurements. Unfortunately, not all of the non-

destructive measurement methods have been welcomed by engineers; the reasons for this are twofold. First, the methodology has been grossly oversold. That is, while the concept of a noninvasive measurement technique is certainly attractive, there is a gap between concept and field implementation. In short, too much attention was given to the "glamour" of noninvasive methods and not enough to the basic science and engineering required to make it an operational tool. A second detracting factor has been the lack of conceived programs to develop the kind of basic theories and measurement techniques essential in evaluating proposed nondestructive testing methods.

Currently, electromagnetic waves are used in NDE techniques to evaluate concrete structures. However, even though these techniques may be considered mature, they frequently produce more questions than they answer. This uncertainty results from an inadequate knowledge of the medium they are used to probe. That is, the basic knowledge of the electrical properties of concrete structures is not well researched. Therefore, a prior knowledge should be available regarding how, for example, a given section of concrete responds to an electrical impedance measurement as it cures over time. Thus, rather than relying on hypothetical estimates of the variability of the structure, actual measurements should judge whether such a particular defect can be detected. The mechanisms of deterioration in PCC result in changes in local and bulk dielectric properties of the material.

Electromagnetic technology has flourished and advanced considerably during the past four decades. The primary adaptation of this technology to civil engineering has been in geological surveying (Moffat and Puskar, 1976 [2]). While existing radar technology has demonstrated its usefulness to geology and soil exploration (Ellerbruch, 1974 [3]; Feng and Delaney, 1974 [4]; Feng and Sen, 1985 [5]; Hipp, 1971 [7]; Lord et al., 1979 [8]; Lundien, 1971 [9]; McNeill, 1980 [9]), it is desirable to adapt it to the needs and characteristics of measuring concrete structures.

Highway and bridge applications have sought to employ the radar equipment developed for geological and other applications (Carter et al., 1986 [10]; Steinway et al., 1981 [11]). These contact and non-contact methods can rapidly inspect constructed facilities. Pulse radar has shown significant potential for pavement condition surveys.

Applications have included detection of subsurface voids (Steinway et al., 1981 [11]; Clemena et al., 1987 [12]) and detection of layer thickness and subsurface moisture (Maser et al., 1989 [13]; Al-Qadi et al., 1989 [14]; Bell et al., 1963 [15]; Al-Qadi, 1992 [16]).

Portland cement concrete is a composite that contains a wide variety of materials that have different electrical properties. Electromagnetic characterization of PCC can be utilized to reveal information about its composite fabric, which in turn can reveal information about its mechanical response properties. The electrical properties can be related to the composite properties of the aggregates, aggregate size, cast water to cement ratio (w/c), chloride and moisture content, and reinforcing steel.

1.3 Organization of the Thesis

From the discussion present thus far, it is seen that a field application of material characterization measurement system would be beneficial. This section has presented an overview of the two measurement systems that are going to be presented in this thesis as well as the frequency domain applications these systems will implement. The parallel plate measurement system will be the reference we base the accuracy of the capacitance probe measurement system. The layout of the work done in revising the parallel plate algorithms and the complete development of the capacitance probe measurement system as a non-destructive method for material characterization is given below.

Chapter 2 focuses on background information regarding Portland cement concrete and the concepts involved in the deterioration of the concrete. This section then develops the background information regarding dielectric materials and the relation to Portland cement concrete concluding with an explanation of the use of electromagnetic waves in civil infrastructure.

Chapter 3 focuses on the parallel plate measurement system. This section explains the physical construction of the parallel plate setup and the model of a parallel plate capacitor. The calibration algorithms governing the parallel plate calibration are

presented and described. Finally, the calibration standards used as well as measurement methods including results of these methods are presented.

Chapter 4 focuses on the capacitance probe measurement system. This section presents the final design of the physical construction of the capacitance probe including a description of each of the intermediate designs developed throughout the research. The extensive calibration algorithms governing the capacitance probe calibration are presented and described. Finally, the calibration standards used as well as measurement methods including results of these methods are presented.

Chapter 5 verifies the capacitance probe measurement system and provides some applications in which the capacitance probe may be used. Sample measurements will be presented on different concrete specimens and the results provided.

Chapter 6 summarizes the work done during this research. General conclusions of the results obtained will be presented as well as areas that could benefit from future research.

Chapter 2
Dielectric Materials

A dielectric material in an electric field can be viewed as a free-space arrangement of microscopic electric dipoles that are composed of positive and negative charges whose centers do not quite coincide. These electric charges are not free, and they cannot contribute to the conduction process. Rather, they are bound in place by atomic and molecular forces and can only shift positions slightly in response to external fields; therefore, they are called bound charges. Free charges, on the other hand, determine a material's conductivity (Hayt, 1981 [16]).

The characteristic common to all dielectric materials whether they are solid, liquid, or gas; crystalline or amorphous, is their ability to store electric energy. This electric energy storage characteristic takes place by means of a shift in the relative positions of the internal bound positive and negative charges against the normal molecular and atomic forces. This displacement against a restraining force is analogous to lifting a weight or stretching a spring and represents potential energy. The separation

of charges in a certain medium is called polarization. The phenomenon of polarization is accompanied by an increase in the capacitance when a capacitor is filled with a dielectric medium (Hayt, 1981 [16]).

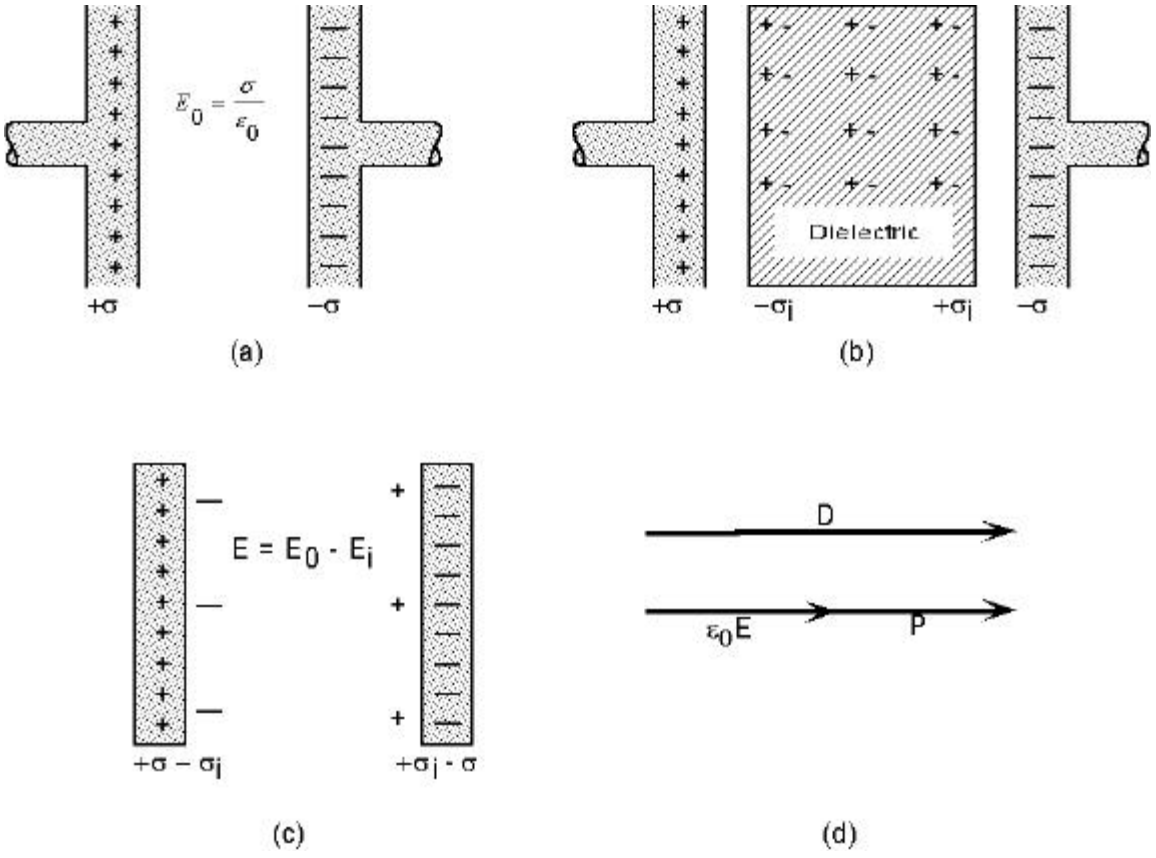

Figure 2.1 A schematic representation of charge distribution within a dielectric filled space between two plates. (a) vacuum filled space (b) dielectric filled space (c) resulting applied electronic field (d) electronic flux density, D, related to the summation of the polarization vector P and the product of the applied field and the dielectric constant of the vacuum (after Tamboulian, 1965 [17]).

Figure 2.1(a) illustrates the concepts involved in assuming a material to be placed between two charged metallic plates. When the intervening space is free of matter, equal and opposite free surface charge densities, $+\sigma$ and $-\sigma$, are present on the plates. The electric intensity, E_o , is uniform and is given by σ/ε_o (ε_o is the vacuum dielectric

constant). When a dielectric medium is inserted between the plates, induced dipoles are formed, as shown in Figure 2.1(b). Unlike the free charges, which transfer to the metallic plates of the capacitor in the charging process, the induced charges belong to a system of dipoles and are bound. In the interior of the dielectric medium, the net charges in a given volume remain equal to zero, and the polarization is assumed to be uniform (Tamboulian, 1965 [17]).

As the field arises from all charges present, the following results:

$$D = \varepsilon_o E + P \tag{2.1}$$

where,

D = Electric displacement current (C/m^2);

E = Electric field (V/m);

ε_o = Dielectric constant of vacuum (8.84×10^{-12} F/m); and

P = Polarization vector (C/m^2).

Charge density (σ) is related to displacement (D) as follows:

$$\sigma = \int_S D \cdot dA \tag{2.2}$$

where,

A = Area of charged surface; and

S = Surface of charged surface.

The polarization vector (P) is related to the electric field (E) as follows:

$$P = \varepsilon_o \chi E \tag{2.3}$$

where,

χ = Electric susceptibility.

Substituting equation 2.3 in equation 2.1 yields:

$$D = \varepsilon_o (1 + \chi) E = \varepsilon E \qquad (2.4)$$

where,

ε = Dielectric constant of the medium.

Materials described by equation 2.4 are categorized as lossless dielectric. Other materials (e.g., PCC) are considered lossy dielectrics due to losses attributed to conduction and relaxation time (Debye's losses). These types of losses yield a complex dielectric constant given as follows:

$$\varepsilon^* = \varepsilon' - j\varepsilon'' \qquad (2.5a)$$

where,

ε' = Real dielectric constant;

ε" = Imaginary dielectric constant; and

$j = \sqrt{-1}$.

Equation 2.5a may be written as a function of the vacuum dielectric constant, and is given as follows:

$$\varepsilon_r^* = \varepsilon_r^{'} - j\varepsilon_r^{''} \qquad (2.5b)$$

where, $\varepsilon_r^* = \frac{\varepsilon^*}{\varepsilon_o}$; $\varepsilon_r^{'} = \frac{\varepsilon^{'}}{\varepsilon_o}$; and $\varepsilon_r^{''} = \frac{\varepsilon^{''}}{\varepsilon_o}$.

The possible polarization forms in PCC at the radio frequency (RF) band are caused by ionic, electronic, dipolar, and heterogeneous (Maxwell-Wagner) effects, as shown in Figure 2.2 (Jastrzebski, 1977 [18]; Wilson and Whittington, 1990 [19]). Both

the amount of the applied field and the attraction of the nucleus atoms determine the magnitude of displacement and thus the amount of polarization. Ionic contribution to the polarization process is caused by the displacement and deformation of charged atoms with respect to other atoms in a molecule or in a crystal lattice. Electronic polarization is due to the displacement of electron cloud with respect to the nucleus within the individual atoms. Dipolar polarization arises in a substance built up of polar molecules possessing a permanent electric dipole moment. Under an applied electric field, polar molecules tend to rotate and orient themselves with the applied electric field.

Heterogeneous polarization (Maxwell-Wagner effect) occurs in dielectric materials in which conducting volumes are distributed. A relaxation effect takes place at some critical frequency. If the applied frequency is much less than the critical frequency, the charge carriers can redistribute themselves within the conducting particles, giving rise to an enhanced dielectric constant and low electrical loss, which is associated with a low value of conductivity. However, if the applied frequency of the field is greater than the critical frequency, then the charge carriers cannot redistribute fully. This causes a reduction in dielectric constant and an increase in conductivity.

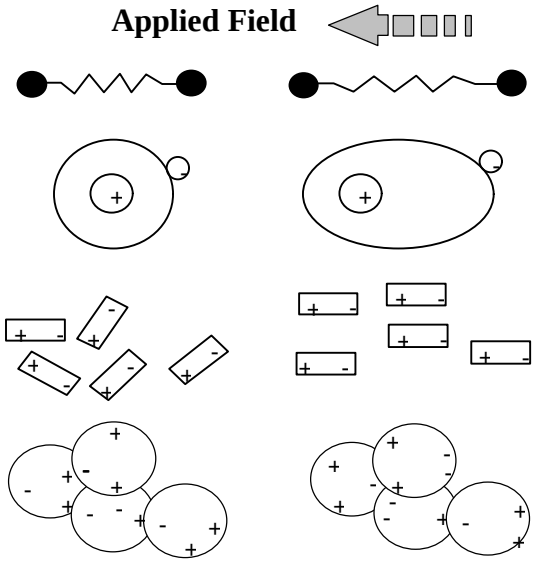

Figure 2.2 A schematic representation of different forms of polarization: (a) ionic; (b) electronic; (c) dipolar; (d) heterogeneous (after Jastrzebski, 1977 [18]; Wilson and Whittington, 1990 [19]).

In order to understand the relationship of PCC chemistry to its dielectric behavior, an understanding of the dispersion of solids and the absorption of water is essential. This is accompanied by a discussion of dipolar and heterogeneous polarization; electronic and ionic polarization which are frequency independent.

The dielectric constant of many liquids and solids depends on the frequency of the measurement. The dependence generally decreases from a static value, ε_s, at low frequencies to a smaller limiting value, ε_∞, at high frequencies. In the transition region of anomalous dispersion, there is "absorption conductivity" yielding a complex dielectric constant, ε_r^*.

In an alternating electric field, the orientation of polar molecules is opposed by the effect of the thermal agitation and molecular interaction (Cole and Cole, 1941 [20]). Debye (1929) [21] models the second effect by a viscous damping, where the molecules are regarded as spheres in a continuous medium with the macroscopic viscosity shown in Figure 2.3.

Theoretical analysis of this behavior is presented in Debye's equations:

$$\varepsilon' = \varepsilon_\infty + \frac{\varepsilon_s - \varepsilon_\infty}{\left(1 + (\omega\tau_o)^2\right)} \tag{2.6}$$

$$\varepsilon'' = \frac{(\varepsilon_s - \varepsilon_\infty)\omega\tau_o}{\left(1 + (\omega\tau_o)^2\right)} \tag{2.7}$$

where

ω = Angular frequency, $2\pi f$;

ε_∞ = Dielectric constant at infinite frequency;

ε_S = Static dielectric constant;

τ_o= Relaxation time (sec); and

f = Frequency.

For a static field, τ_o ranges from 10^{-6} to 10^{-13} sec. The relaxation time depends on temperature, chemical composition, and structure of the dielectric.

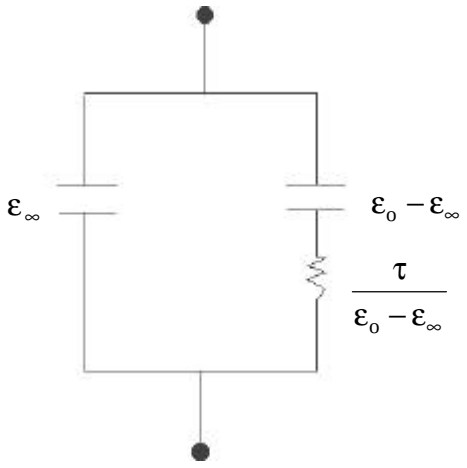

Figure 2.3 A model representation of the molecular interaction effect (after Debye, 1929 [21]).

In heterogeneous materials, consisting of two or more components having a discrepancy in the conductivity potentials, a dispersion known as the Maxwell-Wagner effect arises. This dispersion can be modeled using Debye's equations after modifying ε_S and ε_∞ values. For a two-phase material with any inclusion shape at low concentration, Sillars (1937) [22] suggested the following:

$$\varepsilon_\infty = \frac{\varepsilon_1\{\varepsilon_1 + [A(1-\nu_2)+\nu_2](\varepsilon_2-\varepsilon_1)\}}{\varepsilon_1 + A(1-\nu_2)(\varepsilon_2-\varepsilon_1)} \tag{2.8}$$

$$\varepsilon_s = \frac{\varepsilon_1\{\sigma_1 + [A(1-\nu_2)+\nu_2](\sigma_2-\sigma_1)\}}{\{\sigma_1 + A(1-\nu_2)(\sigma_2-\sigma_1)\}} + \nu_2\sigma_1\frac{[\sigma_1 + A(\sigma_2-\sigma_1)](\varepsilon_2-\varepsilon_1)}{\{\sigma_1 + A(1-\nu_2)(\sigma_2-\sigma_1)\}^2} + \nu_1\sigma_2\frac{[\varepsilon_1 + A(\varepsilon_2-\varepsilon_1)(\sigma_2-\sigma_1)]}{\{\sigma_1 + A(1-\nu_2)(\sigma_2-\sigma_1)\}^2} \tag{2.9}$$

$$\tau = \frac{\varepsilon_o[\varepsilon_1 + A(1-\nu_2)(\varepsilon_2-\varepsilon_1)]}{4\pi[\sigma_1 + A(1-\nu_2)(\sigma_2-\sigma_1)]} \tag{2.10}$$

where,

ε_1 and ε_2 = Dielectric constant of host and inclusion materials, respectively;

σ_1 and σ_2 = Conductivity of host and inclusion materials, respectively;

ν_1 and ν_2 = Proportions of host and inclusion materials of the total volume, respectively;

A = Depolarization factor of the inclusions, (depends on the geometry or axial ratio as well as the material nature); and

τ = Relaxation time for two-phase material (sec).

Equations 2.8 through 2.10 provide a physical explanation for aqueous porous materials with different pore axial ratios, related to the frequency range at which minimum losses occur. These equations indicate that Maxwell-Wagner losses decrease gradually as the ratio of pore axes increases. Where a distribution of relaxation time is observed, a distribution of depolarization factors (that is, axial ratios) may be indicated. Hasted (1973) [23] showed that the agreement between Maxwell-Wagner equations and experimental results is reasonable only at low inclusion concentrations.

Cole and Cole (1941) [20] proposed a method for checking equations 2.6 and 2.7 based on constructing a complex plane locus in which the imaginary part, ε", of the complex dielectric constant is plotted against the real part, ε', where each point corresponds to one frequency:

$$\left(\varepsilon' - \frac{\varepsilon_s + \varepsilon_\infty}{2}\right)^2 + (\varepsilon'')^2 = \left(\frac{\varepsilon_s + \varepsilon_\infty}{2}\right)^2 \qquad (2.11)$$

A plotting of ε" versus ε' yields a semicircle with a radius $(\varepsilon_s - \varepsilon_\infty) / 2$ and a center located at $(\varepsilon_s + \varepsilon_\infty) / 2$ from the origin on the ε' abscissa. The intersection points with the abscissa provide ε_s and ε_∞ values, as shown in Figure 2.4. This is based on the assumption of a single relaxation time, which may not always be the case. Cole and Cole

(1941) [20] showed that an experimental curve is usually a circular arc, but with its center lying below the abscissa.

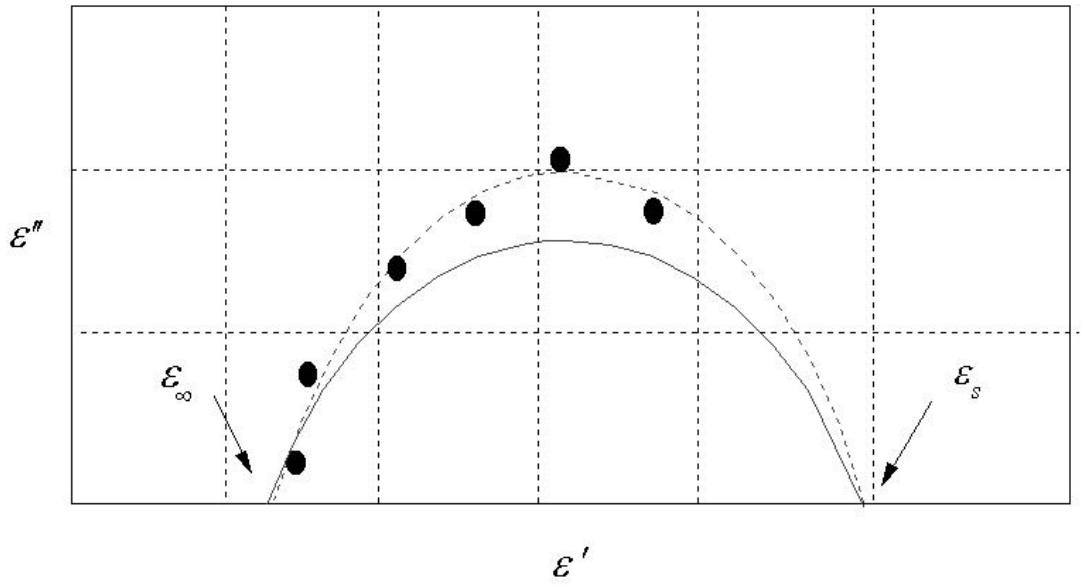

Figure 2.4 A schematic representing: (a) Cole-Cole diagram according to Debye's equation (solid line) and (b) Cole-Cole for experimentally obtained dielectric properties for a lossy material (dotted line) (after Cole and Cole, 1941 [20]).

Each dipole has its own intrinsic relaxation time in each of the different cases. When an average measurement is taken over spatial conditions, a spread of relaxation times distributed around the most probable value will generally result in the following:

$$\varepsilon = \varepsilon_{\infty} + (\varepsilon_s - \varepsilon_{\infty}) \int_0^{\infty} \frac{G(\tau)}{1 + \omega\tau j} d\tau \qquad (2.12)$$

where, $G(\tau)$ is the distribution function of the relaxation times.

Different distribution functions have been proposed (Böttcher, 1952 [24]), however, neither a satisfactory distribution function, $G(\tau)$, nor a general theory for the dependence of ε' and ε" on the frequency was found. Fuoss and Kirkwood (Böttcher, 1952 [24]) suggested that the experimental data could be presented by the following empirical relation:

$$\varepsilon'' = \varepsilon''_m \operatorname{sech}[\beta \ln(\omega/\omega_m)] \tag{2.13}$$

where β is a parameter and ω_m is the angular frequency corresponding to the maximum value of ε" over the whole spectrum of frequency (ε_m").

A modified Debye's empirical formulae considering the effect of relaxation time distribution was given by Cole and Cole (Böttcher, 1952 [24]):

$$\varepsilon - \varepsilon_\infty = \frac{\varepsilon_s - \varepsilon_\infty}{1 + (\omega\tau_o j)^n} \tag{2.14}$$

where n = 1-h; h is a constant and accounts for the extent of the distribution of the relaxation times (ranging from 0 to 1). The larger h is, the larger is the extent of the distribution of relaxation times. Thus, equations 2.6 and 2.7 may be modified as follows:

$$\varepsilon' = \varepsilon_\infty - (\varepsilon_s - \varepsilon_\infty)\frac{1 + (\omega_o\tau)^n \cos\frac{n\pi}{2}}{1 + 2(\omega_o\tau)^n \cos\frac{n\pi}{2} + (\omega\tau_o)^{2n}} \tag{2.15}$$

$$\varepsilon'' = (\varepsilon_s - \varepsilon_\infty)\frac{(\omega_o\tau)^n \sin\frac{n\pi}{2}}{1 + 2(\omega_o\tau)^n \cos\frac{n\pi}{2} + (\omega\tau_o)^{2n}} \tag{2.16}$$

Merging equations 2.15 and 2.16 yields:

$$\left[\varepsilon' - \frac{\varepsilon_S + \varepsilon_\infty}{2}\right]^2 + \left[\varepsilon'' + \frac{\varepsilon_S + \varepsilon_\infty}{2}\operatorname{cotan}\frac{n\pi}{2}\right]^2 = \left[\frac{\varepsilon_s + \varepsilon_\infty}{2}\operatorname{cosec}\frac{n\pi}{2}\right]^2 \tag{2.17}$$

Equation 2.17 represents a circle with its center at $\left(\frac{\varepsilon_s + \varepsilon_\infty}{2}\right),\left(-\frac{\varepsilon_s + \varepsilon_\infty}{2}\operatorname{cotan}\frac{n\pi}{2}\right)$ and a radius of $\frac{\varepsilon_s - \varepsilon_\infty}{2}\operatorname{cosec}\frac{n\pi}{2}$.

Certain dielectrics display conductivity that arises from the effect of polarization on the displacement current. An actual charge transporting such conduction would

normally be described by a volume conductivity, σ (ohm^{-1}cm^{-1}), and the effect would be to add an additional term to the dielectric loss:

$$\varepsilon'' = \varepsilon''_{\text{dielectric}} + \frac{\sigma}{\omega}\left(\frac{1}{4\pi x 9 x 10^{11}}\right) \tag{2.18}$$

where $\varepsilon''_{\text{dielectric}}$ is the dielectric loss resulting from the non-linear behavior of the material.

The frequency variation of dielectric loss might also be described as a frequency variation of apparent conductivity arising from the relaxation process. The conductivity may therefore be given as follows:

$$\sigma = \frac{(\varepsilon_s - \varepsilon_\infty)\omega^2\tau}{1+\omega^2\tau^2} \tag{2.19}$$

Let $\sigma_\infty = (\varepsilon_s - \varepsilon_\infty)\tau$, then

$$\sigma = \frac{\sigma_\infty \omega^2\tau^2}{1+\omega^2\tau^2} \tag{2.20}$$

Equation 2.20 describes the elevation of dielectric conductivity from its zero value at zero frequency (σ_S) to σ_∞ at infinite frequency, thus rewriting (2.20) as follows:

$$\sigma = \sigma_s + \frac{(\sigma_\infty - \sigma_s)\omega^2\tau^2}{1+\omega^2\tau^2} \tag{2.21}$$

Since PCC is a heterogeneous material consisting of solid substance, hydrated and unhydrated cement products, and water (at different states), the previous discussion would relate to water relaxation losses, Maxwell-Wagner effect, and conductivity which could coexist in PCC. A successful description of PCC dielectric behavior using either of the models given by equations 2.11 or 2.17 would make it possible to sense changes in PCC dielectric properties, due to deterioration and/or change in basic properties, through evaluating ε_∞, ε_s, and τ_o using Cole-Cole diagram principles. This could be accomplished, especially at microwave frequencies, when the Maxwell-Wagner effect disappears.

Adopting this procedure would provide a better understanding of the effect of different deteriorations on the PCC dielectric properties, and at the same time would provide more confidence in the conclusion because the evaluation parameters are calculated from a spectrum of frequencies rather than from a single value.

At low RF, the low conductivity of the PCC solid substance is compared to the very high conductivity of the capillary ionized water; this provides the conditions necessary to produce heterogeneous polarization. At this range of frequency, it seems difficult to evaluate ε_∞, ε_s, and τ_o because of the difficulty of estimating the pore water (considered, in this case, the inclusion) conductivity and dielectric constant due to the continuous changes in the water content, state, and ion type and content in PCC. In addition, it is difficult to estimate a quantitative value for the relaxation time for PCC ingredients.

The conductivity losses in PCC could arise from: (a) the conductivity of PCC, (b) the direct conductivity through the water in the pores, and (c) the interfaces' conductivity. The electric phenomena associated with a surface layer can include two-dimensional surface conductivity. Such a conductivity can occur in a system in which the mobility of charge carriers is large along the surface but small when normal to it. At low frequency, the pores act as a conducting inclusion, with high conductivity along the pore walls because of the adsorbed water layer. Thus, changing the inclusion size and shape due to further hydration would result in reduction of such conductivity. The conductivity losses decrease or even disappear completely when RF is replaced by the microwave frequencies. Thus, in the latter range, relaxation losses dominate.

2.1 Portland Cement Concrete

Portland cement concrete is the most widely used construction material. It is a composite material consisting of cement, water, and coarse and fine aggregate. When water reacts with the cement, PCC hardens due to the formation of hydration products. The usual primary requirement of a good PCC in its hardened state is a satisfactory compressive strength. Other desired properties of PCC concomitant with high strength

are: density, durability, tensile strength, low permeability, and resistance to sulfate attack.

The hydration process of cement shapes the internal structure of PCC. The final internal structure depends on the mix ingredients including the type of cement used, the stage of hydration, and curing and temperature conditions. The aggregate, although considered to be a filler in ordinary strength PCC, plays an important role in shaping the PCC structure, and therefore, its durability. The aggregate influences the physical and chemical nature of the interfacial region between aggregate and hydrated cement paste (HCP) which is called the transition zone (dependent on the chemistry and size of aggregate), and its physical properties, which include density, strength, and porosity (Mehta, 1986 [25]). In spite of PCC's apparent simplicity, it is quite complex due to the heterogeneous distribution of the solid components and the pores (which are of varying sizes).

Immediately upon contact of cement with water, an exchange of ionic species is initiated between the solid and the liquid phases. The high solubility of some of the clinker components leads to a rapid increase of ion concentration in the liquid phase. The liquid phase quickly becomes saturated with different ionic species. The hydration of PCC is a complicated process that includes chemical reactions, ion production, hydration products, and pore structure development. A series of chemical reactions between cement and water result in HCP; one may refer to Mindess and Young (1981) [26] for the chemical reactions that take place during the hydration process.

The pore size distribution of cementitious materials can be obtained experimentally by the Mercury Intrusion Porosimetry (MIP) techniques (Lowell and Shield, 1987 [27]). An increase in hydration and/or lower w/c ratio would result in a higher percentage of finer pores (Young, 1974 [28]; Abdel-Jawad and Hansen, 1989 [29]). It is important to note that the pore size affects the form in which water is presented in the PCC pore system: capillary, adsorbed, and interlayer. The water in the large voids (>50nm) is considered free, while the water in smaller capillaries (5 to 50nm) is usually held by capillary tension. The adsorbed water is physically bound to the hydrated cement paste (HCP) surface under the influence of attractive forces. Up to six

molecular layers of water (15Å) can be held by hydrogen bonding. The interlayer water is strongly held between the layers of calcium silicate hydrate (C-S-H) by hydrogen bonding.

The pore size distribution in PCC is coarser and the porosity is higher than that of the corresponding HCP (at the same w/c ratio) due to the effect of the transition zone (Winslow and Cohen, 1994 [30]). The size of the transition zone is proportional to the aggregate size and the PCC mix. The transition zone, therefore, contributes to reducing the durability and strength of PCC. In addition, it causes the non-linearity in the stress-strain diagram of PCC. The aggregate chemistry proved to have great influence on the microstructure of the HCP in the transition zone (Ping et al., 1991 [31]).

2.2 Deterioration in Portland Cement Concrete

Deterioration in PCC may result from physical and/or chemical effects. One of the most common forms of deterioration is corrosion of the reinforcing steel caused by chloride intrusion. Therefore, an understanding of the mechanism of chloride intrusion is necessary.

If the chloride ions in the pore solution of PCC reach a certain threshold level, 0.71 kg/m^3 of PCC (at the PCC-steel contact surface), the reinforcing steel will begin to corrode (Al-Qadi et al., 1993 [32]). The chloride ions reach the pore solution through cracks or diffusion through the PCC's pore water. Additionally, chlorides may exist in PCC through poor quality control of the mixing water.

Corrosion of steel in PCC occurs due to an electrochemical reaction. The corroding system consists of an anode (where electrochemical reduction takes place), a cathode, an electrical conductor, and an electrolyte (in this case, it is the cement paste pore solution). Free Cl^- ions, moving through the PCC pore system, react with the positively-charged Fe^{2+}, after destroying the protective film around the reinforcing steel, and form $FeCl_2$. In the presence of moisture, further reaction with $FeCl_2$ leads to the formation of iron hydroxide and the release of more Cl^- and H^+ ions. The iron hydroxide reacts with oxygen and results in the formation of Fe_2O_3 (rust). This final compound,

after further stages of reaction, enlarges to up to six times the original steel volume (Bradford, 1992 [33]). This phenomenon results in the reduction of the steel effective area and creates tensile stresses in the surrounding PCC, causing cracks, delamination, and ultimately spalls in the PCC structure. The vertical cracks created allow more chlorides to intrude in to the PCC pore system and thus aggravate the problem.

2.3 Electromagnetic Waves in Civil Infrastructure

Electromagnetic (EM) waves have been used for different engineering applications in the field and in the laboratory. These applications include determining and/or evaluating depth of water wells and ice glaciers, bridge deck conditions, pavement thickness and conditions, and moisture in hot-mix asphalt. In addition, low RF EM waves were used to study PCC at very early stages to assess the hydration process of PCC. Different setups were used to achieve different ranges of frequency in the radio and microwave bands, such as ground penetration radar (GPR) systems, coaxial transmission line (CTL), and simple capacitors.

Electromagnetic waves were used to study the hydration process of Portland cement and PCC at the radio and microwave frequencies through evaluating the conductivity and/or the complex dielectric constant. Radio wave frequency bands were used to monitor cement hydration and structure development. McCarter and Curran (1984) [34] studied the electrical response characteristics of cement-water-electrolyte at 1 kHz frequency. Taylor and Arulanandan (1974) [35] explored the physical properties of Portland cement by studying its electrical properties (the dielectric constant and conductivity). Measurements of conductivity and the dielectric constant were experimentally determined over a frequency range of 1 MHz to 100 MHz by measuring both the resistance and the capacitance, respectively. Testing of different w/c ratios determined both the relative dielectric constant and the conductivity. The study showed that conductivity increased with frequency and decreased with more hydration, while the relative dielectric constant decreased with frequency and/or hydration.

Similarly, Perez-Pena and Roy (1989) [36], Moukwa et al. (1991) [37], Wittmann and Schlude (1975) [38], and De Loor (1962) [39] studied the dielectric properties of PCP over the RF and microwave frequencies. Measurements of dielectric properties of PCC over RF were performed by Hansson and Hansson (1983) [40], McCarter and Curran (1984) [34], McCarter et al. (1985) [41], Wilson and Whittington (1990) [42], Whittington et al. (1981) [43], and McCarter and Whittington (1981) [44]. Hasted and Shah (1964) [45] and Shah et al. (1965) [46] measured the dielectric properties of bricks, Portland cement, and PCC at different w/c ratios. Results were compared to the theoretically obtained values.

Chapter 3
Parallel Plate Measurement System

The parallel plate capacitor was chosen for materials characterization because of simplicity, its suitability for the low RF frequency range, and the convenience of casting or cutting parallel-faced PCC specimens. The parallel plate capacitor uses a uniform electric field over a fairly large volume of space. This means that large specimens can be measured with acceptable accuracy. The fixture allows an adjustable separation between its plates, hence allowing flexibility in specimen sizes. A parallel plate capacitor fixture was custom-made to hold the evaluated PCC specimens. An HP-4195A Network/Spectrum Analyzer (Hewlett-Packard Co., Santa Clara, Calif.) was connected to the fixture to measure the capacitor impedance. Rectangular-shaped specimens used for this setup simplified both the design and the casting mold required.

3.1 System Design and Setup

Figure 3.1 shows the experimental setup used in this study. The capacitor plates are mounted in a horizontal direction. Each stress-relieved plate is approximately 46 x 46 x 1.3 cm and is made of steel. A supporting rod at each corner fixes the upper plate. The lower plate is mounted on a threaded rod located at its center, allowing the lower plate to move vertically. Five-cm-long sleeves on the supporting rods maintain the lower plate in a horizontal position, allowing a range of 5 to 13 cm displacement between the two plates.

The PCC is placed at the center of the parallel plate capacitor. Carefully-cast rectangular PCC blocks (due to polishing or casting) allow for complete surface contact with the plates. Attention should also be paid to the amount of pressure that is exerted to maintain contact between the plates and the PCC sample. Results have shown that saturated samples are sensitive to such pressure at low frequencies.

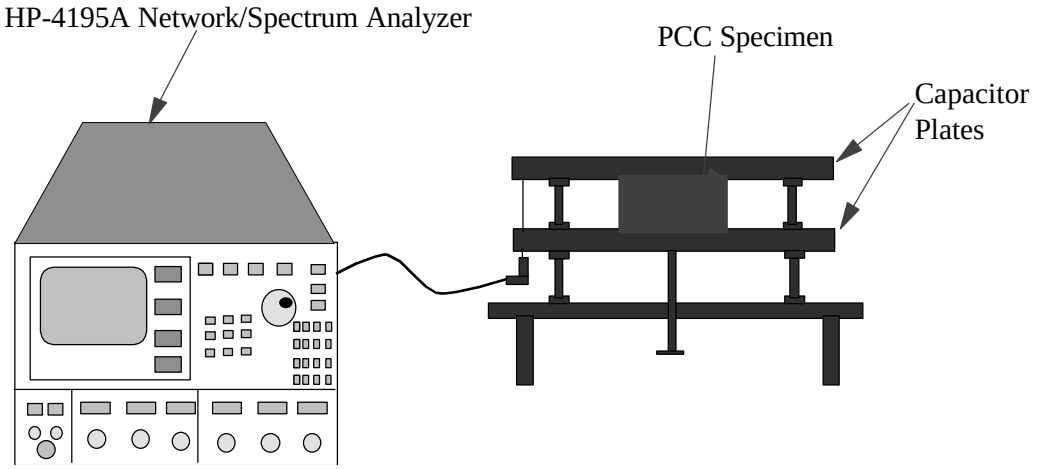

Figure 3.1: A schematic setup for the parallel plate capacitor.

The impedance of the capacitor is measured using a HP-4195A Network/Spectrum Analyzer. EM fields will emanate from the capacitor plates and excite the test medium. The distribution of EM fields will govern the impedance of the measurement system. Impedance measurements of this probe will result in information related to the average dielectric performance of the bulk media in the EM field. Internal

flaws including chloride presence will alter the field distribution and dielectric properties, thus bringing a change in the impedance of the measurement system.

3.2 Theoretical Background of the Parallel Plate Capacitor

The measurement techniques are based on planar transmission line principles. The measuring device assumes a plane transmission line in the form of a parallel plate capacitor configuration. The specimen under test forms the dielectric media for some part between the plates. To ensure a uniform electric field in the middle of the plates where the specimen is placed (see Figure 3.2), each plate should be at least three times the largest dimension of the tested specimen to minimize edge diffraction effect (Al-Qadi, 1992 [15]). Thus, the uniform electric field equation can be used (see equation 2.7).

$$D = \varepsilon^* E \tag{3.1}$$

and

$$V_0 = -\int_d^0 EdL = \rho_s \frac{d}{\varepsilon^*} \tag{3.2}$$

where

V_o = Potential (V);

d = Thickness of the dielectric specimen in the direction of EM wave propagation (m); and

ρ_S = Surface charge density (C/m^2).

As

$$Q = CV_o \tag{3.3}$$

where, Q is the total charge (C) and C is the capacitance (F).

From equations 3.1, 3.2, and 3.3,

$$C = \varepsilon^* \frac{S}{d} \tag{3.4}$$

where S is the surface area of the specimen in contact with one plate and perpendicular to the direction of wave propagation (m^2). Equation 3.4 is valid for an infinite plate capacitor that guarantees low edge disturbance.

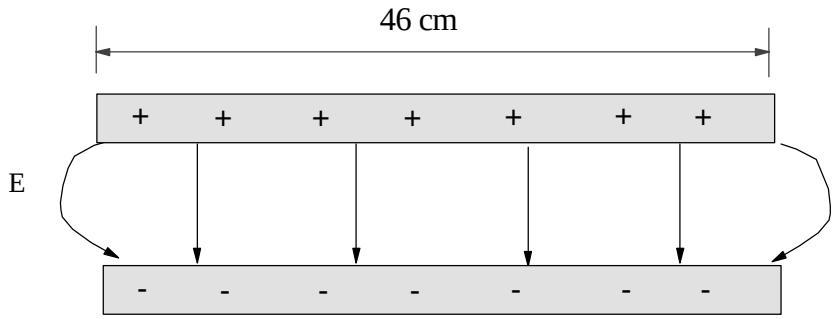

Figure 3.2: Electric field distribution between the two plates of the parallel plate capacitor.

3.3 Parallel Plate Capacitor Model

The calibrated impedance is assumed to be due to the complex capacitance, C*, given by:

$$Y_L = \frac{1}{Z_L} = j2\pi f (C^* - C_0) = G_L + jB_L \tag{3.5}$$

where

Y_L = the complex load admittance, = ½L;

G_L and B_L = the load conductance and susceptance, respectively;

f = frequency; and

$j = \sqrt{-1}$.

C_0 is the capacitance due to an equivalent sample of air (air capacitance), as illustrated in Figure 3.3. In equation 3.5, the difference ($C^* - C_0$) is used since C_0 is included as part of the open circuit calibration.

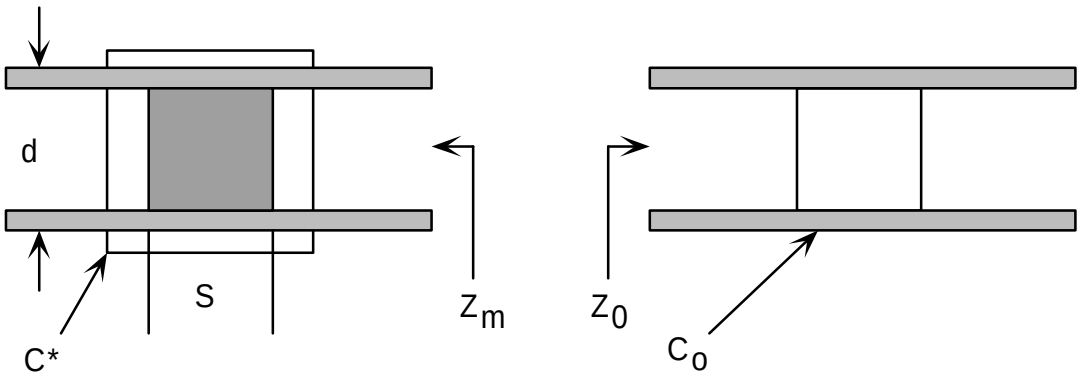

Figure 3.3. Capacitor with and without specimen under test.

With the assumption of uniform electric field distribution at the center of the capacitor and homogeneous specimen, the complex capacitance is given by:

$$C^* = \varepsilon_0 \varepsilon_r^* \frac{S}{d} = \varepsilon_0 \left(\varepsilon_r' - j\varepsilon_r'' \right) \frac{S}{d} \qquad (3.6)$$

where ε_o is the free space permittivity (ε_0 = 8.854 x 10^{-14} F/cm); ε^*_r is the complex relative permittivity of the specimen; ε'_r and ε''_r are the dielectric constant and the dielectric loss factor, respectively; and S and d are the cross-sectional area and the thickness of the specimen being measured, respectively.

The capacitance of the air-filled capacitor is given as follows:

$$C_0 = \varepsilon_0 \frac{S}{d} \qquad (3.7)$$

Hence, the complex permittivity is given in terms of the calibrated load as follows:

$$\varepsilon_r' = 1 + \frac{Bd}{2\pi fS} \tag{3.8}$$

$$\varepsilon_r'' = \frac{Gd}{2\pi fS} \tag{3.9}$$

For simplicity, the loss tangent can be defined as follows:

$$\tan\delta = \frac{\varepsilon_r''}{\varepsilon_r'} \tag{3.10}$$

The designed capacitor fixture can be treated as a waveguiding system consisting of two parallel plates of large extent confining a dielectric region between them. The mode of propagation is the principle mode or the transverse electromagnetic (TEM) field mode. The electric field lies vertically between the plates, while the magnetic field lies along the width. The wave propagates between the conducting planes with a phase velocity equal to the free space velocity of light (air dielectric). Assuming a width of b' and a thickness of a' at the center (of the PCC specimen), the following parameters can be defined for such a transmission line:

Capacitance, C: Capacitance per unit length of a parallel plate transmission line may be expressed as follows:

$$C = \frac{b\varepsilon}{a'} \tag{3.11}$$

Phase velocity, v_P: The phase velocity is found using the following expression:

$$v_p = \frac{1}{\sqrt{\mu\varepsilon}} \tag{3.12}$$

Resistance, R: The resistance per unit length may be expressed as follows:

$$R = \frac{2R_s}{b'} \tag{3.13}$$

where R_s is the surface resistivity in ohms.

Characteristic Impedance, Z_0: The characteristic impedance has the following expression:

$$Z_0 = \frac{1}{v_p C} \tag{3.14}$$

Dimensions of the fixture are:

Length, l = 46 cm;

Width, w = 46 cm;

Height, a' = 7.6 cm;

R_s (for steel) = 188 x 10^{-6} $\sqrt{f}$; and

Width (of PCC specimen), b' = 10.2 cm.

With the values given above, the electrical parameters of interest can be evaluated for an air-filled transmission line as:

C = 2 x (8.856 x 10^{-12}) F/m;

v_p = 3 x 10^8 m/s;

R = 25 x 10^{-6} $\sqrt{f}$; and

Z_0 = 188.38 Ω.

Higher order modes can also exist in a parallel plate transmission line. The higher order waves or the complementary waves can exist for a nonzero incidence angle on the conducting plates. The following expression gives the cut-off frequency (f_c) for higher order modes for both transverse electric (TE) field mode and transverse magnetic field (TM) mode:

$$f_c = \frac{nv_p}{2a'} \tag{3.15}$$

where n = 1, 2,… any integer value denoting the order of the modes.

With a' = 7.6 cm, the value for cut-off frequency (f_c) for an air-dielectric line is given by $f_c = (2 \times 10^9)\, n = 2n$ GHz.

A lumped element model has been assumed in the development the equations governing the parallel plate measurement system when in fact the material under test is actually a distributed element. This distributed element can be viewed in the parallel plate test fixture as a open terminated transmission line. Figure 3.4 shows the material under test in the parallel plate fixture and the corresponding open circuited transmission line model associated with the material under test.

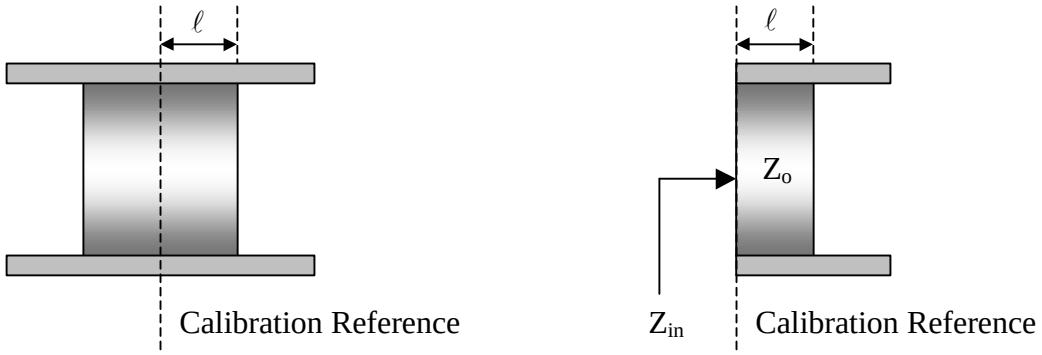

Figure 3.4: (a) The parallel plate fixture containing a material under test and (b) the corresponding transmission line model.

The input impedance, Z_{in}, for an open circuited transmission line is given as:

$$Z_{in\_distributed} = -jZ_o \cot\beta\ell \tag{3.16}$$

where,

ℓ = length of the transmission line;

$\beta = \frac{2\pi}{\lambda}$, λ = wavelength; and

Z_o = characteristic impedance of the transmission line.

For the lumped element assumption, the value of ℓ is very small. Knowing this we can estimate the value of Z_{in} for the lumped element model by using the following relationship:

$$\cot x \approx \frac{1}{x} \text{ , @ x = small number} \tag{3.17}$$

Using this identity, solving for Z_{in} of the lumped element model results in the following:

$$Z_{in\_lumped} = -\frac{jZ_o}{\beta\ell} \tag{3.18}$$

We can developed the percent of error associated with the lumped element versus the distributed elements by the following:

$$\frac{Z_{in\_distributed} - Z_{in\_lumped}}{Z_{in\_distributed}} = 1 - \frac{\tan\beta\ell}{\beta\ell} \tag{3.19}$$

Figure 3.5 shows the percent error between the lumped and distributed models for sample material under test having a width of 7.6cm (ℓ = 3.8cm) between the frequency range of .1MHz and 40MHz.

The relationship between the impedance of the lumped element and the dielectric constant needs to be considered so that a error calculation can be performed. Assuming a lossless case, the characteristic impedance is related to lumped elements as follows:

$$Z_o = \sqrt{\frac{L}{C}} \tag{3.20}$$

where,

L = inductance per unit length; and

C = capacitance per unit length.

Also in the lossless case, the propagation constant reduces to the following:

$$\gamma = j\beta = j\omega\sqrt{LC} \tag{3.21}$$

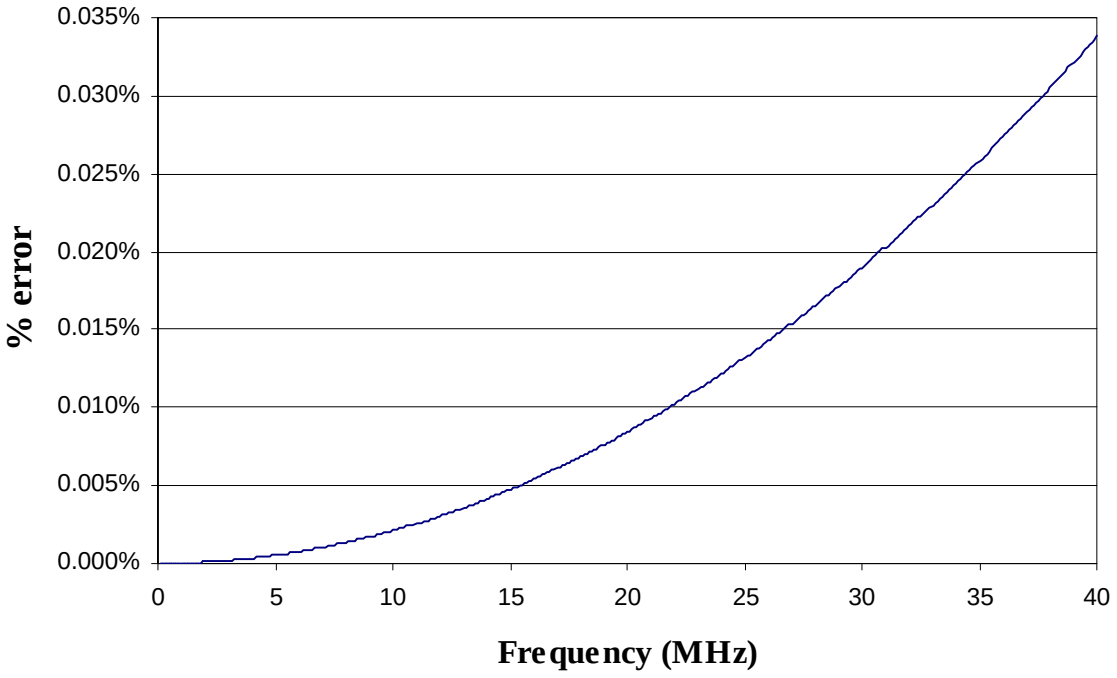

Figure 3.5: A graph showing the percent error between the impedance of the lumped element model versus the distributed element model.

Substituting equation (3.20) and equation (3.21) into equation (3.18) gives us the following relationship:

$$Z_{in\_lumped} = -\frac{jZ_o}{\beta L} = \frac{\sqrt{\frac{L}{C}}}{\omega\sqrt{LC}\ell} = -j\frac{1}{\omega C_T} \propto \frac{1}{\varepsilon} \tag{3.22}$$

where,

C_T = the total capacitance of length, ℓ.

The corresponding error relating to the dielectric constant, plotted in Figure 3.6, can be found in equation 3.23 as shown:

$$\frac{\frac{1}{\varepsilon_{distributed}} - \frac{1}{\varepsilon_{lumped}}}{\frac{1}{\varepsilon_{distributed}}} = 1 - \frac{\beta L}{\tan \beta L} \tag{3.23}$$

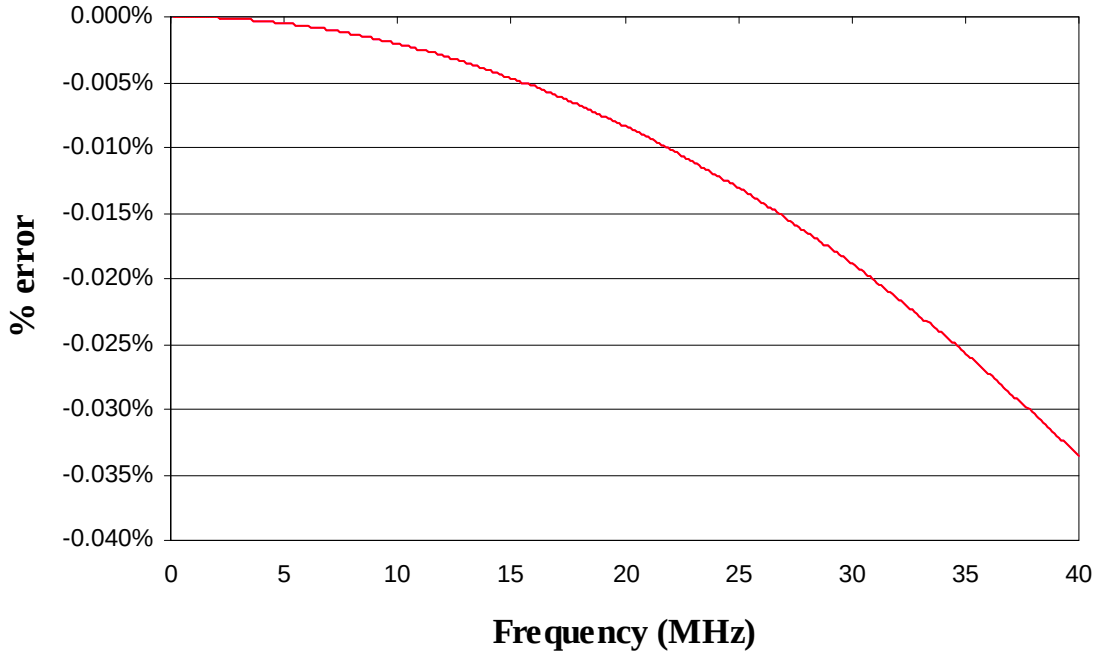

Figure 3.6: A graph showing the percent error of the dielectric constant due to the assumption of a lumped element model versus the distributed element model.

3.4 Parallel Plate Calibration Standards

Before defining of the calibration equations in the next section, the parallel plate capacitor system will use three calibration measurements for error compensation. These measurements are an open standard, a load standard, and a short standard. We need to use known standards when performing these measurements and this section will describe the construction of the calibration standards used for the parallel plate measurement system.

3.4.1 Open Calibration Standard

The open calibration standard is simply an air dielectric between the plates of the parallel plate system. We can acknowledge that using air as an open calibration standard introduces a small amount of error due to the capacitance that will be present between the plates. This error is taken into consideration with the simulation performed to find the average of this capacitance value over different spacing between the parallel capacitor plates. It would be very difficult to make a high quality open calibration standard for this system due to the system's physical attributes, so an air dielectric is used for this calibration measurement. Since the capacitance measurement is dependant on the distance between the plates, the distance for each of the calibration standards must be the same as the distance between the plates when measuring the material with unknown dielectric constant.

3.4.2 Load Calibration Standard

The load standard is a 50Ω resistor. This calibration standard will have to have the ability to be adjusted for different distances between the plates for the same reason mentioned in the open calibration standard section. Shown in Figure 3.7 are the designed calibration standard and the standard's maximum dimensions. The standard is constructed of two solid brass pieces with six low tolerance three hundred ohm (300Ω) resistors in series with a dielectric medium separating the plates where the resistors are

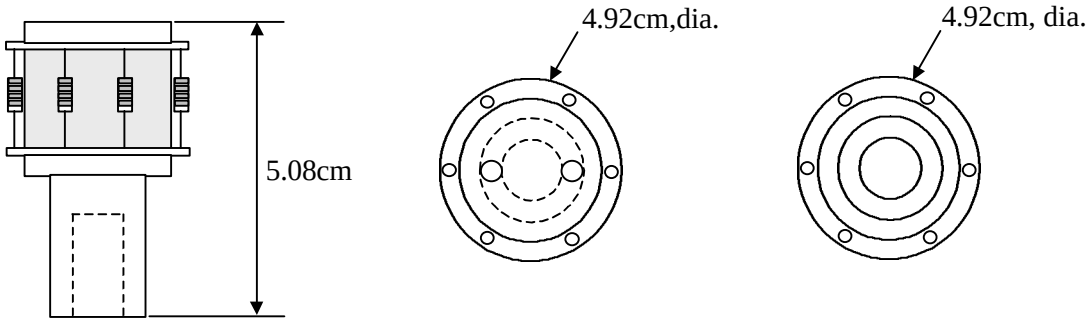

Figure 3.7. Parallel plate load calibration standard

connected. There is a milled out hole on the underside of the standard that is used for the placement of a brass spring to allow plate distance adjustment.

The narrow end of the load calibration standard containing the spring can be inserted into a base. The spring will press the load standard and the base against each of the conducting plates. Two bases were constructed having different heights to allow for a wide range (≈ 7.3cm to 11.12cm) of parallel plate measurement distances. Having multiple bases will allow us the flexibility of measuring different sized samples in the system. The base diagrams are shown in Figures 3.8 and 3.9.

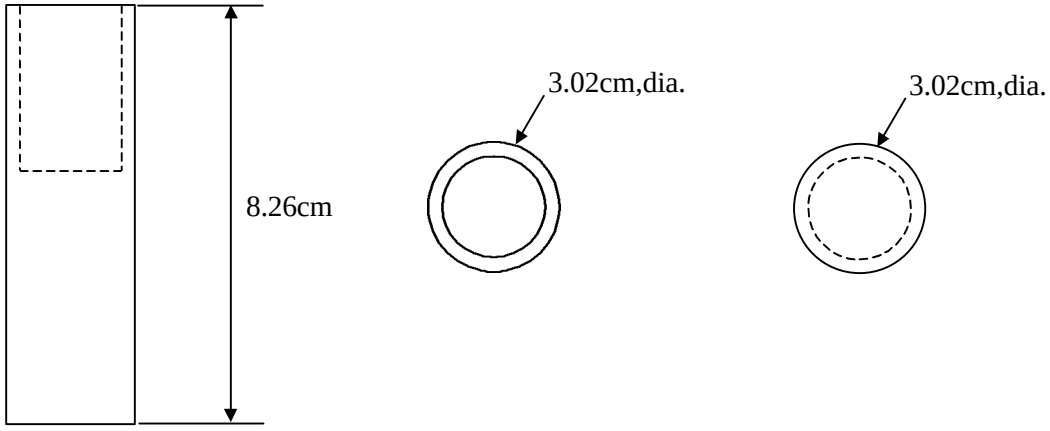

Figure 3.8. Large height calibration standard base

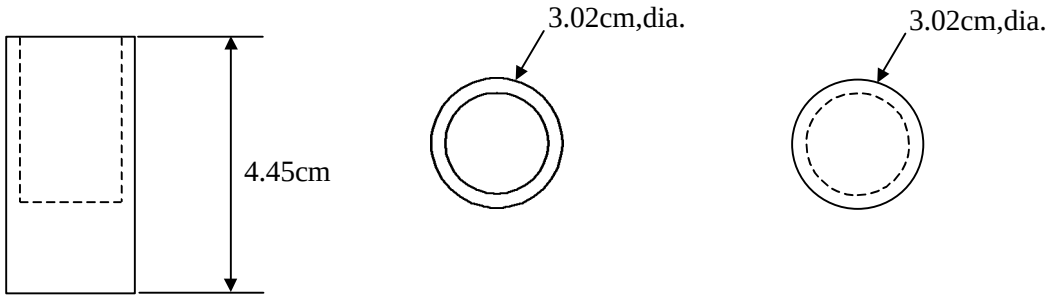

Figure 3.9. Small height calibration standard base

3.4.3 Short Calibration Standard

The short calibration standard is shown in Figure 3.10. This calibration standard is a solid piece of brass with a milled hole in the underside for the placement of the spring. This standard will also work with the two calibration bases shown in Figures 3.8

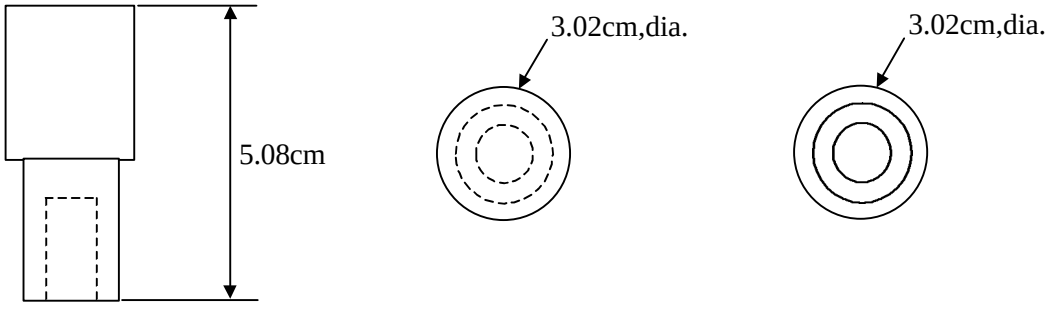

Figure 3.10. Short circuit calibration standard

and 3.9. Making a perfect short calibration standard is easier than making an open calibration standard due to the fact that you do not have the effects of a parasitic capacitance and/or other noise contributions. Since the quality of this type of short is very high, we have assumed this short calibration standard to be a perfect short in the previous section.

3.5 Equations Governing the Parallel Plate System

A scattering parameter matrix is a valuable representation of a multiport network. The scattering matrix of any n port device is unique to that device and is independent of the loads at the n ports. In the case of the parallel plate test fixture, we have a total of two ports (n=2) consisting of ports at the measurement plane and at the reference plane as illustrated in Figure 3.11. This two port device has historically had a network analyzer connected to the reference port and various loads (open, short, matched load, known dielectric material or unknown dielectric material such as PCC) connected to the measurement port. The open, short, and matched loads are employed in order to determine the scattering parameters of the matrix. Once these parameters are defined at a

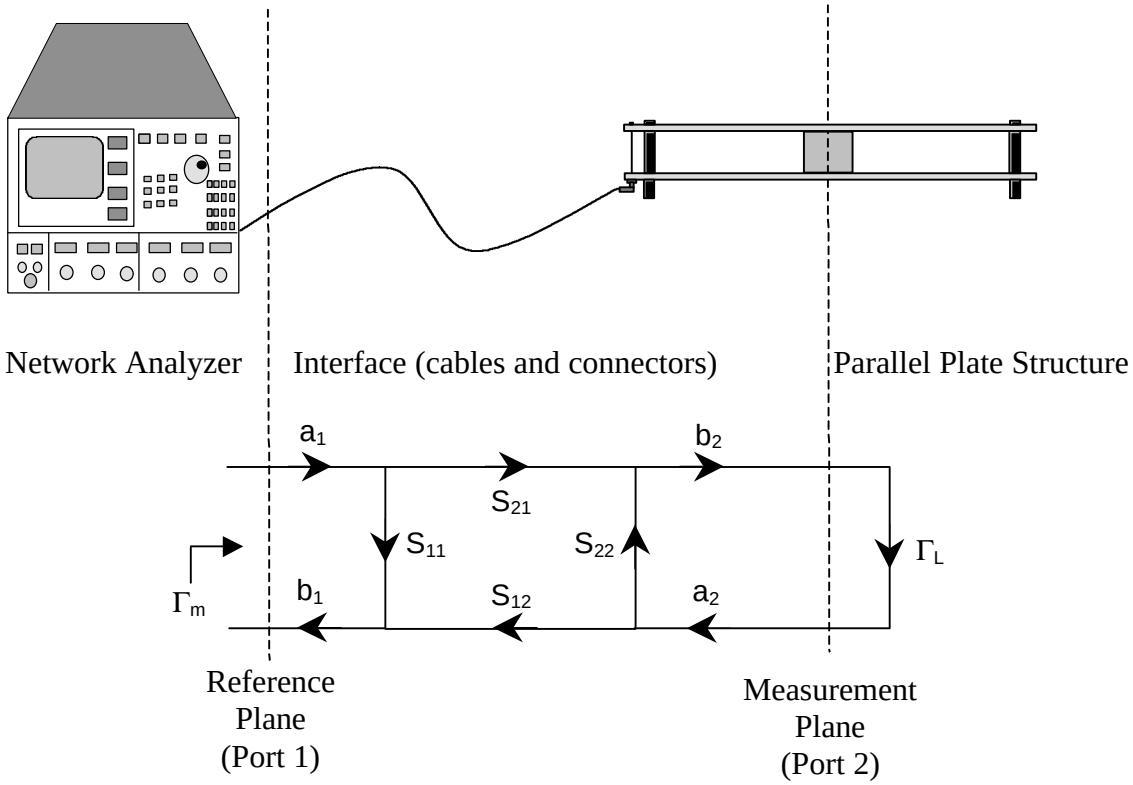

Figure 3.11. Parallel plate measurement system and model

given frequency, the test fixture is defined and a unique relationship is established between the unknown loads and the reflection coefficient measured by the network analyzer. Figure 3.11 is a schematic of the measurement system including the two port scattering parameters,

where

$a_1 \equiv$ voltage wave input by network analyzer

$b_1 \equiv$ voltage wave reflected by the entire measurement system to the network analyzer

$a_2 \equiv$ voltage wave reflected by load at the measurement plane between parallel plates

$b_2 \equiv$ voltage wave incident to load at the measurement plane between parallel plates

$\Gamma_M \equiv$ reflection coefficient measured by network analyzer at the reference plane (= b_1/a_1)

$\Gamma_L \equiv$ reflection coefficient of the load at the measurement plane between the parallel plates at the measurement plane (= a_2/b_2), Γ_L is what is desired to be determined from the measured Γ_M.

For the 2 port, parallel plate capacitor fixture, the scattering matrix is as follows:

$$\begin{bmatrix} b_1 \\ b_2 \end{bmatrix} = \begin{bmatrix} S_{11} & S_{12} \\ S_{21} & S_{22} \end{bmatrix} \begin{bmatrix} a_1 \\ a_2 \end{bmatrix}. \tag{3.24}$$

Evaluating the scattering matrix results in the following equations:

$$b_1 = S_{11}a_1 + S_{12}a_2 \tag{3.25}$$

$$b_2 = S_{21}a_1 + S_{22}a_2 \tag{3.26}$$

Recall that the point of the parallel plate capacitor calibration scheme is to define the four scattering parameters (S_{11}, S_{21}, S_{12}, and S_{22}).

Dividing equation 3.25 by a_1 yields the following equation for Γ_m:

$$\Gamma_m = \frac{b_1}{a_1} = S_{11} + S_{12}\left(\frac{a_2}{a_1}\right). \tag{3.27}$$

Dividing equation 3.26 by a_2 yields the following equation for Γ_L^{-1}:

$$\frac{1}{\Gamma_L} = \frac{b_2}{a_2} = S_{22} + S_{21}\left(\frac{a_1}{a_2}\right) \tag{3.28a}$$

Rearranging equation 3.28a results in the following relation between a_2 and a_1:

$$\frac{a_2}{a_1} = \frac{\Gamma_L S_{21}}{1 - \Gamma_L S_{22}}. \qquad (3.28b)$$

Substituting equation 3.28a into equation 3.27 yields the following equation for the reflection coefficient at the reference plane in terms of the reflection coefficient at the measurement plane and the scattering parameters:

$$\Gamma_M = S_{11} + \frac{S_{12} S_{21} \Gamma_L}{1 - S_{22} \Gamma_L} \qquad (3.29)$$

The four scattering parameters are a property of the test fixture and are independent of the load or the network analyzer. The following sections will describe each of the three calibration measurements in detail and how they are used for error compensation. The calibration coefficients, consisting of the scattering parameters, will then be applied to generate an expression for the complex dielectric constant of a material with unknown permittivity.

The impedance of the parallel plate measurement system is measured using a network analyzer. The analyzer is connected to the parallel plate measurement setup through an interface network which is formed mainly of a cable and an adapter. The analyzer is used to measure the reflection coefficient, Γ, at its reference plane. This reflection coefficient is a function of the S-parameters of the interface network (S_{int}) as well as the impedance of the parallel plate when the PCC material is inserted. The measured Γ is used to evaluate the complex impedance (real and imaginary parts) of the PCC material as a function of frequency

To ensure proper evaluation of the dielectric properties of the PCC structural element under test, a one port calibration method is used. This method uses three calibration standards for error compensation. These three calibration measurements are an open circuit (Y_a), a short circuit ($Y_s = \infty$), and a 50Ω load (Y_L) between the conducting plates of the system; where Y is an admittance. These three calibration measurements are used to solve a three-unknown calibration model. The unknowns generated by the model are the scattering parameters of the model, S_{11}, the product $S_{21}S_{12}$, and S_{22}; where S_{11} and S_{21} represent the reflection and transmission, respectively, at the plane of reference and

S_{22} and S_{12} represent the same parameters at the plane of measurement. The capacitor plates are assumed large enough that the fields near the measurement are vertical between the plates in the area that the measurement is taken (the measurements are assumed to be independent of fringing effects). The general calibration model is shown in Figure 3.12.

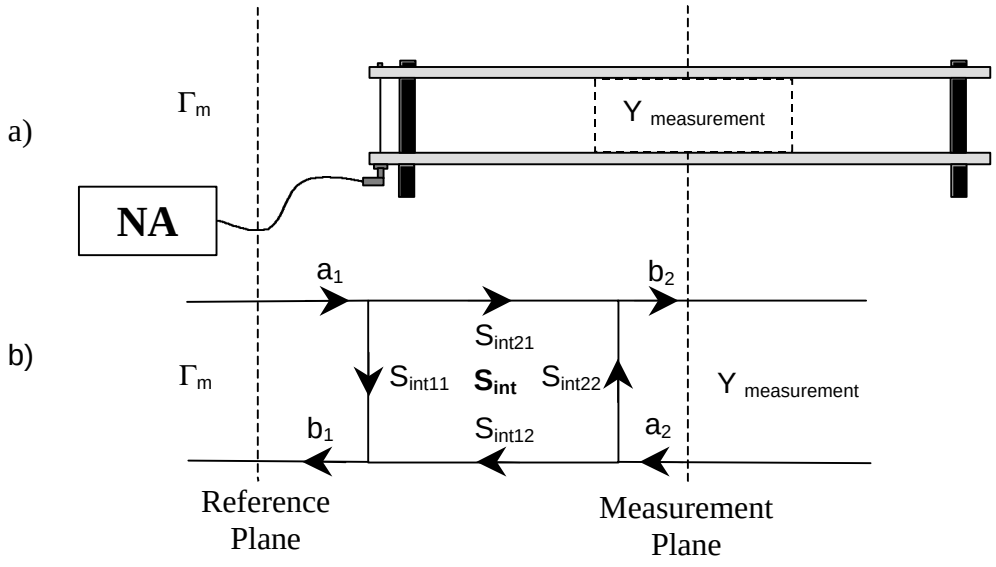

Figure 3.12. (a) General parallel plate system model and (b) general S-parameter model.

At this point, two calibration issues need to be addressed; they are:

1. the load standard used is not exactly equal to 50Ω; and,
2. the open circuit standard is in fact a capacitive load.

These two issues are addressed in the following manner,

1. The effect of the load standard, Y_L.

   For convenient analysis of this calibration problem, the error admittance, Y_L-Y_O, (where, Y_O = 1/50Ω) will be imbedded with the S-parameters of the interface network to yield what we will refer to as the combined S-parameter model. By grouping Y_{err} = Y_L-Y_O with the combined S-parameters, the effective load to the measurement system becomes Y – Y_{err} which results in:

   Y_L-Y_{err} = Y_O = 1/50Ω for the load standard;

$Y_S - Y_{err} = \infty$ for the short circuit standard;

$Y_a - Y_{err} = Y_{op}$ for the open circuit standard; and,

$Y_m - Y_{err} = Y_{MUT}$ for the material sample.

This grouping results in simpler equations for the data reduction of the calibration process, which will be seen later.

2. The effect of the open circuit standard capacitance, C_a.

   It is relevant to state that the measurement perform here is a substitution measurement. This is because the material sample to be measured replaces the air portion of the parallel plate fixture. Hence, the value of Y_a (open circuit standard) in fact corresponds to the admittance of the air portion replaced by the material sample under measurement. Consequently, $Y_a = 1/j\omega C_a$, where C_a is the capacitance of an air sample having exactly the same dimensions as the material sample measured.

3.5.1 Load Calibration

Shown in Figure 3.13, the load calibration model also includes the admittance of the load calibration standard, Y_L, and the admittance compensation for the load standard, Y_{err} (which can also be written as $Y_L - Y_O$, where Y_O is the admittance of the 50Ω reference line). The resistance and capacitance values of the load standard were found to be R_L=50.7Ω and C_L=3.4pF, respectively. This initial step in the load calibration description corrects the measured value of the 50Ω load calibration standard by compensating for the admittance of the 50Ω line (Y_O). As previously discussed, the quantity $Y_L - Y_O$ is embedded into the S-parameter model, leaving Y_O as the only value outside the S-parameter model. By placing the admittance compensation for the load (Y_{err}) inside the S-parameter model, the reflection coefficient at the measurement plane generated from the load standard (Γ_{ml}) is simplified. By including this value within the model, the complexity of the entire equation set can be reduced. Y_{err} can be written as follows:

$$Y_{err} = Y_L - Y_O \tag{3.30a}$$

$$Y_{err} = (G_L - G_O) + j\omega C_L \qquad (3.30b)$$

where,

$j = \sqrt{-1}$;

$\omega = 2\pi f$ where, f = frequency (Hz);

G_O = conductance of a 50Ω load;

G_L = conductance of the load standard ($1/R_L$);

C_L = capacitance of the load standard.

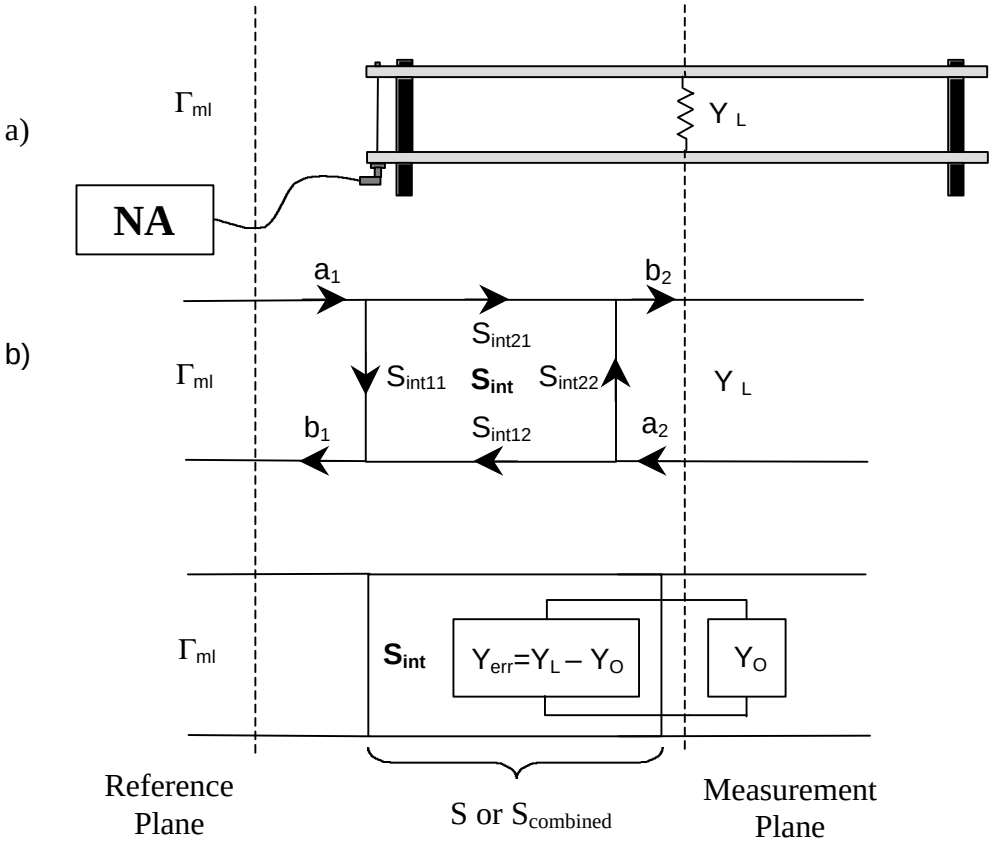

Figure 3.13. (a) Load parallel plate system model and (b) load S-parameter model.

The reflection coefficient at the reference plane of the load measurement is as follows:

$$\Gamma_L = \frac{Y_o - Y_o}{Y_o + Y_o} = 0 \tag{3.31}$$

The reflection coefficient, Γ_L, reduces to zero by leaving only the Y_O term outside the S-parameter load model. After obtaining the value for Γ_L, Γ_{ml} can be found as shown in Figure 3.13. Using the S-parameter model, the reflection coefficient of the parallel plate system with a 50Ω load calibration standard, Γ_{ml}, is equal to S_{11} as follows:

$$\Gamma_{ml} = S_{11} \tag{3.32}$$

3.5.2 Open Calibration

The admittance compensation for the load, Y_{err}, must be accounted for in all of the calibration measurements and is embedded into the open S-parameter model, shown in Figure 3.14. As a result, the effective admittance of the open circuit standard becomes:

$$Y_{op} = Y_a - Y_{err} \tag{3.33a}$$

$$Y_{op} = (G_O - G_L) + j\omega(C_a - C_L) \tag{3.33b}$$

The admittance of the open calibration standard, Y_a, was found through the use of various simulations in which the parallel plate measurement system was simulated and the value of C_a, the capacitance of the air between the plates, was extracted. The equation for Y_a is developed from the simulated value of C_a as follows:

$$Y_a = j\omega C_a \tag{3.34}$$

where,

$C_a \approx C_a$ is the capacitance of an air sample having exactly the same dimensions as the material sample measured.

The reflection coefficient of the open calibration measurement, Γ_{op} is as follows:

$$\Gamma_{op} = \frac{Y_o - Y_{op}}{Y_o + Y_{op}} \tag{3.35}$$

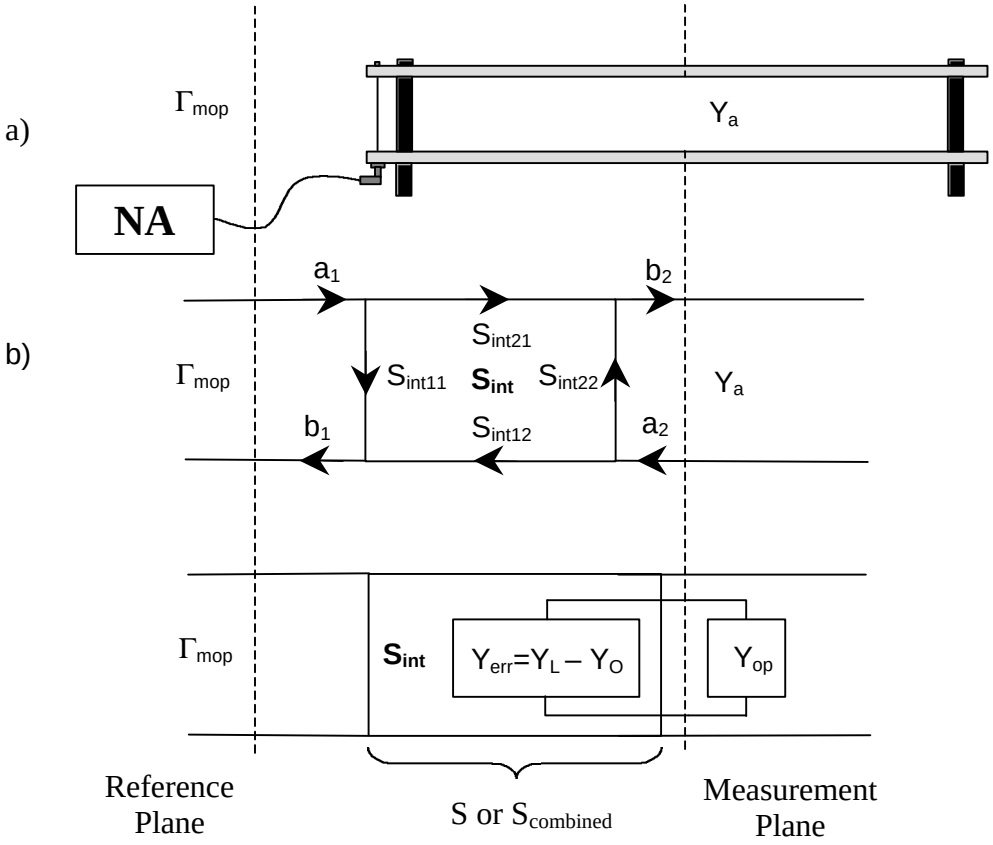

Figure 3.14. (a) Open parallel plate system model and (b) open S-parameter model.

After obtaining the value for Γ_{op}, Γ_{mop} can be found as shown in Figure 3.14. Using the S-parameter model, the reflection coefficient of the parallel plate measurement system using an open calibration standard, Γ_{mop}, may be obtained as the following:

$$\Gamma_{mop} = S_{11} + \frac{S_{12}S_{21}\Gamma_{op}}{1 - S_{22}\Gamma_{op}} \tag{3.36}$$

3.5.3 Short Calibration

Since the short circuit standard presents an infinite admittance to the calibration model, the Y_{err} correction will not alter the effective admittance of the standard:

$$Y_s = \infty - Y_{err} = \infty \tag{3.37}$$

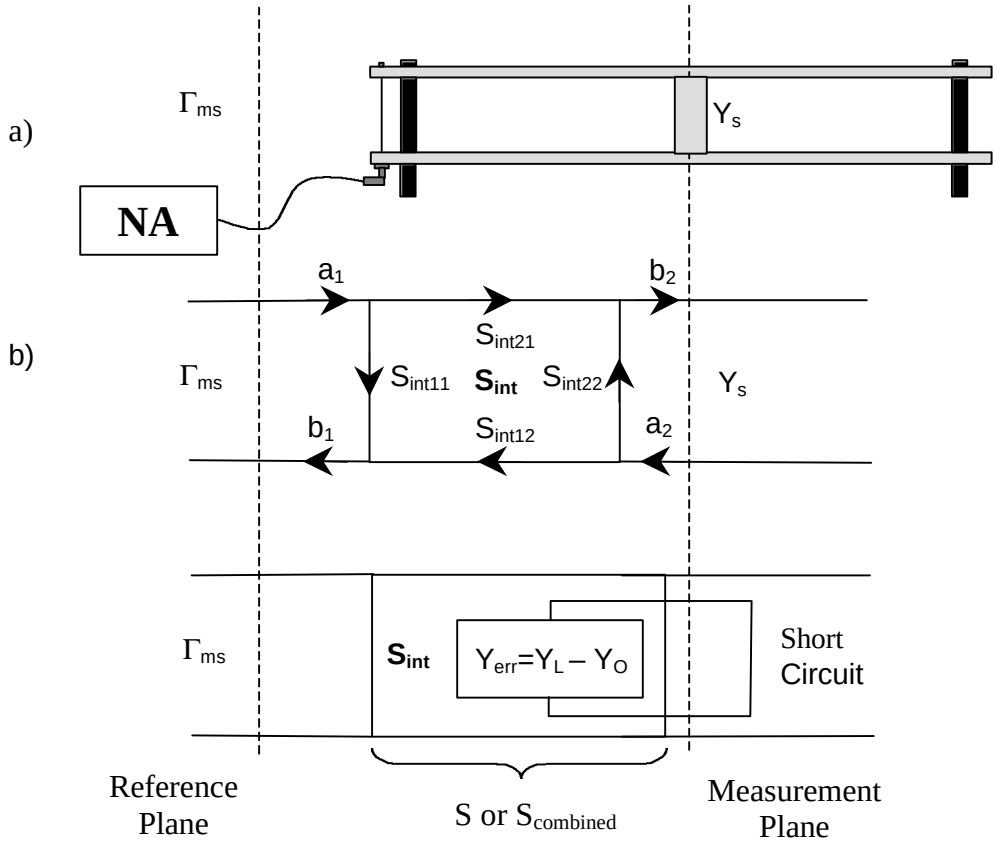

Figure 3.15. (a) Short parallel plate system model and (b) short S-parameter model.

The reflection coefficient of the short measurement, Γ_s, is given as:

$$\Gamma_s = \frac{Y_o - \infty}{Y_o + \infty} = -1 \tag{3.38}$$

After obtaining the value for Γ_s, Γ_{ms} can be found as shown in Figure 3.15. Using the S-parameter model, the reflection coefficient of the capacitor probe system using a short calibration standard, Γ_{ms}, is given as:

$$\Gamma_{ms} = S_{11} - \frac{S_{12}S_{21}}{1 + S_{22}} \tag{3.39}$$

Summary of S-Parameter Model

The S-parameters to be evaluated for calibrating the measurement system are those of the combined network. The s-parameter models and the corresponding equations are summarized below in Table 3.1.

Table 3.1. Reflection coefficients from the measured calibration standards.

Calibration	Reflection Coefficient (Γ_m)
Load	$\Gamma_{ml} = S_{11}$
Open	$\Gamma_{mop} = S_{11} + \frac{S_{12}S_{21}\Gamma_{op}}{1 - S_{22}\Gamma_{op}}$
Short	$\Gamma_{ms} = S_{11} - \frac{S_{12}S_{21}}{1 + S_{22}}$

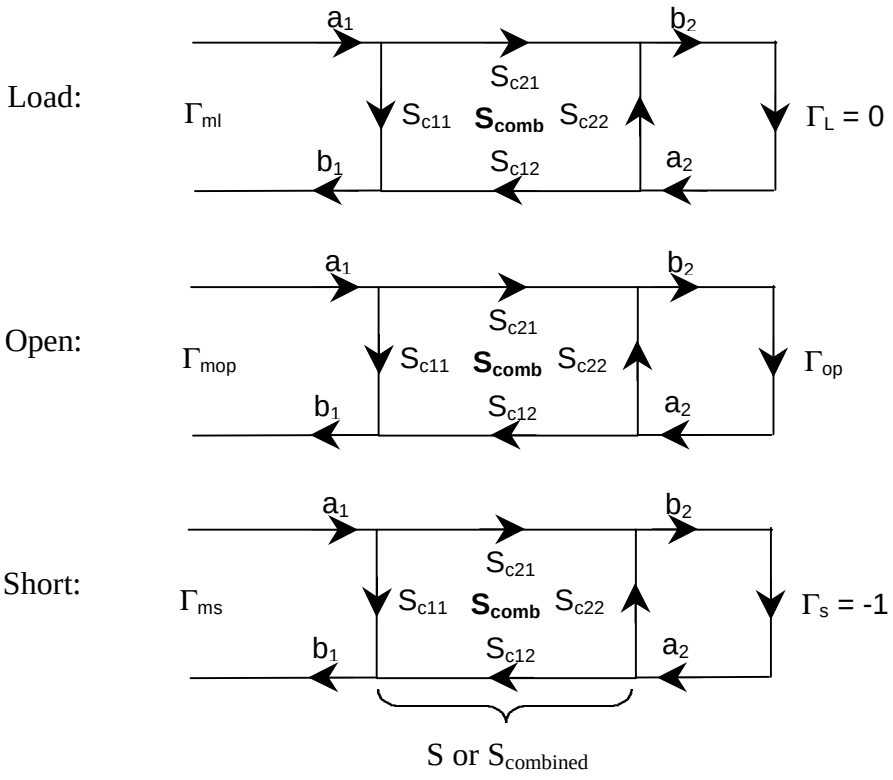

Defining the product of $S_{21}S_{12}$ as S_p,

$$S_p = S_{21}S_{12} \tag{3.40}$$

it is clear that the three standard measurements: Γ_{ml}, Γ_{mop}, Γ_{ms} can be used to evaluate the three error models: S_{11}, S_p, and S_{22}.

3.5.4 Determination of Remaining Unknowns

The analysis begins by developing a solution based on the equations shown in Table 3.1. One of the unknowns, S_{11}, has already been determined since it was found to be equal to the reflection coefficient of the capacitor probe system with the load calibration standard, Γ_{ml}. Subtracting the load reflection coefficient from the short reflection coefficient yields:

$$\Gamma_{ms} - \Gamma_{ml} = \frac{-S_p}{1+S_{22}} \tag{3.41}$$

Subtracting the load reflection coefficient from the open reflection coefficient yields:

$$\Gamma_{mop} - \Gamma_{ml} = \frac{S_p\Gamma_{op}}{1-S_{22}\Gamma_{op}} \tag{3.42}$$

Equations 3.41, and 3.42 can be reduced to obtain an equation which we will denote as the variable, Q. Equation 3.43 was obtained by dividing the expression found in equation 3.41 by the expression found in equation 3.42.

$$\frac{\Gamma_{ms} - \Gamma_{ml}}{\Gamma_{mo} - \Gamma_{ml}} = -\frac{1-S_{22}\Gamma_{op}}{\Gamma_{op}(1+S_{22})} = Q \tag{3.43}$$

Equation 3.43, referred to as Q, can now be solved for S_{22}. The result is as follows:

$$S_{22} = -\frac{1+Q\Gamma_{op}}{\Gamma_{op}(Q-1)} \tag{3.44}$$

Using the results from equation 3.32 and equation 3.39, S_p can be written as follows:

$$S_p = (\Gamma_{ml} - \Gamma_{ms})(1 + S_{22}) \tag{3.45}$$

The equations that are developed for determining the dielectric constant of a material under test (MUT) will now be addressed. As mentioned previously for the calibration measurements, the admittance compensation for the load (Y_{err}) is common to all of the measurements and is introduced into the S-parameter model, shown in Figure 3.16. As done for the calibration measurements, the admittance of the MUT, Y_m, must be corrected using the admittance compensation, Y_{err}. By placing the positive value of the admittance compensation into the S-parameter model, the corrected admittance value of the MUT, Y_{mut}, is given as:

$$Y_{mut} = Y_m - Y_{err} \tag{3.46}$$

The reflection coefficient of the MUT measurement (Γ_{mut}), developed from the equation given above for Y_{mut}, is given as follows:

$$\Gamma_{mut} = \frac{Y_o - Y_{mut}}{Y_o + Y_{mut}} \tag{3.47}$$

After obtaining the value for Γ_{mut}, Γ_{mm} can be determined as shown in Figure 3.16. Using the S-parameter model, the reflection coefficient of the MUT (Γ_{mm}) is given as:

$$\Gamma_{mm} = S_{11} + \frac{S_p \Gamma_{mut}}{1 - S_{22}\Gamma_{mut}} \tag{3.48}$$

The expression for Γ_{mm} from equation 3.48 can be rewritten in terms of Γ_{mut} as:

$$\Gamma_{mut} = \frac{\Gamma_{mm} - \Gamma_{ml}}{S_p + S_{22}(\Gamma_{mm} - \Gamma_{ml})} \tag{3.49}$$

From equation 3.48, a numerical value for the reflection coefficient of the MUT in equation 3.49 can be obtained using known parameters determined by calibration.

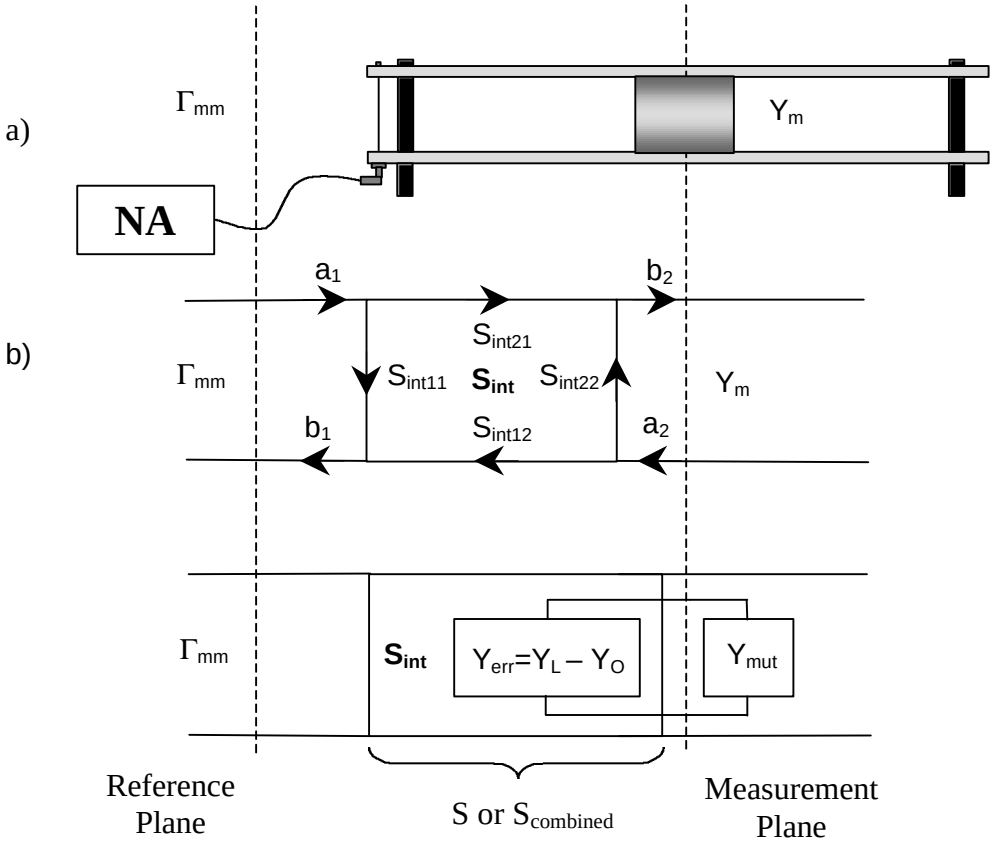

Figure 3.16. (a) MUT parallel plate system model and (b) MUT S-parameter model.

We may then rearrange equation 3.47 in terms of Y_{mut} as follows:

$$Y_{mut} = Y_O \frac{(1-\Gamma_{mut})}{(1+\Gamma_{mut})} \tag{3.50}$$

From equation 3.46, the admittance of the MUT, Y_m, is known and can be expressed as follows:

$$Y_m = Y_{mut} + Y_{err} \tag{3.51a}$$

$$Y_m = G_m + j\omega C_m \tag{3.51b}$$

Substituting in the classical equations for a parallel plate capacitor and conductivity (equations 3.52 and 3.53 respectively), shown below, we obtain the new form of the admittance of the MUT shown in equation 3.54.

$$C = \frac{\varepsilon_o \varepsilon_r A}{d} \tag{3.52}$$

$$G = \frac{\sigma A}{d} \tag{3.53}$$

$$Y_m = \frac{\sigma A}{d} + j\omega \frac{\varepsilon_o \varepsilon_r A}{d} \tag{3.54}$$

We can now divide both sides of equation 3.54 with the following expression:

$$j\omega \frac{\varepsilon_o A}{d} \tag{3.55}$$

The resulting form of equation 3.54 is as follows:

$$\frac{Y_m}{j\omega \frac{\varepsilon_o A}{d}} = \varepsilon_r - j\frac{\sigma}{\omega \varepsilon_o} \tag{3.56}$$

The final two identities needed to complete the solution are given as follows:

$$\varepsilon_r'' = \frac{\sigma}{\omega \varepsilon_o} = \frac{\varepsilon''}{\varepsilon_o} = -\mathrm{Im}\left[\frac{Y_m}{j\omega \frac{\varepsilon_o A}{d}}\right] \tag{3.57}$$

$$\varepsilon_r' = \varepsilon_r = \mathrm{Re}\left[\frac{Y_m}{j\omega \frac{\varepsilon_o A}{d}}\right] \tag{3.58}$$

Equations 3.57 and 3.58 are the real and imaginary portions of the complex dielectric constant (ε' and ε", respectively) extracted from equation 3.56.

An alternate presentation style involves the specification at ε_r' and tan δ instead of ε_r' and ε_r''. The loss tangent, tan δ, is defined as:

$$\tan\delta = \frac{\varepsilon_r''}{\varepsilon_r'} \tag{3.59}$$

3.6 Calibration Schemes

When the developed calibration standards were used as the sole standards in the calibration process, the output was slightly noisy and repeatability was difficult to achieve. This noise could be a result of our estimation of the true value of the standards. Two methods were developed to optimize the calibration scheme (shown in Figure 3.17). These two methods involve calibrating the system up to a certain point using HP's calibration standards, then completing the calibration with the developed standards. The first scheme used the HP standards to calibrate the vector network analyzer directly at the measurement device. This scheme was found to slightly decrease the noise, but the fact that we also had trouble with repeatability using this method caused us to look at a final alternative calibration. The final method used was to calibrate the vector network analyzer at the end of the cable that connects the analyzer to the parallel plate test fixture. This calibration scheme developed the best measurement results in both noise reduction and repeatability and was used as the calibration scheme for future measurements. An example of the results obtained on a sample of extruded nylon with each of the calibration schemes are plotted in Figures 3.18 and 3.19 showing the real and imaginary parts of the dielectric constant, respectively.

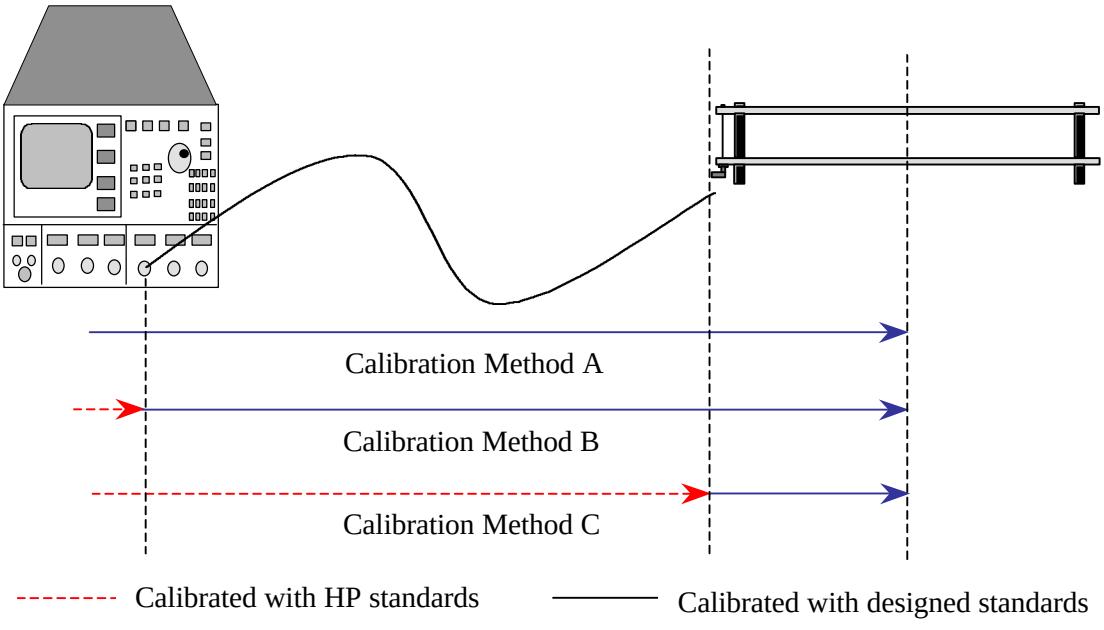

Figure 3.17. Methods of calibrating the parallel plate measurement fixture.

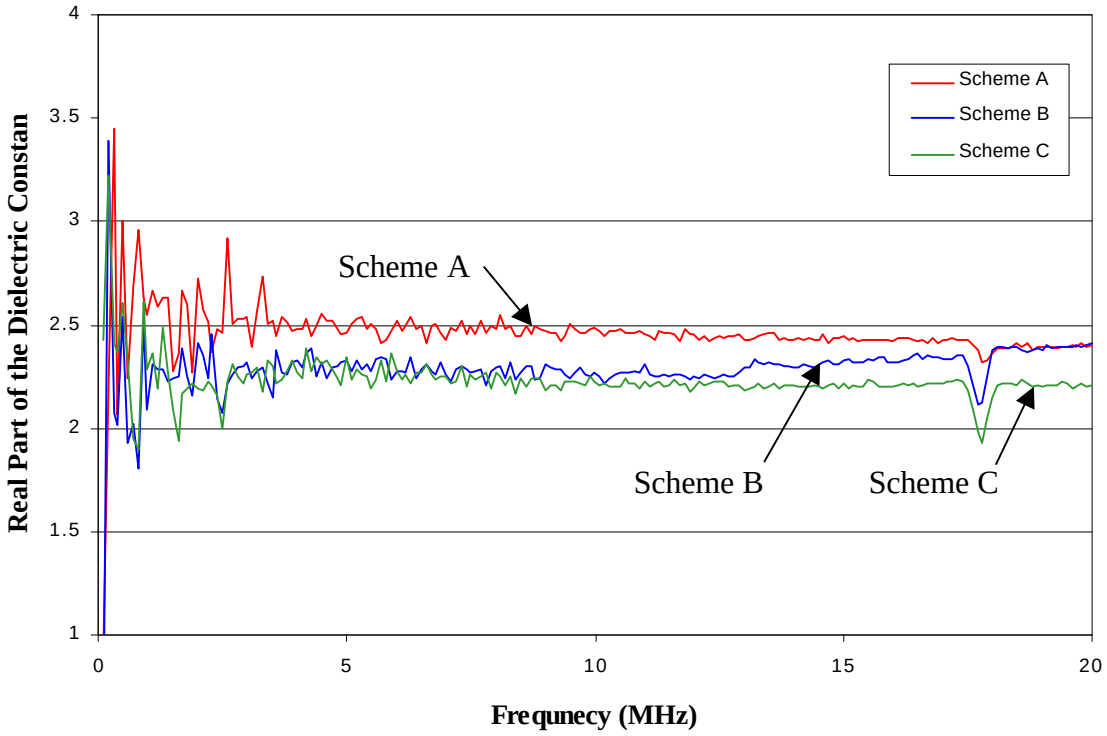

Figure 3.18: The real part of the dielectric constant of extruded nylon using different calibration schemes.

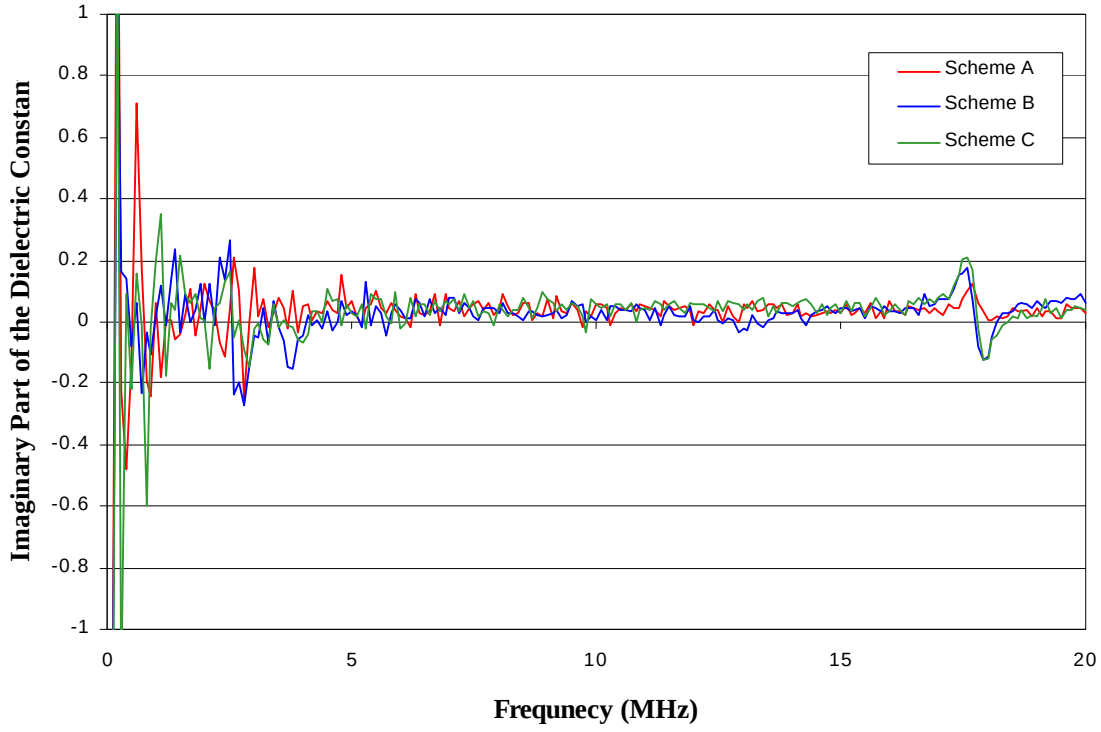

Figure 3.19: The imaginary part of the dielectric constant of extruded nylon using different calibration schemes.

3.7 Conclusions

This section introduced the parallel plate capacitance system for the purposes of material characterization. The theory behind the parallel plate capacitor design was explained along with the design and construction of the test fixture.

The developed standards used to calibrate the parallel plate measurement system were also introduced. A system calibration using three calibration measurements was employed on the parallel plate measurement system to solve for the scattering parameters, S_{11}, S_{22}, and $S_{21}S_{12}$, used to model interface consisting of the cables and adapters connecting the parallel plate measurement fixture to a vector network analyzer. From these calibration measurements the dielectric constant of a test specimen was calculated. Finally, the calibration schemes used in the measurements were described and explained. The scheme that produced the least amount of error was used in the measurements.

The parallel plate capacitor system will be used as a reference in the following section to validate the results generated by the capacitor probe.

Chapter 4
Capacitance Probe Measurement System

The capacitor probe will be implemented as a field-ready measurement tool to characterize the physical properties of Portland cement concrete (PCC) based on the materials dielectric constant. The capacitance probe was designed, as a surface probe, to measure the capacitance properties of materials. From these capacitance measurements, the dielectric constant of the material under test can be found. The capacitance probe, in design, resembles a parallel-plate capacitor in the sense that it consists of two conducting plates with a known separation. However, a parallel-plate capacitor does not allow for nondestructive in-situ measurements. In order to achieve the desired qualifications of a portable field test unit: a probe needed to be designed and tested, and an easily transportable measurement instrument needed to be acquired.

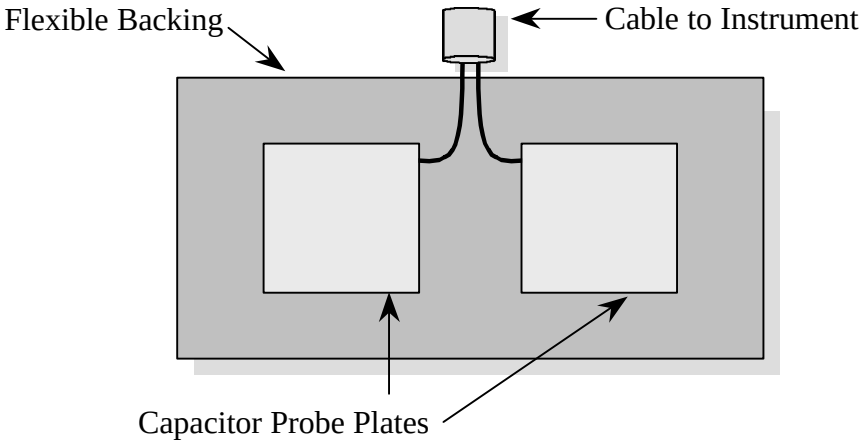

Figure 4.1. The capacitor probe.

The capacitor probe, shown in Figure 4.1, was developed so that in-situ measurements of the dielectric properties of PCC can be readily performed. In this regard, the capacitor probe was designed to be small, lightweight, and durable. Conceptually, the capacitor probe resembles a simple two-plate capacitor structure where both plates are placed against the surface of the structure under test.

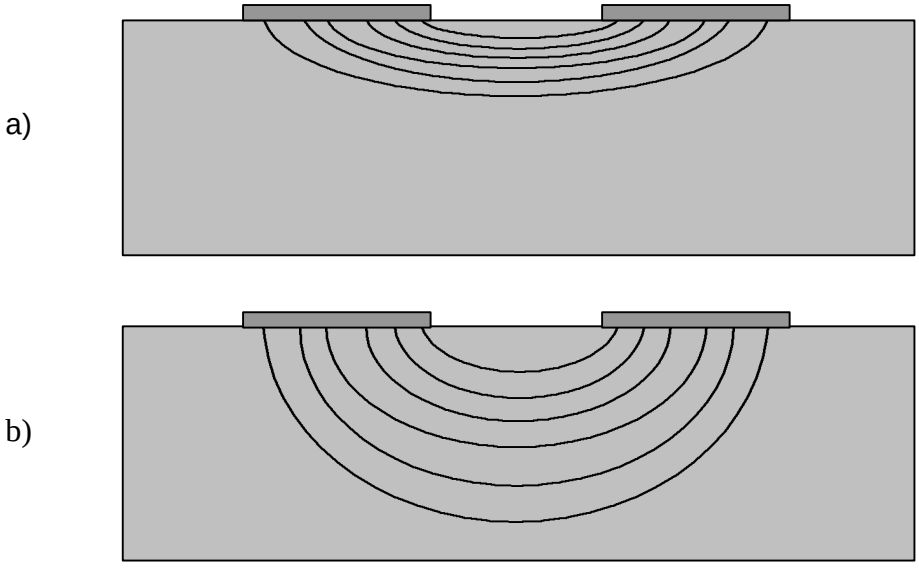

Figure 4.2. Schematic of EM field distribution at (a) high frequency and (b) low frequency.

The plates are manufactured of “flexible” metal sheet (e.g., copper or brass) which allows complete contact when placed on the PCC structural element. Rubber backing is used for mechanical strength, handling, and protection purposes. The probe is flexible so that it may conform to different geometric shapes such as the curved surface of a pile. Different sizes were considered for this purpose, however, typically the overall length is on the order of 50 to 100mm to ensure adequate bulk averaging of the constituents of the structures concrete.

As shown in Figure 4.2, EM fields will emanate from the capacitor plates and excite the test medium. The distribution of EM fields will govern the impedance of the probe. Impedance measurements of this probe will result in information related to the average dielectric performance of the bulk media in the EM field. Internal flaws including chloride presence will alter the field distribution and dielectric properties, thus bringing a change in the impedance of the probe. In addition, by changing the frequency of the EM excitation and/or adjusting the distance between the plates, it is possible to reveal different information at different depths in the PCC structure.

The capacitor probe NDE system includes a portable frequency domain measurement instrument and a portable personal computer for on-site data acquisition and processing. The system is calibrated using known standards to ensure accurate determination of the electrical properties of the structure under test.

The capacitor probe is designed to maximize the interaction of the EM fields and the PCC material. In addition, the frequency used should be in the range where specific polarization (such as the ionic polarization in the case of chloride penetration or alkali-silica reaction) is dominant over other effects. Based on the size, shape, and the location of the probe, in addition to the excitation frequency of the EM waves, the degree of interaction and the depth of penetration of EM waves in the PCC structural element can be controlled.

The capacitor probe will be implemented as a field-ready measurement tool to characterize the physical properties of Portland cement concrete (PCC) based on the materials dielectric constant. The Capacitance probe was designed, as a surface probe, to measure the capacitance properties of materials. From these capacitance measurements,

the dielectric constant of the material under test can be found. The capacitance probe, in design, resembles a parallel-plate capacitor in the sense that it consists of two conducting plates with a known separation. However, a parallel-plate capacitor does not allow for nondestructive in-situ measurements. In order to achieve the desired qualifications of a portable field test unit: a probe needed to be designed and tested, and an easily transportable measurement instrument needed to be acquired.

4.1 Physical Construction of the Capacitance Probe

Several probes have been built during this project with each new design more adaptive to a field environment. The four types of capacitance probes, which have been designed and tested, will be discussed in this section.

4.1.1 Capacitance Probe Design

Plexiglas Probe

An initial capacitance probe was built using a 60.96cm x 60.96cm x 0.635cm sheet of Plexiglas as a base with two 7.62cm square brass plates (0.3175cm thick with a 5.08cm separation) acting as the electrical conducting plates. These plates were mounted to the Plexiglas by using brass posts that were inserted into holes in the Plexiglas and fastened with wing nuts. This capacitance probe utilized M-type connectors to be used with the existing Hewlett-Packard Spectrum/Network Analyzer (Model 4195A). The outer conductor of the coaxial-type connecting cable connects to one of the plates while the inner conductor connects to the remaining plate. A 60.96cm x 60.96cm x 30.48cm wooden box was constructed (using no metallic connectors) and filled with Ottawa sand. This sandbox was designed to be used to determine if the preliminary capacitance probe design could detect changes in the dielectric properties of sand due to insertion and relative placement of inhomogeneities. While measurement of the actual dielectric constant of the sand and any inserted inhomogeneities was unsuccessful due to the fact

the calibration system was not completed, it was determined that changes in the dielectric properties of the sand could be detected due to changes in the measurements.

Rubber-Backed Capacitance Probe

A second capacitance probe was built using a 30.48cm x 20.32cm x .3175cm natural rubber sheet as a backing material and two 7.62cm square brass sheets (0.00381cm thick with a 5.08cm separation) as electrodes. Initially, computer jumper stands and pins were to be used as connectors to attach the Capacitance probe to a cable. However, after unsuccessful attempts to locate a commercial source, DC power adapter plugs and jacks were used as interface connectors. It was decided that the DC adapter would not be used due to questions about its suitability, therefore a change in the connector was considered. The question of the connectors suitability came from the fact that this connector was not designed to be used with a coaxial fixture. The brass electrodes were affixed to the backing material by means of 0.15875cm thick double-sided tape. This design was very well suited for field use due to the rubber backing's high durability and flexibility. The effects of the rubber backing and the double-sided tape on this design, as well as the Plexiglas in the initial design, will be seen later to have a minimal effect in the measurements. The reason for this is the addition of an error parameter inserted into the calibration model to compensate for the space above the probe.

Tape-Backed Capacitance probe

A third Capacitance probe, resembling the rubber-backed Capacitance probe in appearance, was built using masking tape as a backing material using similar contact pads (without the double-sided tape) in the same geometric configuration. By using the masking tape, intentions were to reduce the effects (if any) of the backing material on the measurements and to have a means of fastening the probe to the material under test. A RCA connector was used to connect the Capacitance probe to a cable as opposed to the DC adapter plug due to the RCA connector's specific design for work with a coaxial-type fixture. The outer conductor of the RCA plug makes solid contact around the entire connector (which was connected to the S/NA).

Final Capacitance Probe Design

A final capacitance probe design consists of the rubber backing, resembling that used in the second capacitance probe, the only difference being the thickness, which is reduced to 0.0625cm. Along with the natural rubber backing, conducting adhesive copper tape purchased from 3M will be used as the conducting plates. The copper tape is also 7.62cm wide and can be cut to any desired length to conform to the previous designs. The usage of the tape allows easy change of the electrical conducting plates in the field. The RCA connectors will continue to be used in all of the final designs.

4.2 Capacitance Probe Plate Configurations

Different models of the final design were constructed with respect to the size and spacing of the conducting plates. These models were constructed to research whether a different plate configuration would result in more precise data or allow the user to determine some type of depth measurement. Eventually, the spacing between the plates will be used to control the depth of the measurement into the sample. The dimensions of the different constructions of capacitance probes are described in Table 4.1. Illustrations of different constructions of capacitance probes are located in Appendix A: Figures A1 to A6. Most of the capacitance probe configurations produced similar results for a uniform sample of Portland cement concrete (slab: 45.72 x 30.48 x 10.16cm) with a water to cement ratio of .45 and a 6% air content. It will be shown shown in Chapter 5, however, that a similar sample of Portland cement concrete with an air void 7.5mm thick at a depth of 50mm produced different results between each of the different capacitance probe designs. The distance between the capacitance probe will correlate to a change in the depth of the measurement. This will be acknowledged by noticing the reduction in the dielectric constant as the separation increases. As the penetration increases, the air void containing a dielectric constant of one, $\varepsilon_o = 1$, has a greater effect on the measurements, thus reducing the effective dielectric constant of the measurement.

Table 4.1. Plate size and spacing of the different capacitance probes.

Capacitance Probe	Plate Size	Plate Spacing
A	7.62cm x 7.62cm (3.00in. x 3.00in.)	5.08cm (2.00in.)
B	7.62cm x 7.62cm (3.00in. x 3.00in.)	5.08cm (3.00in.)
C	7.62cm x 7.62cm (3.00in. x 3.00in.)	5.08cm (4.00in.)
D	5.08cm x 5.08cm (2.00in. x 2.00in.)	5.08cm (2.00in.)
E	12.70cm x 5.08cm (5.00in. x 3.00in.)	5.08cm (2.00in.)
F	7.62cm x 7.62cm (3.00in. x 3.00in.)	5.08cm (6.00in.)

4.3 Capacitor Probe Calibration Standards

After defining of the calibration equations in the previous section, the capacitor probe system will use four calibration measurements for error compensation. These measurements are an open standard, a load standard, a short standard, and a material of known dielectric constant. We need to use known standards when performing these measurements and this section will described the construction of the calibration standards used for the capacitance probe measurement system.

4.3.1 Open Calibration Standard

The open calibration standard is simply an air dielectric between the plates of the capacitance probe system. We can acknowledge that using air as an open calibration

standard introduces a small amount of error due to the capacitance that will be present between the plates. This error is taken into consideration with the fourth calibration measurement performed as explained in the previous section, which describes the calibration process. It would be very difficult to make a high quality open calibration standard for this system due to the system's physical attributes, so an air dielectric is used for this calibration measurement.

4.3.2 Load Calibration Standard

The load standard is a 50Ω equivalent resistance. Shown in Figure 4.3 are the designed calibration standard and the standard's maximum dimensions. The standard is constructed of two solid brass plates with six (6) low tolerance three hundred ohm (300Ω) resistors in series mounted on two long pieces of thin plexiglas. The plates were attached to the plexiglas using standard epoxy. As mentioned previously, this design and constructed standard was measured in the laboratory over the frequency range of interest and the resistance was found to be 50.5Ω and the capacitance was found to be 71.0pF.

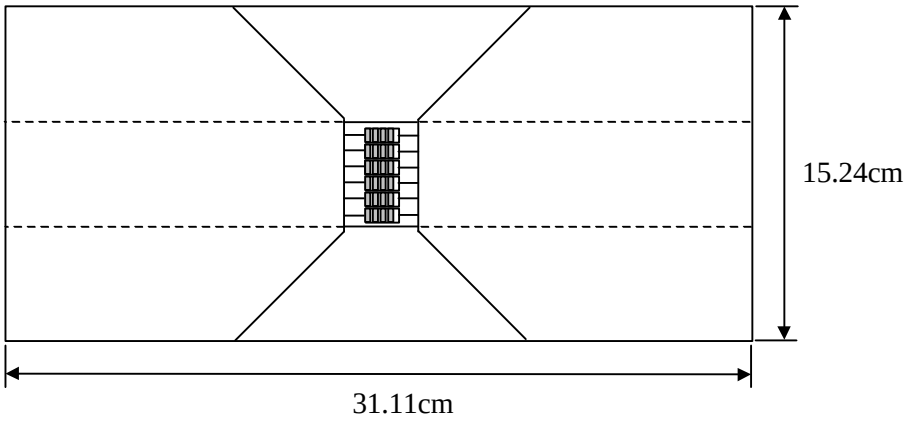

Figure 4.3. Capacitor probe load calibration standard.

4.3.3 Short Calibration Standard

The short calibration standard is shown in Figure 4.4. This calibration standard is a solid sheet of brass. Making a perfect short calibration standard is easier than making an open calibration standard due to the fact that you do not have the effects of a parasitic capacitance and/or other noise contributions. Since the quality of this type of short is very high, we have assumed this short calibration standard to be a perfect short as in the previous section.

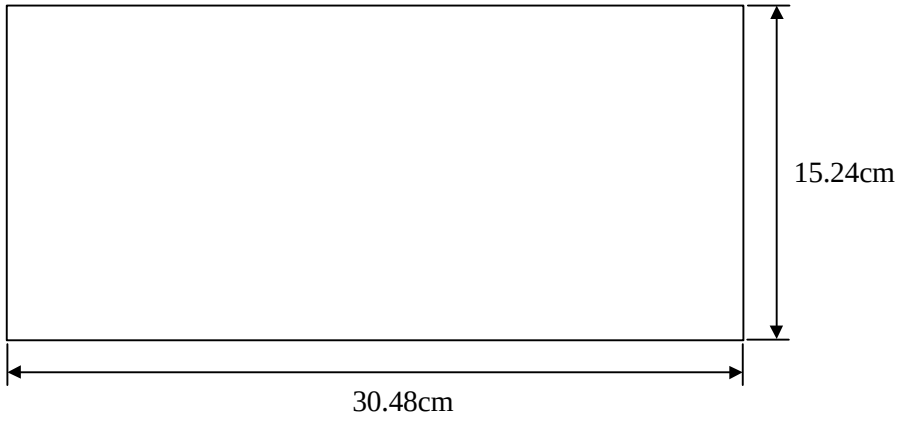

Figure 4.4. Capacitor probe short calibration standard.

4.3.4 Known Dielectric Material Calibration Standard

The materials used for this calibration are either a sample of Portland cement concrete (slab: 45.72 x 30.48 x 10.16cm) or of ultra high molecular weight (uhmw) polyethylene (slab: 45.72 x 30.48 x 10.16cm). The dielectric constant obtained from the parallel plate capacitor measurement system is used as the reference value for the dielectric constant of the known material in the calibration equations of the capacitance probe measurement system, $\varepsilon^*_{r\,m1}$.

4.4 Equations Governing the Capacitance Probe System

The impedance across the capacitor probe is measured using a network analyzer. The analyzer is connected to the capacitor probe through an interface network which is

formed mainly of a cable and an adapter. The analyzer is used to measure the reflection coefficient, Γ, at its reference plane. This reflection coefficient is a function of the S-parameters of the interface network (S_{int}) as well as the impedance of the capacitor probe when applied to the PCC material. The measured Γ is used to evaluate the complex impedance (real and imaginary parts) of the PCC material as a function of frequency

To ensure proper evaluation of the dielectric properties of the PCC structural element under test, four calibrations are used. Three calibration measurements are taken with the capacitor probe open-circuited, short-circuited, and terminated in a nominal 50Ω load at the terminals of the capacitor. The fourth calibration measurement is taken while the probe is applied to a material of known dielectric properties (ε^*_{m1}) at the frequencies

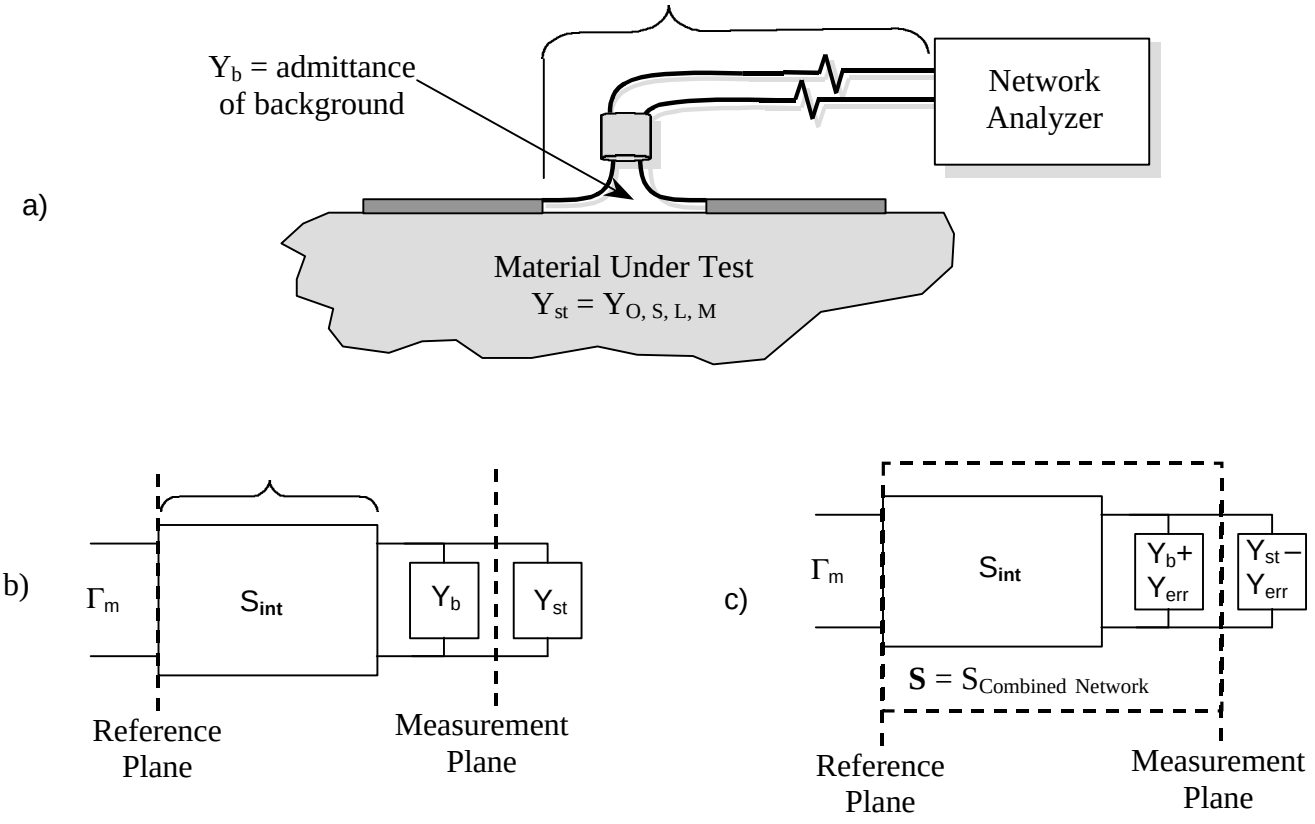

Figure 4.5. (a) General capacitor probe model, (b) general S-parameter model of the interface network, and (c) general S-parameter model of the combined network.

desired. The admittance of the four calibration standards are Y_a, $Y_s = \infty$, Y_L, and Y_M for the open (air), short, load, and material terminations, respectively.

The general calibration model, shown in Figure 4.5, can be simplified by including the admittance of the back side of the capacitor probe, Y_b, into the S-parameter model of the combined network (lumping the unknowns). The error $Y_L - Y_O$, representing the deviation of Y_L from its nominal value (1/50Ω), is also combined in the S-parameters of the combined network.

These four calibration measurements are used to solve a four-unknown calibration model. The unknowns generated by the model are the admittance of air (Y_a) and S_{11}, the product $S_{21}S_{12}$, and S_{22}, where S_{11}, S_{21}, S_{12}, and S_{22} represent the scattering parameters of the combined network.

4.4.1 Load Calibration

Shown in Figure 4.6, the load calibration model also includes the admittance of the load calibration standard, Y_L, and the admittance compensation for the load standard, Y_{err} (which can also be written as Y_L-Y_O, where Y_O is the admittance of the 50Ω line). The resistance and capacitance values of the load standard were found to be R_L=50.5Ω and C_L=71.0pF, respectively. This initial step in the load calibration description corrects the measured value of the 50Ω load calibration standard by compensating for the admittance of the 50Ω line (Y_O).

Next, the admittance value Y_b and the quantity Y_L-Y_O are introduced into the S-parameter model, leaving Y_O as the only value outside the S-parameter model. By placing the admittance compensation for the load, Y_{err}, inside the S-parameter model, the reflection coefficient at the measurement plane generated from the load standard (Γ_{ml}) is simplified. By including these two values within the model, the complexity of the entire equation set can be reduced. The reflection coefficient at the reference plane of the load measurement is as follows:

$$\Gamma_L = \frac{Y_o - Y_o}{Y_o + Y_o} = 0 \qquad (4.1)$$

The reflection coefficient, Γ_L, reduces to zero by leaving only the Y_O term outside the S-parameter load model. After obtaining the value for Γ_L, Γ_m can be found as shown in Figure 4.5. Using the S-parameter model, the reflection coefficient of the capacitor probe system with a 50Ω load calibration standard, Γ_{ml}, is equal to S_{11} as follows:

$$\Gamma_{ml} = S_{11} \tag{4.2}$$

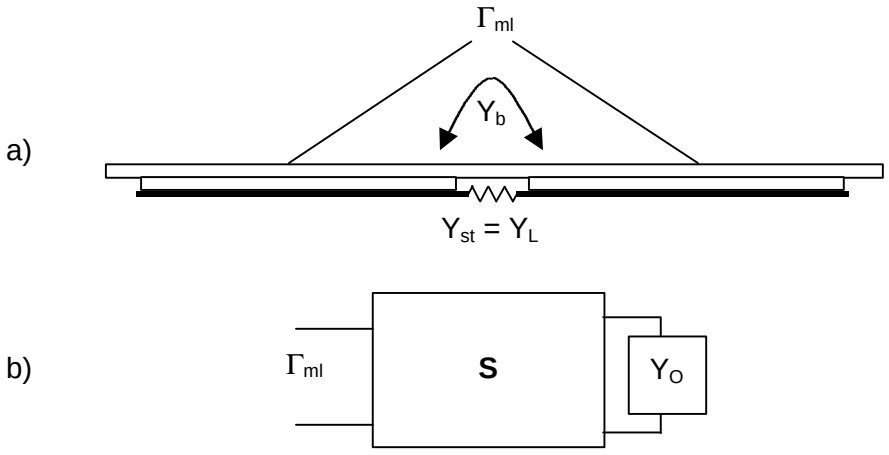

Figure 4.6. (a) Load capacitor probe model and (b) load S-parameter model.

4.4.2 Open Calibration

The admittance value of air above the capacitor probe, Y_b, is common to all the calibration measurements. Therefore, it can be introduced into the open S-parameter model, shown in Figure 4.7, as in the load calibration measurement. The admittance compensation for the load, Y_{err}, must also be included in the open S-parameter model. To accomplish this, the admittance of the air calibration standard, Y_a, is corrected to account for the admittance compensation. The positive value of the admittance compensation, Y_{err}, is then placed into the S-parameter model, leaving the corrected admittance of the open calibration standard (Y_{op}) and the negative value of the load

admittance compensation outside the S-parameter model. Thus, the actual value for the unknown Y_a is as follows:

$$Y_{op} = Y_a - Y_{err} \tag{4.3}$$

The admittance of the open calibration standard, Y_a, can be described in terms of a capacitance-containing variable F. Replacing Y_a as one of four unknowns that will be determined through the four calibration measurements, the value of F is as follows:

$$Y_a = j\varpi\varepsilon_o F \tag{4.4}$$

where

$j = \sqrt{-1}$;

$\omega = 2\pi f$, where f = frequency (Hz);

ε_O = permittivity of free space, 8.85×10^{-12} [F/m]; and

$F \approx C/\varepsilon_O$, resulting from the general admittance equation, $Y=j\omega C$.

The reflection coefficient of the open calibration measurement, Γ_{op}, is as follows:

$$\Gamma_{op} = \frac{Y_o - Y_{op}}{Y_o + Y_{op}} \tag{4.5}$$

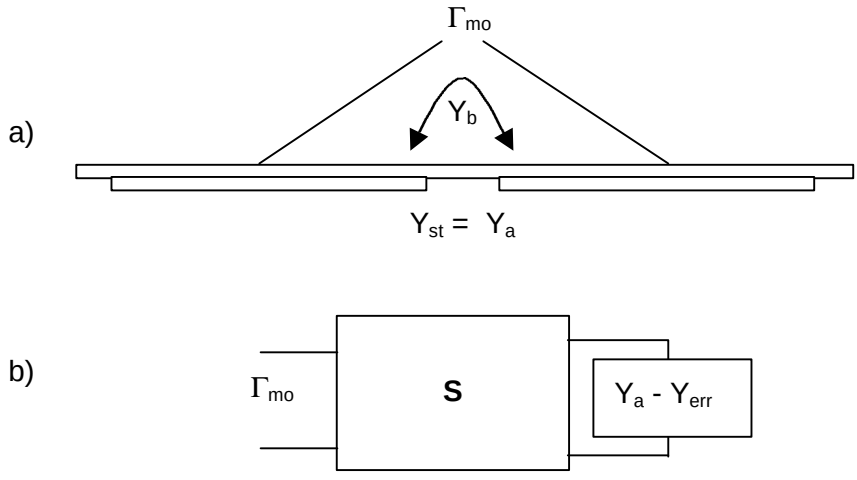

Figure 4.7. (a) Open capacitor probe model and (b) open S-parameter model.

After obtaining the value for Γ_{op}, Γ_m can be found as shown in Figure 4.5. Using the S-parameter model, the reflection coefficient of the capacitor probe system using an open calibration standard, Γ_{mo}, may be obtained as the following:

$$\Gamma_{mo} = S_{11} + \frac{S_{12}S_{21}\Gamma_{op}}{1 - S_{22}\Gamma_{op}} \tag{4.6}$$

4.4.3 Calibration Using Material of Known Dielectric Constant

Upon completion of the open calibration standard, the calibration measurement involving a material of known dielectric constant can begin. As mentioned previously, the admittance value of air above the capacitor probe (Y_b) is common to all the calibration measurements. This background admittance is introduced into the S-parameter model, shown in Figure 4.8, as with the load and open calibration measurements. Also, the admittance compensation for the load, Y_{err}, must be included in the material S-parameter model. As with the load and open calibration measurements, the admittance of the material calibration measurement, Y_{m1}, must be corrected using the

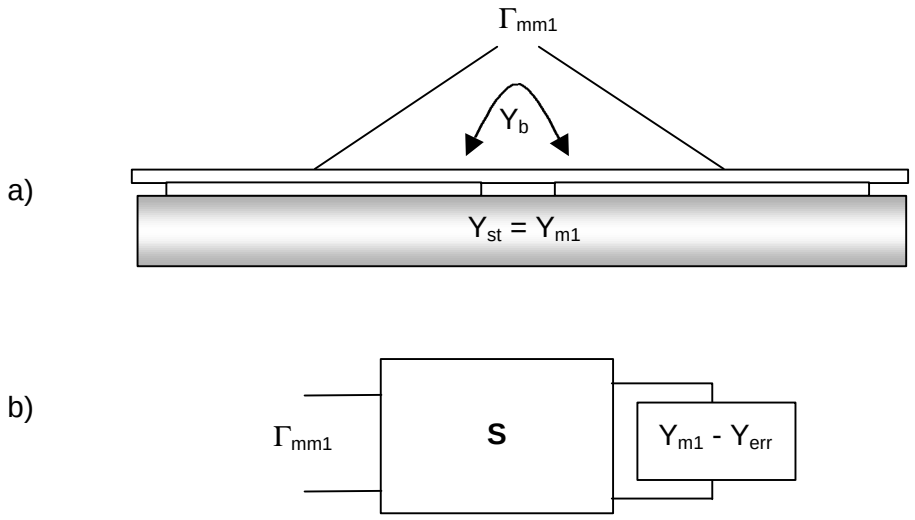

Figure 4.8. (a) Material capacitor probe model and (b) material S-parameter model.

admittance compensation, Y_{err}. By placing the positive value of the admittance compensation into the S-parameter equation, the corrected admittance of the material calibration measurement, Y_{m1e}, is as follows:

$$Y_{m1e} = Y_{m1} - Y_{err} \tag{4.7}$$

The admittance of the material calibration standard, Y_{m1}, can also be described in terms of the unknown variable, F. Equation 4.8 yields Y_{m1}, where ε_{m1}* is the known dielectric constant of the calibration material:

$$Y_{m1} = j\varpi\varepsilon^{*}_{m1} F \tag{4.8}$$

where $F \approx C/\varepsilon^{*}_{m1}$, resulting from the general admittance equation, $Y=j\omega C$.

The reflection coefficient of the material measurement, Γ_{m1}, can be given as follows:

$$\Gamma_{m1} = \frac{Y_o - Y_{m1e}}{Y_o + Y_{m1e}} \tag{4.9}$$

After obtaining the value for Γ_{m1}, Γ_m can be found as shown in Figure 4.5. Using the S-parameter model, the reflection coefficient of the capacitor probe system using the known material calibration standard, Γ_{mm1}, can be determined as:

$$\Gamma_{mm1} = S_{11} + \frac{S_{12}S_{21}\Gamma_{m1}}{1 - S_{22}\Gamma_{m1}} \tag{4.10}$$

4.4.4 Short Calibration

The short calibration measurement is assumed to be a perfect short. By making this assumption, the short S-parameter model, shown in Figure 4.9, decreases in complexity since no correction parameters (i.e., Y_b and Y_{err}) are needed to complete the model. As for any short, the admittance is equal to infinity. Thus, the admittance for the measured short, Y_s, is as follows:

$$Y_s = \infty \tag{4.11}$$

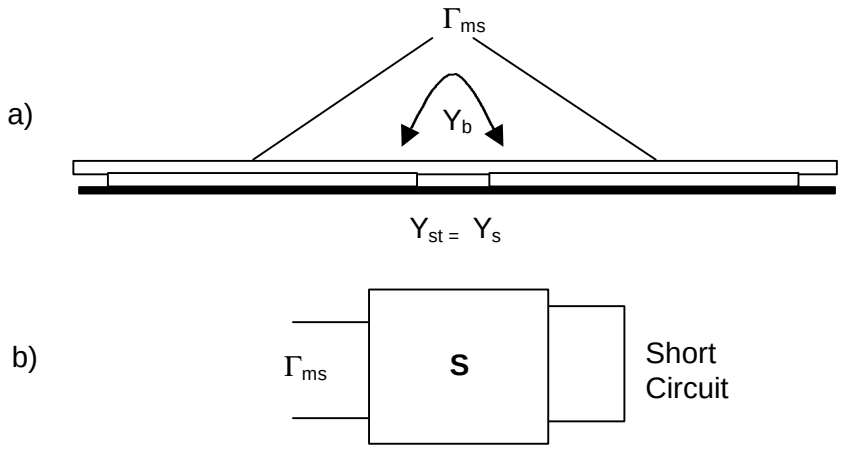

Figure 4.9. (a) Short capacitor probe model and (b) short S-parameter model.

The reflection coefficient of the short measurement, Γ_s, is given as:

$$\Gamma_s = \frac{Y_o - \infty}{Y_o + \infty} = -1 \tag{4.12}$$

After obtaining the value for Γ_s, Γ_m can be found as shown in Figure 4.5. Using the S-parameter model, the reflection coefficient of the capacitor probe system using a short calibration standard, Γ_{ms}, is given as:

$$\Gamma_{ms} = S_{11} - \frac{S_{12}S_{21}}{1+S_{22}} \tag{4.13}$$

Solving for the scattering parameters, the product of $S_{21}S_{12}$ can be written as S_p:

$$S_p = S_{21}S_{12} \tag{4.14}$$

The equations developed above are summarized in Table 4.2. These equations represent the reflection coefficients at the input side of the system, denoted as Γ_{ml}, Γ_{mo}, $\Gamma_{mm1,}$ and Γ_{ms}, in Figures 4.6 through 4.9, respectively.

Table 4.2. Reflection coefficients from the measured calibration standards.

Calibration	Reflection Coefficient (Γ_m)
Load	$\Gamma_{ml} = S_{11}$
Open	$\Gamma_{mo} = S_{11} + \frac{S_{12}S_{21}\Gamma_{op}}{1 - S_{22}\Gamma_{op}}$
Material	$\Gamma_{mm1} = S_{11} + \frac{S_{12}S_{21}\Gamma_{m1}}{1 - S_{22}\Gamma_{m1}}$
Short	$\Gamma_{ms} = S_{11} - \frac{S_{12}S_{21}}{1 + S_{22}}$

4.4.5 Determination of Remaining Unknowns

The analysis begins by developing three new equations from those shown in Table 4.2. One of the unknowns, S_{11}, has already been determined since it was found to be equal to the reflection coefficient of the capacitor probe system with a 50Ω load calibration standard, Γ_{ml}. This is a main reason for placing the load compensation admittance into the S-parameter model. Subtracting the load reflection coefficient from the short reflection coefficient yields:

$$\Gamma_{ms} - \Gamma_{ml} = \frac{-S_p}{1 + S_{22}} \tag{4.15}$$

Subtracting the load reflection coefficient from the open reflection coefficient yields:

$$\Gamma_{mo} - \Gamma_{ml} = \frac{S_p \Gamma_{op}(F)}{1 - S_{22}\Gamma_{op}(F)} \tag{4.16}$$

where Γ_{op} is a function of F.

Subtracting the load reflection coefficient from the material reflection coefficient yields:

$$\Gamma_{mm1} - \Gamma_{ml} = \frac{S_p \Gamma_{m1}(F)}{1 - S_{22}\Gamma_{m1}(F)} \tag{4.17}$$

where Γ_{m1} is also a function of F.

Equations 4.15, 4.16, and 4.17 can be reduced to obtain two equations with two unknowns. Equation 4.18 was obtained by dividing the expression found in equation 4.17 by the expression found in equation 4.15. Equation 4.19 was determined by dividing the expression found in equation 4.16 by the expression found in equation 4.15. The two unknowns remaining in these equations are the values of F and S_{22}. The values Γ_{m1} and Γ_{op} are functions of the variable F.

$$\frac{\Gamma_{mm1} - \Gamma_{ml}}{\Gamma_{ms} - \Gamma_{ml}} = -\frac{\Gamma_{m1}(1 + S_{22})}{1 - S_{22}\Gamma_{m1}} = A \tag{4.18}$$

$$\frac{\Gamma_{mo} - \Gamma_{ml}}{\Gamma_{ms} - \Gamma_{ml}} = -\frac{\Gamma_{op}(1 + S_{22})}{1 - S_{22}\Gamma_{op}} = B \tag{4.19}$$

Equations 4.18 and 4.19, referred to as A and B, need to be solved simultaneously to yield the two unknowns. The values of A and B are known quantities since all of the variables on the left of the first equality sign are measured values.

Equations 4.18 and 4.19 can be written in terms of the reflection coefficients, Γ_{m1} and Γ_{op}, respectively. The resulting equations are as follows:

$$\Gamma_{op} = \frac{1}{S_{22}(1 - A) - A} \tag{4.20}$$

$$\Gamma_{m1} = \frac{1}{S_{22}(1 - B) - B} \tag{4.21}$$

Equations 4.5 and 4.9 need to be written in terms of Y_{op} and Y_{m1e} as follows:

$$Y_{op} = Y_o \frac{1 - \Gamma_{op}}{1 + \Gamma_{op}} \tag{4.22}$$

$$Y_{m1e} = Y_o \frac{1 - \Gamma_{m1}}{1 + \Gamma_{m1}} \tag{4.23}$$

Substituting equations 4.20 and 4.21 into equations 4.22 and 4.23, respectively, we obtain the following two equations:

$$Y_{op} = Y_o \frac{S_{22}(1-A)-A-1}{S_{22}(1-A)-A+1} \tag{4.24}$$

$$Y_{m1e} = Y_o \frac{S_{22}(1-B)-B-1}{S_{22}(1-B)-B+1} \tag{4.25}$$

Using the relation found in equation 4.4, we can write an equation for Y_a using the expression for Y_{op} found in equation 4.24. Equation 4.5 relates Y_a to the unknown variable F.

$$Y_a = Y_o \frac{S_{22}(1-A)-A-1}{S_{22}(1-A)-A+1} + Y_{err} = j\omega\varepsilon_o F \tag{4.26}$$

Similarly, Using the relation found in equation 4.7, we can write an equation for Y_{m1} using the expression for Y_{m1e} found in equation 4.28. Equation 4.8 relates Y_{m1e} to the unknown variable F.

$$Y_{m1} = Y_o \frac{S_{22}(1-B)-B-1}{S_{22}(1-B)-B+1} + Y_{err} = j\omega\varepsilon_o \varepsilon^*_{rm1} F \tag{4.27}$$

The result shown in equation 4.27 uses the relation for the dielectric constant in terms of the relative complex dielectric constant of the material, ε^*_{rm1}, multiplied by the dielectric constant of air, ε_o and shown in equation 4.28.

$$\varepsilon^*_{m1} = \varepsilon_o \varepsilon^*_{rm1} \tag{4.28}$$

We can obtain an expression for the relative dielectric constant, $\varepsilon^*_{rm1,}$ by dividing the expression found in equation 4.27 by the expression found in equation 4.26. The resulting equation is shown as follows:

$$\varepsilon^*_{rm1} = \frac{Y_o \frac{S_{22}(1-B)-(1+B)}{S_{22}(1-B)+(1-B)} + Y_{err}}{Y_o \frac{S_{22}(1-A)-(1+A)}{S_{22}(1-A)+(1-A)} + Y_{err}} \tag{4.29}$$

Using the relations shown in equations 4.30a and 4.30b, equation 4.29 can be reduced to the expression found in 4.31.

$$C = \frac{1+A}{1-A} \tag{4.30a}$$

$$D = \frac{1+B}{1-B} \tag{4.30b}$$

$$\varepsilon^{*}_{rm1} = \frac{Y_o(S_{22}-D)+Y_{err}(S_{22}+1)}{Y_o(S_{22}-C)+Y_{err}(S_{22}+1)} \tag{4.31}$$

Separating the unknown variable S_{22} from the expressions found in the numerator and denominator of equation 4.31 results in an equation for ε^{*}_{rm1} as follows:

$$\varepsilon^{*}_{rm1} = \frac{S_{22}(Y_o+Y_{err})-DY_o+Y_{err}}{S_{22}(Y_o+Y_{err})-CY_o+Y_{err}} \tag{4.32}$$

The numerator and denominator of equation 4.32 can be divided by Y_o+Y_{err} to isolate S_{22} and the following expressions defined:

$$D' = \frac{-DY_o+Y_{err}}{Y_o+Y_{err}} \tag{4.33a}$$

$$C' = \frac{-CY_o+Y_{err}}{Y_o+Y_{err}} \tag{4.33b}$$

Using the identities found in equations 4.33a and 4.33b, equation 4.32 can be reduced to the expression found in equation 4.34.

$$\varepsilon^{*}_{rm1} = \frac{S_{22}+D'}{S_{22}+C'} \tag{4.34}$$

Solving equation 4.34 in terms of S_{22} will produce the following expression:

$$S_{22} = \frac{D'-\varepsilon^{*}_{rm1}C'}{\varepsilon^{*}_{rm1}-1} \tag{4.35}$$

Using the expression found in equation 4.15, S_p can be written as follows:

$$S_p = (\Gamma_{ml}-\Gamma_{ms})(1+S_{22})$$

The final unknown variable, F, can be obtained using the expression found in equation 4.4. The value of Y_a is obtained from substituting the expression for S_{22} found in equation 4.35 into equation 4.26.

$$F = \frac{Y_a}{j\omega\varepsilon_o} \tag{4.36}$$

The equations that are developed for determining the dielectric constant of a material under test (MUT) are similar to the equations for the material of known dielectric constant for calibration purposes. As mentioned previously for the material calibration measurements, the admittance value of air above the capacitor probe (Y_b) is common to all of the measurements and is introduced into the S-parameter model, shown in Figure 4.10. The admittance compensation for the load, Y_{err}, must again be included in the material S-parameter model. As before, the admittance of the MUT, Y_{m2}, must be corrected using the admittance compensation, Y_{err}. By placing the positive value of the admittance compensation into the S-parameter model, the corrected admittance value of the MUT, Y_{m2e}, is given as:

$$Y_{m2e} = Y_{m2} - Y_{err} \tag{4.37}$$

The admittance of the MUT, Y_{m2}, in terms of the known variable F, is given as follows:

$$Y_{m2} = j\varpi\varepsilon^*_{m2}F \tag{4.38}$$

where ε_{m2}* is the dielectric constant of the MUT.

The reflection coefficient of the MUT measurement (Γ_{m2}), developed from the equations given above for Y_{m2e} and Y_{m2}, is given as follows:

$$\Gamma_{m2} = \frac{Y_o - Y_{m2e}}{Y_o + Y_{m2e}} \tag{4.39}$$

After obtaining the value for Γ_{m2}, Γ_m can be determined as shown in Figure 4.5. Using the S-parameter model, the reflection coefficient of the MUT (Γ_{mm}) is given as:

$$\Gamma_{mm} = S_{11} + \frac{S_p\Gamma_{m2}}{1 - S_{22}\Gamma_{m2}} \tag{4.40}$$

The expression for Γ_{mm} from equation 4.40 can be rewritten in terms of Γ_{m2} as:

$$\Gamma_{m2} = \frac{\Gamma_{mm} - S_{11}}{S_p - S_{11}S_{22} + S_{22}\Gamma_{mm}} \tag{4.41}$$

From equation 4.41, a numerical value for the reflection coefficient of the MUT can be obtained using known parameters determined by calibration. In order to solve for the complex dielectric constant of the MUT, ε^*_{2m}, equation 4.39 needs to be written in terms of Y_{m2e}:

$$Y_{m2e} = Y_o \frac{1 - \Gamma_{m2}}{1 + \Gamma_{m2}} \tag{4.42}$$

Through the use of equations 4.37 and 4.38, the relative complex dielectric constant can be expressed as:

$$\varepsilon^*_{rm2} = \frac{Y_{m2e} + Y_{err}}{j\omega\varepsilon_o F} \tag{4.43}$$

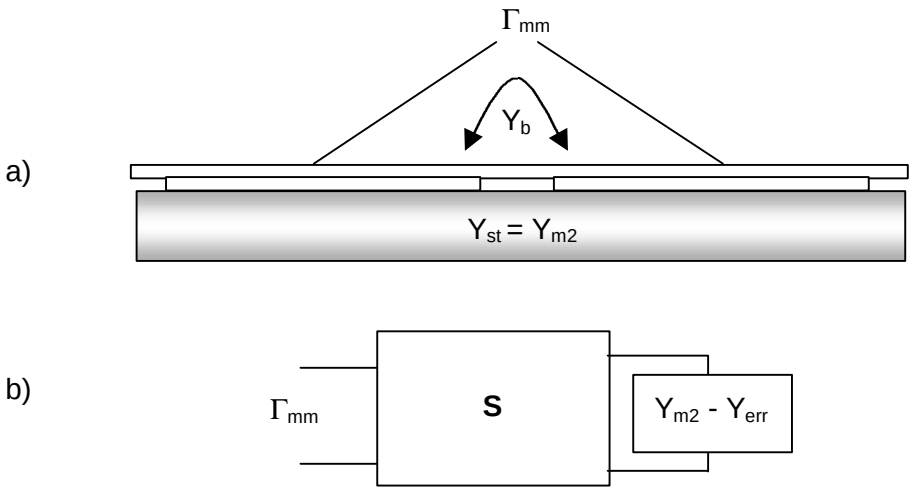

Figure 4.10. (a) MUT capacitor probe model and (b) MUT S-parameter.

4.5 Conclusions

The capacitance probe measurement system was introduced by placing both plates of the parallel plate measurement system in a single plane. This would allow a user to perform non-destructive measurements of structures. The history pertaining to the designs of the capacitance probes was mentioned and the final design was described.

The developed standards used to calibrate the capacitance probe measurement system were also introduced. A system calibration using four calibration measurements was employed on the capacitance probe measurement system to solve for the same scattering parameters as found in the parallel plate system with the addition a fourth measurement to account for the capacitance of air between the conducting plates. The fourth calibration measurement was performed on a material sample of known dielectric constant.

Finally, the equations resulting from the four calibration measurements were solved to obtain the system unknowns. From these unknowns, the dielectric constant of a test specimen was calculated.

Chapter 5
Verification and Application of the Capacitance Probe

The capacitance probe measurement system was designed and calibrated to produce similar results to those generated by the parallel plate measurement system. The scheme used to calibrate the capacitance probe (Chapter 4.4) is extremely complex, yet is not able account for all of the unknown variables. The finite thickness of the specimen measured in the laboratory is known to be a source of error since the radiation pattern of the capacitance probe penetrates through the material and radiates outside the back and sides of the sample. Possible variations in the area behind the capacitance probe due to inconsistent application of the probe is unaccounted for in the calibration and could also be a source of error. A piece of Styrofoam is used to try keep the user and equipment applying the probe on a sample an adequate distance from the measurement surface to minimize errors.

5.1 Correction Function

The correction function is devised to account for the undesirable systematic effects/errors as mentioned in the introduction of this chapter. The correction function is defined as a scaling function to be applied to the values of the dielectric of the material used as a calibration standard. This scaling function is applied such that the calculated dielectric constant of the material sample under test would be identical to the values obtained earlier using the parallel plate capacitor measurement system.

The correction function is developed using an iterative approach where the resulting dielectric constant of the material under test generated by the known dielectric material is compared with a material reference in the range of the material being measured. Using the known dielectric constant of the material standard, the dielectric constant of the material under test is evaluated. The ratio between the dielectric constant values obtained from the capacitance probe to the dielectric constant obtained from the parallel plate is used to scale the dielectric constant of the material used for calibration. Equations 5.1 and 5.2 express the calculation performed to accomplish this scaling:

$$\varepsilon'_{calmat\_used} = \frac{\varepsilon'_{MUT\_pp}}{\varepsilon'_{MUT\_cp}}(\varepsilon'_{calmat\_known}) \tag{5.1}$$

$$\varepsilon''_{calmat\_used} = \frac{\varepsilon''_{MUT\_pp}}{\varepsilon''_{MUT\_cp}}(\varepsilon''_{calmat\_known}) \tag{5.2}$$

where,

ε_{MUT} = the reference(pp) and the generated(cp) dielectric constant data in the range of the dielectric constant of the MUT; and

ε_{calmat} = the scaled and known values of the dielectric constant of the calibration material.

This iterative process was applied until the dielectric constant obtained from the capacitance probe system converged to the results obtained from the parallel plate. The final ratio of the scaled values of the calibration material with the known values is called the correction function:

$$\text{CorrectionFunction} = \frac{\varepsilon^*_{\text{calmat\_used}}}{\varepsilon^*_{\text{calmat\_known}}} \tag{5.3}$$

where,

ε_{used} = the dielectric constant of the calibration material after the iterative process; and,

$\varepsilon_{measured}$ = the known dielectric constant of the calibration material.

The plotted values of the correction functions in the subsequent sections are the separated real and imaginary parts of the complex function as described in equation 5.3.

It is relevant to state that the correction function was fairly consistent throughout different sample and material measurements, i.e. One correction function worked acceptably for measurements of different concrete samples as well as using different material (UHMW and extruded nylon).

5.2 Validation of the Capacitance Probe

To account for these systematic errors, the correction function developed in the previous section will be implemented. This section will consider the validation of the capacitance probe measurement system's results. Two different materials will be used in the calibration of the capacitance probe measurement system; these are UHMW – polyethylene and extruded nylon. We need to keep in mind that the systematic errors mentioned previously are dependent on the material used in calibration as well as the measured material. For this reason, there will be a different correction function for each of the materials used in the system calibration.

5.2.1 Calibration Material: UHMW

A sample of UHMW (slab: 45.72 x 30.48 x 10.16cm) will be considered as the calibration material in this section. The real and imaginary parts of the correction

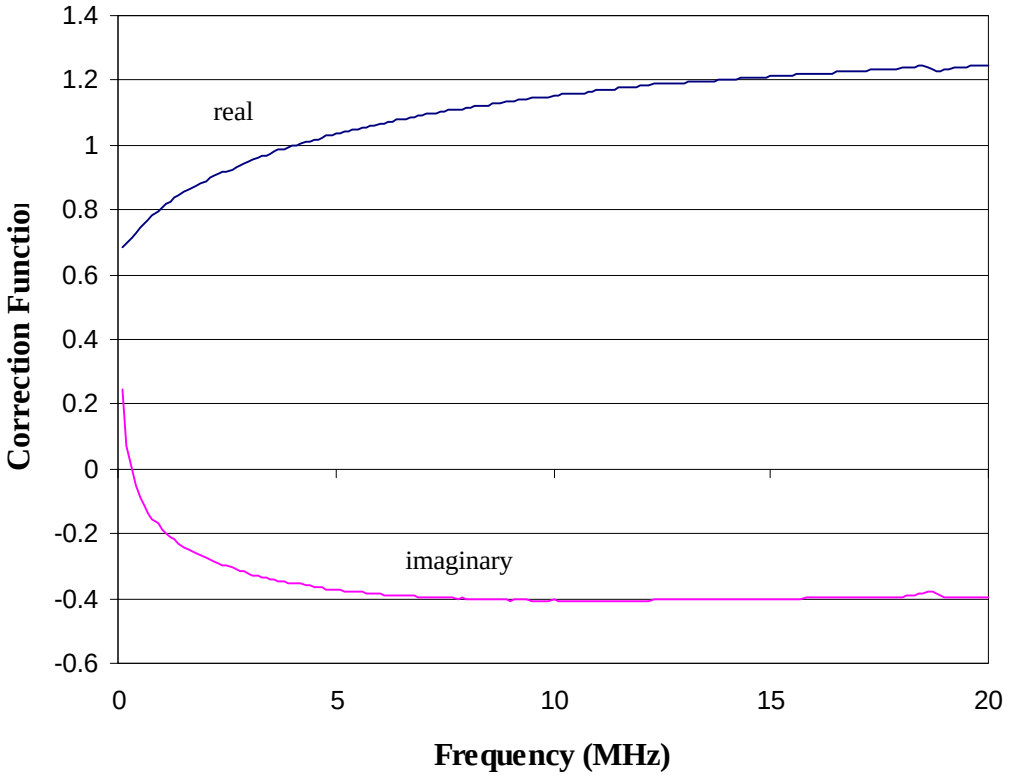

Figure 5.1: The real and imaginary parts of the correction function of the capacitance probe measurement system using UHMW for calibration.

function for UHMW, as described in section 5.1, is shown in Figure 5.1.

A partial influence on the correction function is the actual dielectric constant of the material used for calibration. After reviewing the correction function, it can be seen that the closer the dielectric constant of the material used for calibration is to the material being measured will result in a solution containing a reduced amount of noise. Figure 5.2 shows the real and imaginary parts of the dielectric constant of the UHMW. In the next section, extruded nylon will be used as the calibration material.

To get a general idea of the resulting dielectric constant values obtained from the capacitance probe measurement system using UHMW, a specimen (slab: 45.72 x 30.48 x 10.16cm) of Portland cement concrete will be analyzed. This specimen has a water to cement (w/c) ratio of 0.45. Figures 5.3 and 5.4 show the real and imaginary portions, respectively, of the dielectric constant obtained from this system, with and without the correction function, as well as the measured values from the parallel plate measurement system.

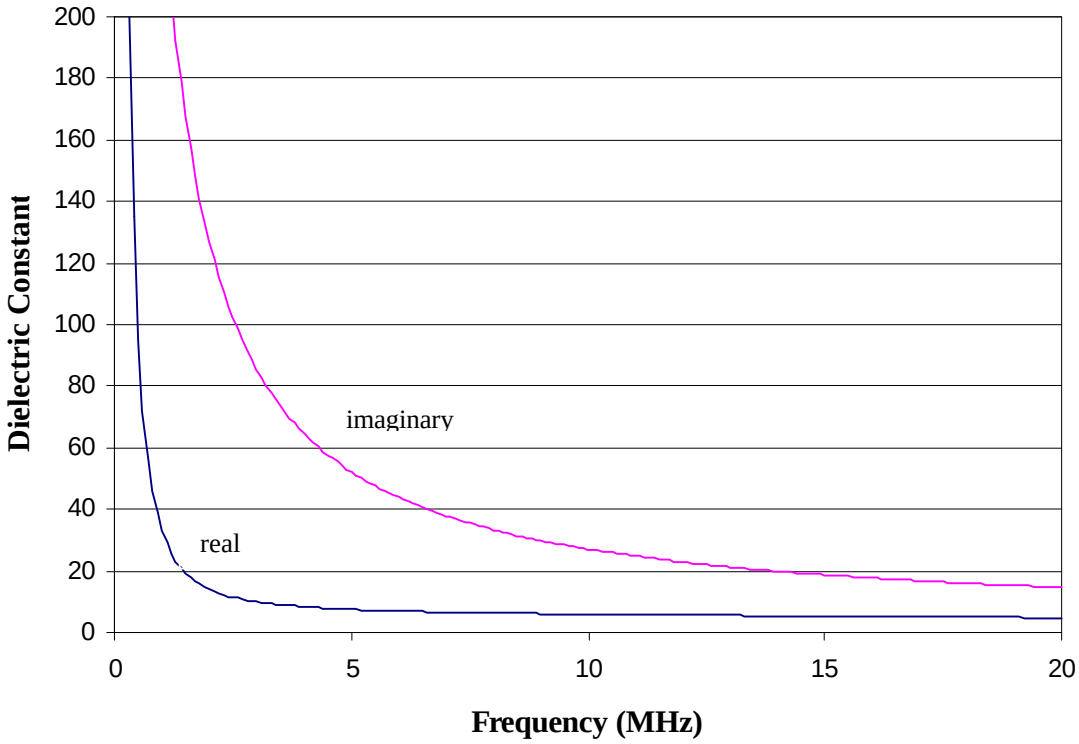

Figure 5.2: The real and imaginary dielectric constant of the UHMW sample used for calibration.

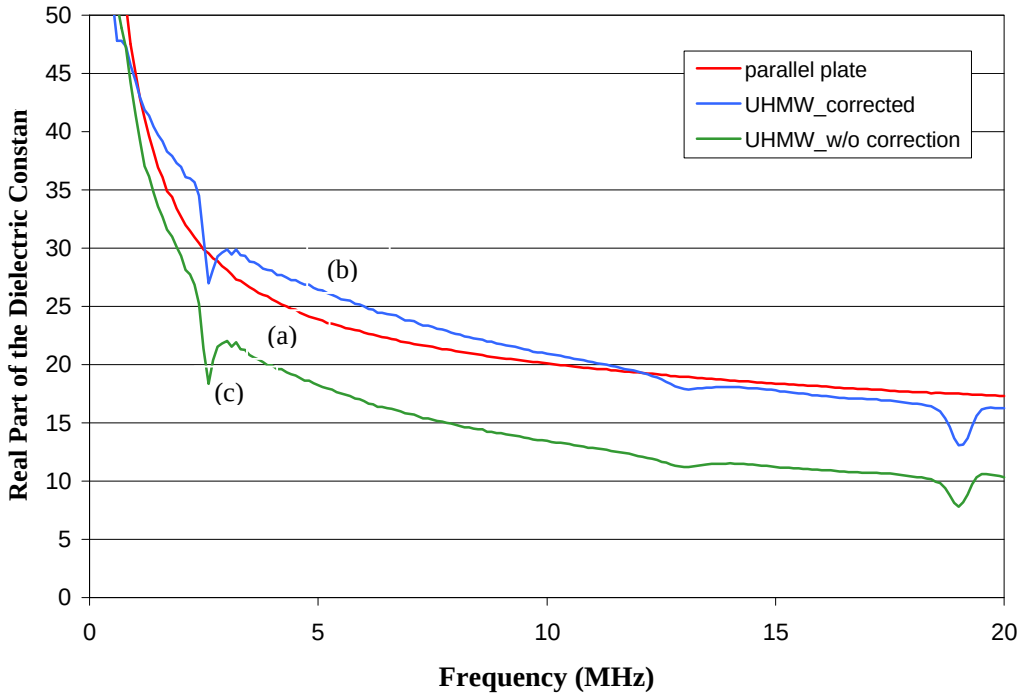

Figure 5.3: The real part of the dielectric constant of a PCC sample using (a) the parallel plate, the capacitance probe (b) with correction, and (c) without correction using UHMW for calibration.

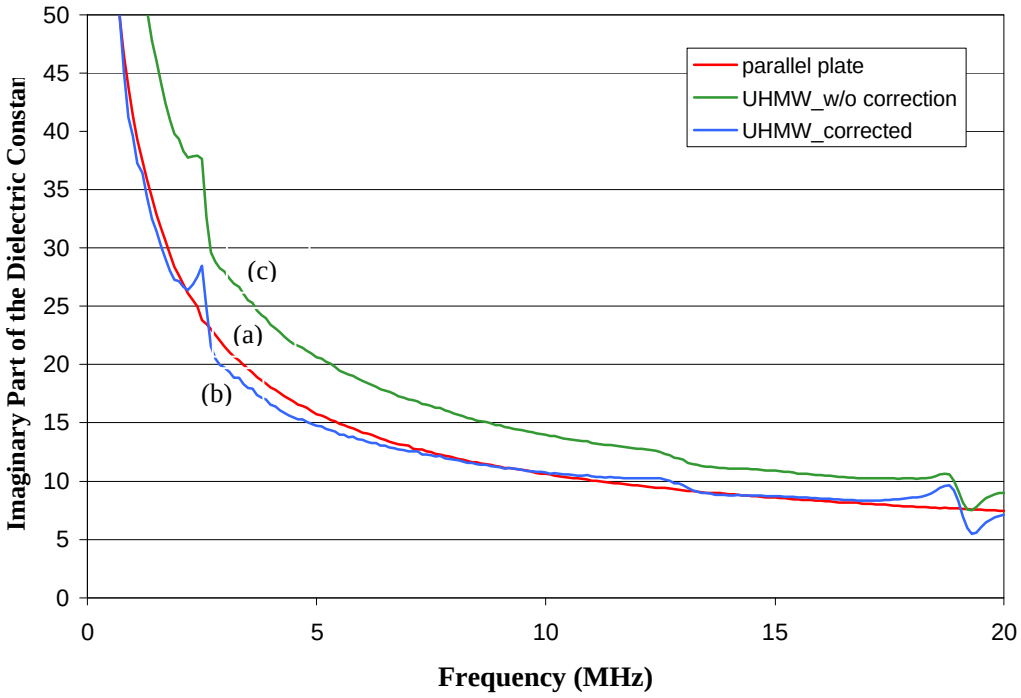

Figure 5.4: The imaginary part of the dielectric constant of a PCC sample using (a) the parallel plate, the capacitance probe (b) with correction, and (c) without correction using UHMW for calibration.

5.2.2 Calibration Material: Extruded Nylon

A sample of extruded nylon (slab: 45.72 x 30.48 x 10.16cm) will be considered as the calibration material in this section. The real and imaginary parts of the correction function for extruded nylon, as described in section 5.1, is shown in Figure 5.5.

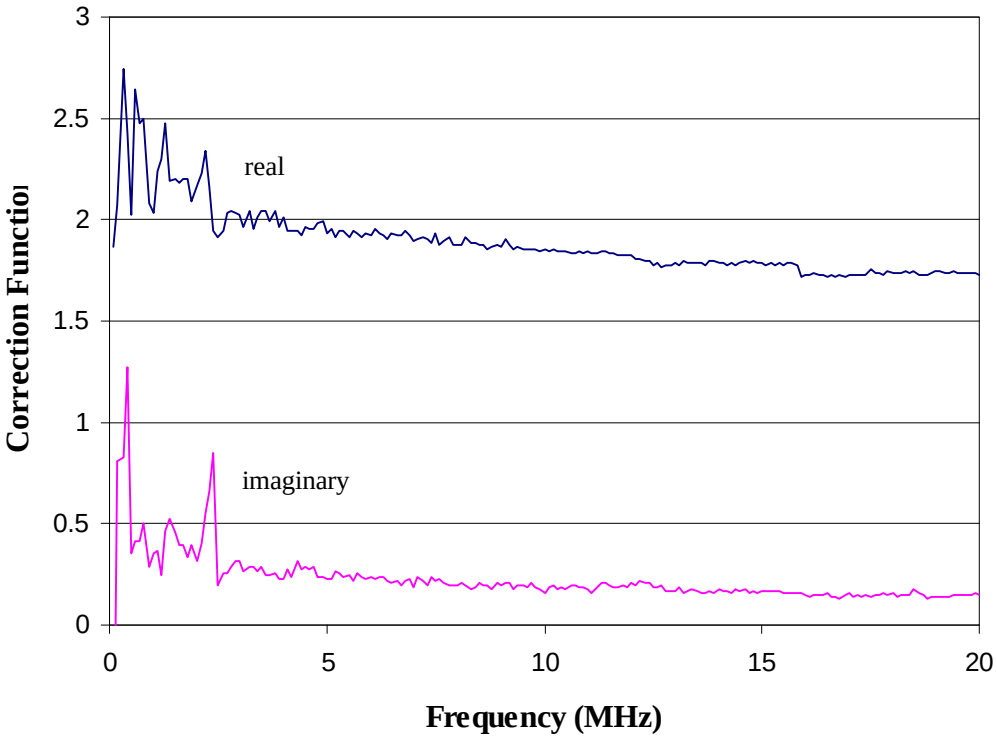

Figure 5.5: The real and imaginary parts of the correction function of the capacitance probe measurement system using extruded nylon for calibration.

As with the UHMW, the actual dielectric constant of the extruded nylon will have an influence partial influence on the correction. Figure 5.6 shows the real and imaginary parts of the dielectric constant of the extruded nylon.

To get a general idea of the resulting dielectric constant values obtained from the capacitance probe measurement system using extruded nylon, the same specimen (slab: 45.72 x 30.48 x 10.16cm) of Portland cement concrete will be analyzed. This specimen has a w/c ratio of 0.45. Figures 5.7 and 5.8 show the real and imaginary portions, respectively, of the dielectric constant obtained from this system, with and without the correction function, as well as the measured values from the parallel plate measurement system.

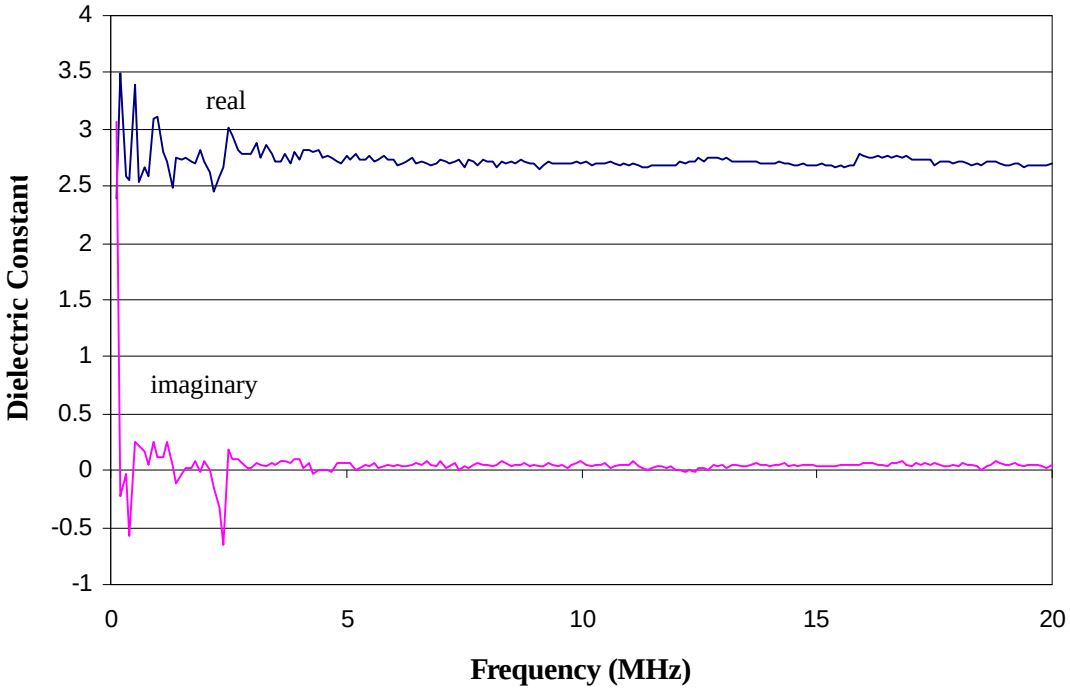

Figure 5.6: The real and imaginary dielectric constant of the extruded nylon sample used for calibration.

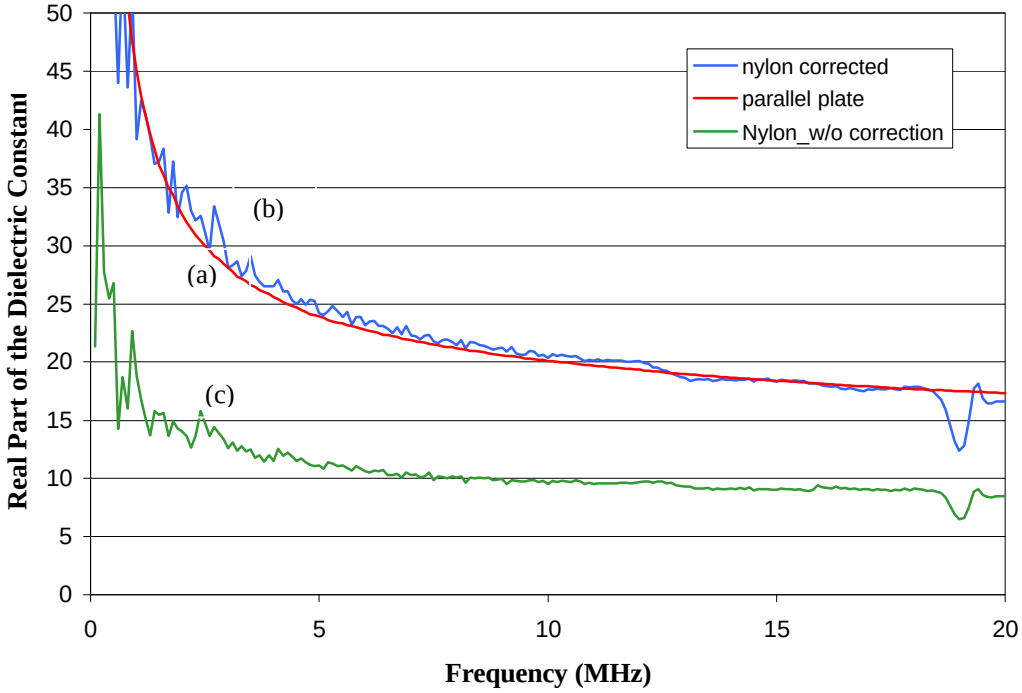

Figure 5.7: The real part of the dielectric constant of a PCC sample using (a) the parallel plate, the capacitance probe (b) with correction, and (c) without correction using extruded nylon for calibration.

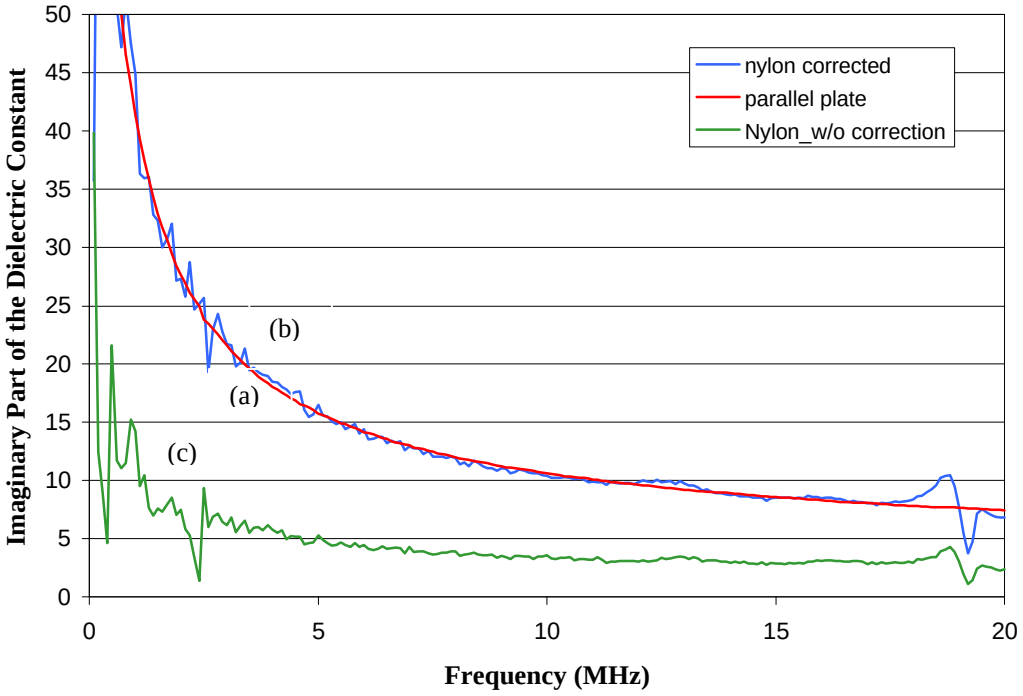

Figure 5.8: The imaginary part of the dielectric constant of a PCC sample using (a) the parallel plate, the capacitance probe (b) with correction, and (c) without correction using extruded nylon for calibration.

5.3 Application of the Capacitance Probe

This section will discuss some of the sample measurements performed in the laboratory with the different models of capacitance probes which were mentioned in the previous chapter and graphically illustrated in Appendix A. Three measurements performed with the capacitance probe measurement system using the various probes will be presented. The first measurement is that of a uniform Portland cement concrete sample (slab: 45.72 x 30.48 x 10.16cm) with a w/c ratio of 0.45. The second measurement will be of a sample of Portland cement concrete (slab: 45.72 x 30.48 x 10.16cm) with the same w/c ratio containing a air void which is 7.5mm in thickness at a depth of 50mm below the surface of the sample. These measurements will be discussed briefly in the following sections.

5.3.1 Uniform PCC Sample

A uniform PCC sample is referred to as a sample that contains no foreign objects or air gaps within the surface of the concrete. When we measure with the different probes containing different plate widths and configurations, we will expect the results to be similar because the sample should look identical at different depths. The small changes found are most likely due to the inhomogeneous nature of PCC. Figures 5.9 and 5.10 show the real and imaginary parts of the dielectric constant found using each of the separate probes, models A through F. As mentioned previously, the results are nearly identical. The next section presents a measurement of a sample containing an air void and it may be useful to refer to the results from this application.

5.3.2 PCC Sample Containing an Air Void

Placing an air void within the sample will cause the effective dielectric constant to reduce as the probes radiate to a specific depth in the sample. This is due to the fact the air void has a dielectric constant of one, $\varepsilon_{r,air} = 1$, which will reduce the dielectric constant seen by the probes that radiate down to the void. Once all of the measurements were completed, it was found that the capacitance probes with the larger spacing resulted in a lower effective dielectric constant, and thus radiated further into the PCC sample. We can conclude from these results that the greater the spacing between the plates of the capacitance probes, the deeper the probe radiates into the sample. We can also notice that the different plate configurations with the same spacing result in almost identical measurements of the dielectric constant. The real and imaginary plots of the measured dielectric constants of the PCC sample containing an air void is shown in Figures 5.11 and 5.12. This gives reasonable proof that the capacitance probes can be used to measure air voids in concrete structures.

With further investigation, the depth, size and location of the air voids or other foreign substances such as sodium deposits or metals could possibly be discovered. These cases and others will be performed in this ongoing research.

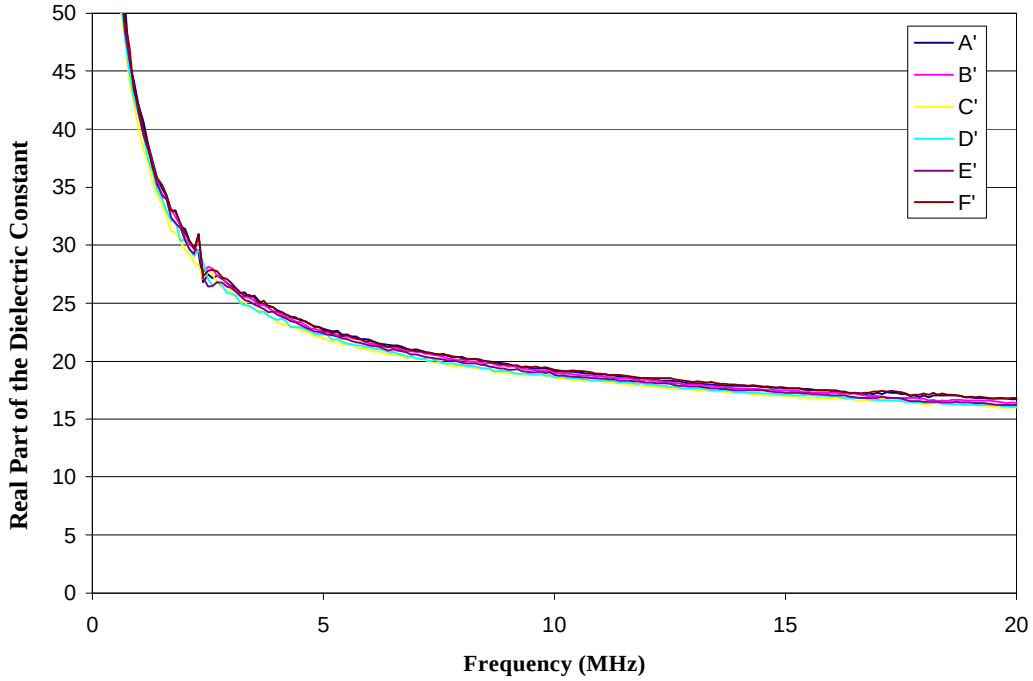

Figure 5.9: The real dielectric constant of a uniform PCC sample using the different developed plate configurations of the capacitance probe system.

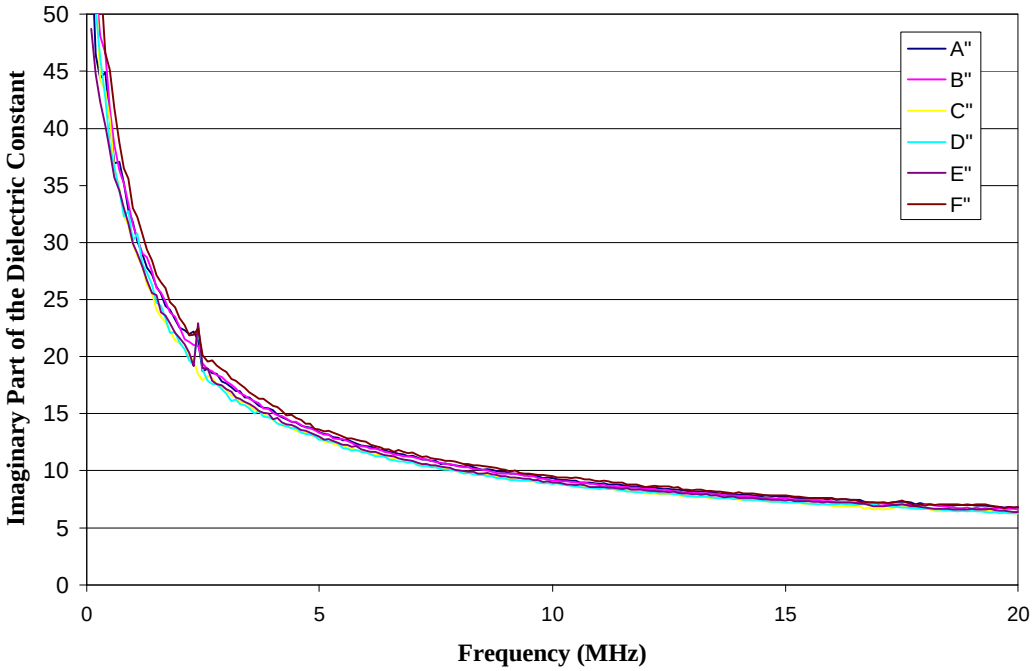

Figure 5.10: The imaginary dielectric constant of a uniform PCC sample using the different developed plate configurations of the capacitance probe system.

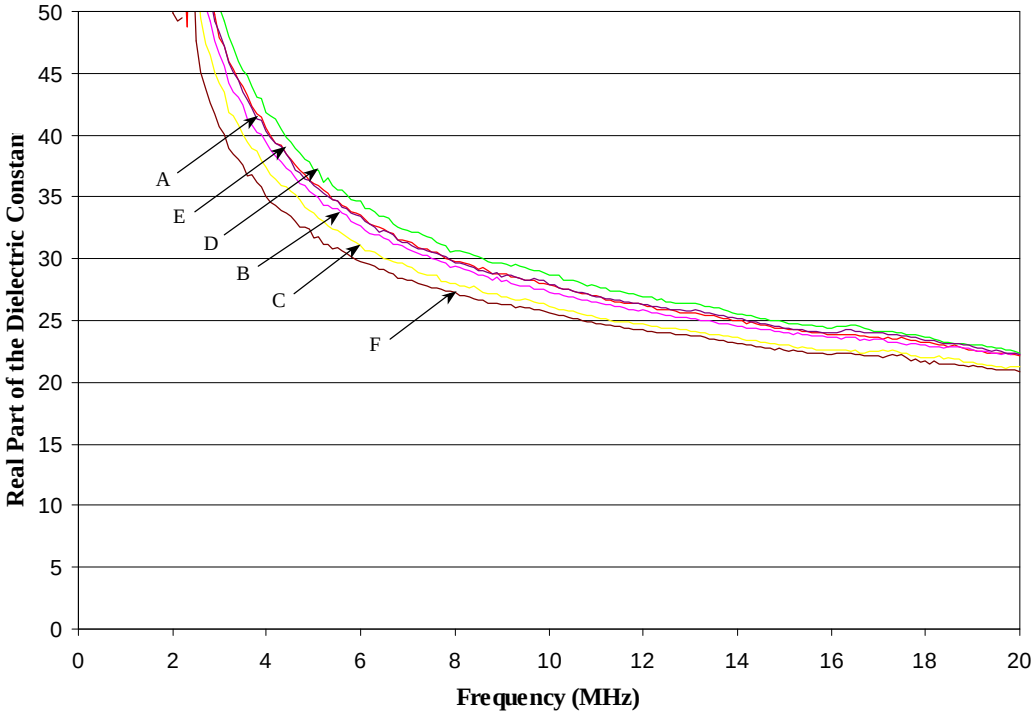

Figure 5.11: The real dielectric constant of a PCC sample containing an air void using the different developed plate configurations of the capacitance probe system.

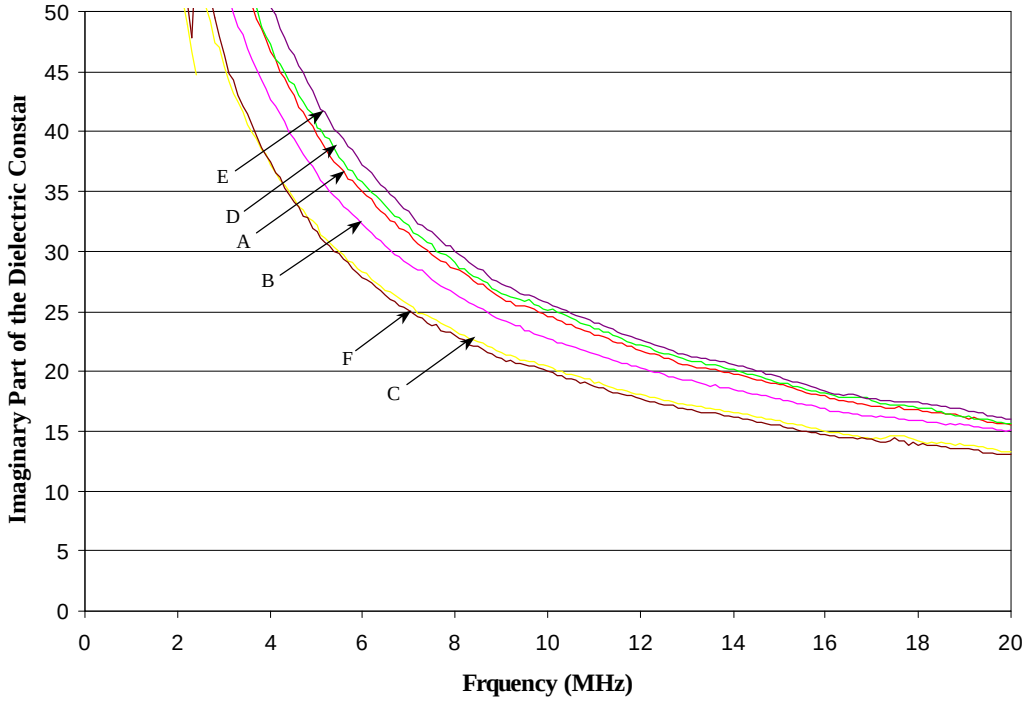

Figure 5.12: The imaginary dielectric constant of a PCC sample containing an air void using the different developed plate configurations of the capacitance probe system.

5.4 Conclusions

This section investigated the correction function used to adjust the capacitance probe measurement system to an optimal value for measuring Portland cement concrete. The system is developed to measure a specimen based on a sample measurement of PCC. This limits the capacitance probe to measuring specimens that the user has an idea of the range of the dielectric constant of the specimen.

The capacitance probe measurement system has been verified by viewing the obtained results along with the results from the parallel plate measurement system. After the correction function was introduced, the amount of error was limited.

The several models of capacitance probes were applied to a couple samples of PCC. It was in these measurements that the capacitance probe was found to be able to detect a subsurface object. It was also found the plate separation is related to the depth penetration of the measurement into the concrete.

Chapter 6
Summary and Conclusions

This research focused on the development of a field portable capacitance measurement system to investigate the material characterization of Portland cement concrete. A capacitance probe has been designed for the non-destructive evaluation of Portland cement concrete through wideband RF measurements in the frequency domain. Measurement techniques focusing on impedance measurements have been investigated. The capacitance probe measurement system resembles a parallel plate capacitor with the difference being that the capacitance probe has both conducting plates in the same horizontal plane. A system calibration, using three calibration measurements, was used on a parallel plate measurement system to solve for the scattering parameters, S_{11}, S_{22}, and $S_{21}S_{12}$, used to model interface consisting of the cables and adapters connecting the parallel plate measurement fixture to a vector network analyzer. A system calibration using four calibration measurements was employed on the capacitance probe measurement system to solve for the same scattering parameters as found in the parallel

plate system with the addition a fourth measurement to account for the capacitance of air between the conducting plates. The fourth measurement is needed due to the unique geometry of the capacitance probe fixture. A correction process based on the results of the parallel plate measurement system has been proposed to rectify systematic discrepancies in the capacitance probe measurement system. The investigation of a correction function was used to adjust the capacitance probe measurement system to an optimal value for measuring Portland cement concrete. The system is developed to measure a specimen based on a sample measurement of PCC. This limits the capacitance probe to measuring specimens that the user has an idea of the range of the dielectric constant of the specimen.

6.1 Results and Conclusions

Based on this research study, the following conclusions can be made:

- An in-situ capacitance probe was designed and constructed;
- The capacitance probe measurement system was successfully calibrated using four calibration measurements;
- The capacitance probe was successfully implemented to measure the dielectric properties of Portland cement concrete;
- Subsurface abnormalities in Portland cement concrete were detected by the capacitance probe when the plate spacing was varied;
- It appears that the capacitance probe has great potential for applications in concrete civil infrastructure condition assessment.

6.2 Suggestions for Future Work

Based on the results of this study, the following recommendations for future research are made:

- Modification in the system design is needed to allow for one person to operate the system

- Further research is needed to quantify the flaw detection in concrete
- A study into a balanced measurement device or the use of a balun with the network analyzer is needed to possibly reduce the noise from the output signal at low frequencies.

Appendix A

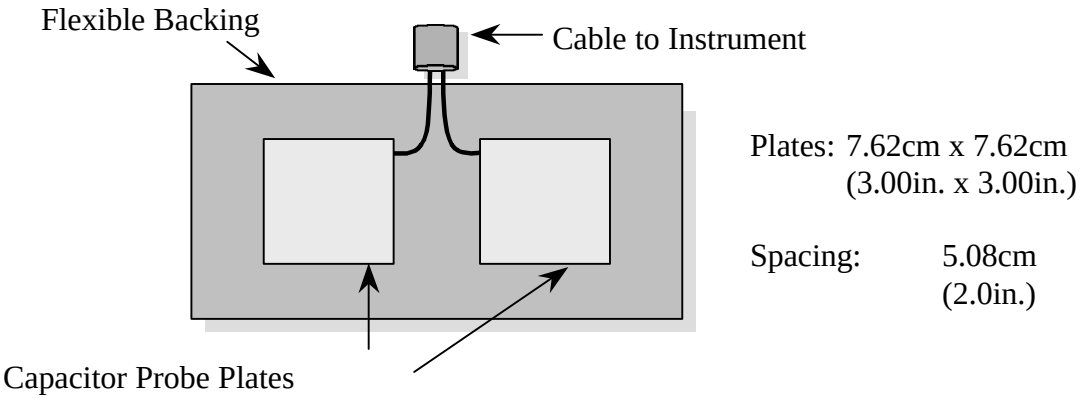

Figure A1. The Capacitor Probe: Model A

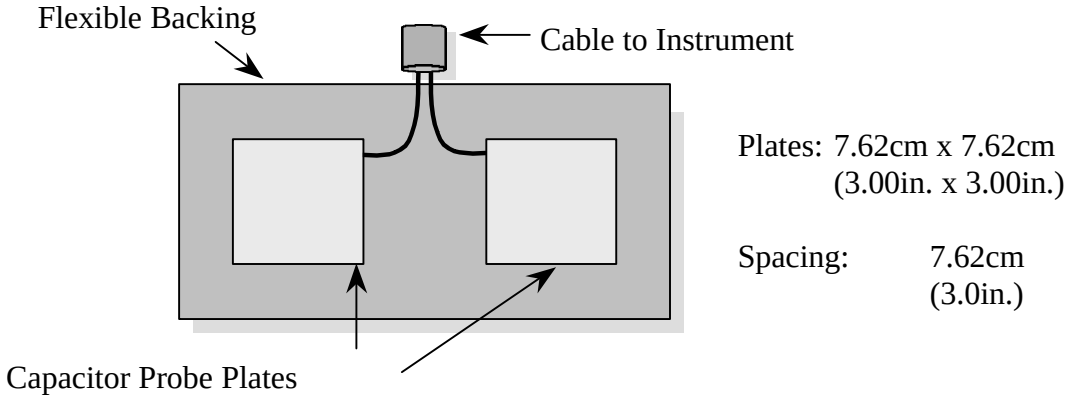

Figure A2. The Capacitor Probe: Model B

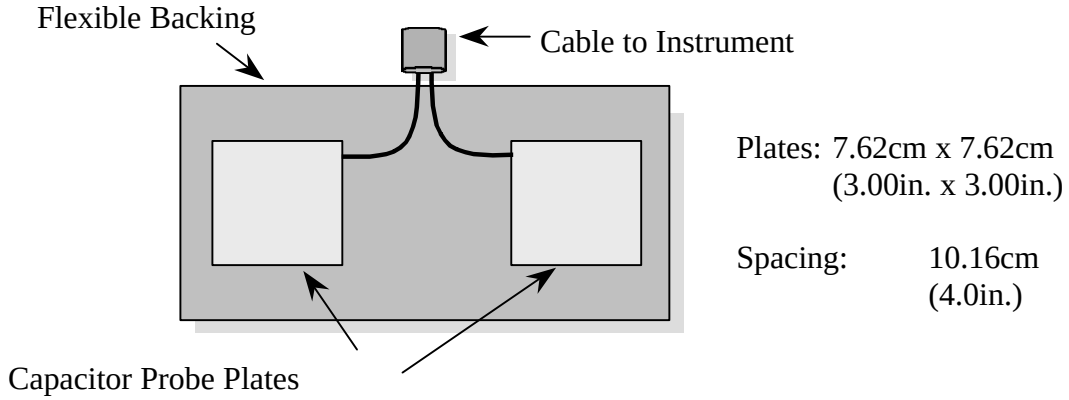

Figure A3. The Capacitor Probe: Model C

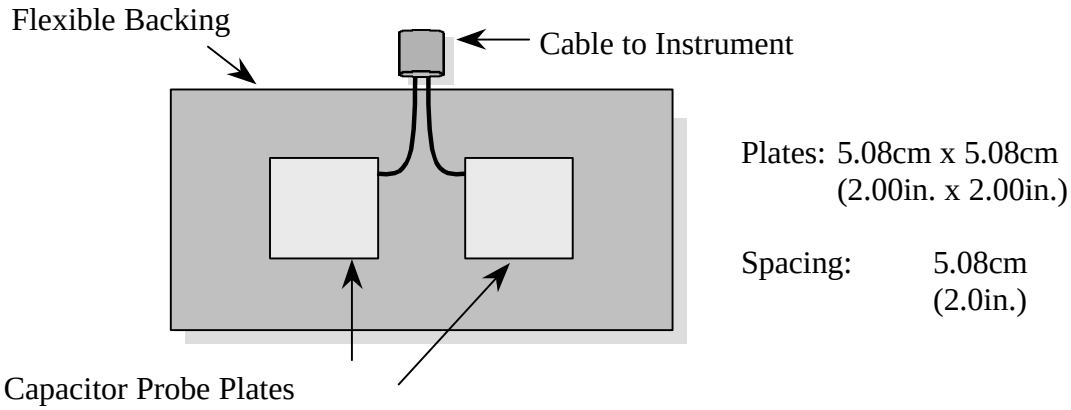

Figure A4. The Capacitor Probe: Model D

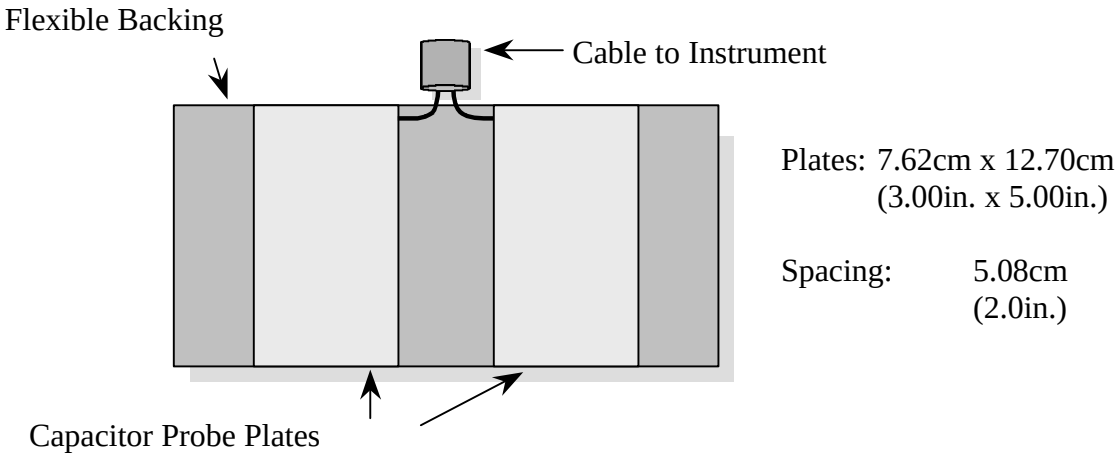

Figure A5. The Capacitor Probe: Model E

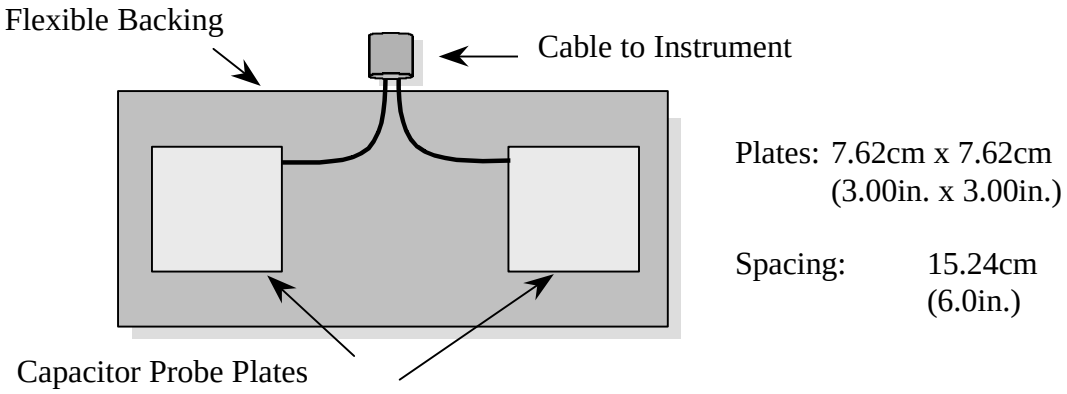

Figure A6. The Capacitor Probe: Model F

References

[1]. Bussey, H. E. (1967) "Measurement of RF Properties of Materials, A Survey." *Proceedings of the Institute of Electrical and Electronics Engineers,* 1046-1053, June.

[2]. Moffat, D. L. and R. J. Puskar. (1981) "A Subsurface Electromagnetic Pulse Radar." *Geophysics,* Vol. 41, No. 3, 605-671, June.

[3]. Feng, S. and A. Delaney. (1974) "Dielectric Properties of Soils at UHF and Microwave Frequencies." *American Geophysical Union.*

[4]. Feng, S. and P. N. Sen. (1985) "Geometrical Model of Conductive and Dielectric Properties of Partially Saturated Rocks." *Journal of Applied Physics,* Vol. 58, No 8, Oct.

[5]. Hipp, J. E. (1971) "Soil Electromagnetic Parameters as a Function of Frequency, Soil Density, Soil Moisture." *Proceedings of the Institute of Electrical and Electronics Engineers,* Vol. 62, No. 1, 98-103, Jan.

[6]. Lord, A. E., Jr., R. M. Koerner, and J. S. Reif. (1979) "Determination of Attenuation and Penetration Depth of Microwaves in Soil." *Geotechnical Testing Journal,* Vol. 2, No. 2, 77-83, June.

[7]. Lundien, J. R. (1971) "Terrain Analysis by Electromagnetic Means. Report 5: Laboratory Measurement of Electromagnetic Propagation Constants in the 1.0-1.5 GHz Microwave Spectral Region." *Technical Report 3-693,* US Army Waterways Experiment Station, MI, Feb.

[8]. McNeill, J. D. (1980) *Electrical Conductivity of Soils and Rocks,* Technical Note TN-5, Geonics Ltd., Oct.

[9]. Carter, C. R., T. Chung, F. B. Holt, and D. Manning. (1986) "An Automated Signal Processing System for the Signature Analysis of Radar Waveforms from Bridge Decks." *Canadian Electrical Engineering Journal,* Vol. 11, No. 3, 128-137.

[10]. Steinway, W. J., J. D. Echard, and C. M. Luke. (1981) "Locating Voids Beneath Pavement Using Pulsed Electromagnetic Waves." *NCHRP Project 10-14*, National Cooperative Highway Research Program, National Research Council, Washington, DC.

[11]. Clemena, G., M. Sprinkel, and R. Long, Jr. (1987) "Use of Ground-Penetration Radar for Detecting Voids Under a Jointed Concrete Pavement." *Transportation Research Board,* No. 1109, Washington, DC, 1-10.

[12]. Maser, K. R., R. Littlefield, and B. Brandemeyer. (1989) "Pavement Condition Diagnosis Based on Multisensor Data." *Transportation Research Record 1196,* Transportation Research Board, National Research Council, Washington DC, 62-72.

[13]. Al-Qadi, I. L., D. K. Ghodgaonkar, V. V. Varadan, and V. K. Varadan. (1989) "Detecting Water Content of Asphaltic Cement Concrete by Microwave Reflection and Transmission Measurement." *91st Annual Meeting of the American Ceramic Society*, Indianapolis, IN, April 23-27.

[14]. Bell, J. R., G. A. Leonards, and W. A. Doch. (1963) "Determination of Moisture Content of Hardened Concrete by its Dielectric Properties." *Proceedings of the American Society for Testing and Materials,* Vol. 63.

[15]. Al-Qadi, I. L. (1992) "Using Microwave Measurements to Detect Moisture in Hot-Mix Asphalt." *Journal of Testing and Evaluation,* ASTM, West Conshohocken, PA, Vol. 20, No. 1, 45-50.

[16]. Hayt, W. H., Jr. (1981) *Engineering Electromagnetics,* Fourth Edition, McGraw-Hill Book, Inc., New York, NY.

[17]. Tamboulian, D. H. (1965) *Electric and Magnetic Fields,* Harcourt, Brace, and World, Inc. New York, NY.

[18]. Jastrzebski, Z. D. (1977) *The Nature and Properties of Engineering Materials,* Second Edition, SI Version, John Wiley and Sons, New York, NY.

[19]. Wilson, J. and H. Whittington. (1990) "Variations in the Electrical Properties of Concrete with Change in Frequency." *IEEE Proceedings*, 137 (5), Part A, 246-254.

[20]. Cole, K. S., and R. H. Cole. (1941) "Dispersion and Absorption in Dielectrics; I. Alternating Current Characteristics." *Journal of Chemical Physics*, Vol. 9, 341-351.

[21]. Debye, P. (1929) *Polar Molecules*, Chapter VI, Chemical Catalog Co., New York, NY.

[22]. Sillars, R. W. (1937) "The Properties of a Dielectric Containing Semi-Conducting Particles of Various Shapes." *Journal of the Institute of Electrical Engineers*, Vol. 80, 378-394.

[23]. Hasted, J. B. (1973) *Aqueous Dielectrics.* Chapman and Hall, Ltd., London, England, 235-267.

[24]. Böttcher, C. J. F. (1952) *Theory of Electric Polarization*, Elsevier Publishing Company, New York, NY.

[25]. Mehta, P. K. (1986) *Concrete: Structure, Properties and Materials*. Prentice Hall, Englewood Cliffs, NJ.

[26]. Mindess, S. and J. F. Young. (1981) Concrete. Prentice Hall, Englewood Cliffs, NJ.

[27]. Lowell, S. and J. E. Shield. (1987) *Powder Surface Area and Porosity.* 3rd Ed., Chapman and Hall.

[28]. Young, J. F. (1974) "Capillary Porosity in Hydrated Tricalcium Silicate Paste." *Powder Technology*, Vol. 9, 173-179.

[29]. Abdel-Jawad, Y., and W. Hansen. (1989) "Pore Structure of Hydrated Cement Determined by Mercury Porosimetery and Nitrogen Sorption Techniques." *Materials Research Symposium Proceedings*, Vol.137, 105-118.

[30]. Winslow, D. N., and M. D. Cohen. (1994). "Percolation and Pore Structure in Mortars and Concrete." *Cement and Concrete Research*, Vol. 24, No. 1, 25-37.

[31]. Ping, X., J. J. Beaudoin, and R. Brousseau. (1991) "Effect of Aggregate Size on Transition Zone Properties of the Portland Cement Paste Interface." *Cement and Concrete Research*, Vol. 21, No. 6, 999-1005.

[32]. Al-Qadi, I. L., R. E. Weyers, N. L. Galagedera, and P. D. Cady. (1993) "Condition Evaluation of Concrete Bridges Relative to Reinforced Corrosion, Vol. 4: Deck Membrane Effectiveness and Method for Evaluating Membrane Integrity." *Report No. SHRP-S/FR-92-10V,* Strategic Highway Research Program, National Research Council, Washington, DC, 143p.

[33]. Bradford, S. A. (1992) *Corrosion Control.* Van Nostrand Reinhold, New York, NY

[34.] McCarter, W. J. and P. N. Curran. (1984) "The Electrical Response Characteristics of Setting Cement Paste." *Magazine of Concrete Research,* 36 (126): Mar, 42-49.

[35]. Taylor, M. A. and K. Arulanandan. (1974) "Relationships Between Electrical and Physical Properties of Cement Pastes." *Cement and Concrete Research,* Vol. 4, No. 4, 881-897.

[36]. Perez-Pena, M., D. M. Roy, and F. D. Tamas. (1989) "Influence of Chemical Composition and Inorganic Admixtures on the Electrical Conductivity of Hydrating Cement Pastes." *Journal of Materials Research,* 4 (1): Jan/Feb, 215-223.

[37]. Moukwa, M., M. Brodwin, S. Christo, J. Chang, and S. P. Shah. (1991) "The Influence of the Hydration Process Upon Microwave Properties of Cements." *Cement and Concrete Research,* Vol. 21, 863-872.

[38]. Wittman, F. H. and F. Schlude. (1975) "Microwave Absorption of Hardened Cement Paste." *Cement and Concrete Research,* 5, 63-71.

[39]. De Loor, G. P. (1962) "The Effect of Moisture on the Dielectric Constant of Hardened Portland Cement Paste." *Applied Scientific Research,* Section B, Vol. 9, 297-309.

[40]. Hansson, I. L., and C. M. Hansson. (1983) "Electrical Resistivity Measurements of Portland Cement Materials." *Cement and Concrete Research,* Vol. 13, 675-683.

[41]. McCarter, W. J., P. N. Curran, J. G. Wilson, and H. W. Whittington. (1985) "The Electrical Response Characteristics of Setting Cement Paste." *Magazine of Concrete Research,* Vol. 37, No. 130, 52-55.

[42]. Wilson, J. and H. Whittington. (1990) "Variations in the Electrical Properties of Concrete with Change in Frequency." *IEEE Proceedings,* 137 (5), Part A, 246-254.

[43]. Whittington, H. W., J. McCarter, and M. C. Forde. (1981) "The Conduction of Electricity Through Concrete." *Magazine of Concrete Research*, 33 (114), 48-60.

[44]. McCarter, W. J., and H. W. Whittington. (1981) "Resistivity Characteristics of Concrete." *Proceedings of Institution of Engineers*, Part 2, Vol. 71, 107-117.

[45]. Hasted, J. B., and M. A. Shah. (1964) "Microwave Absorption by Water in Building Materials." *British Journal of Applied Physics*, Vol. 15, 825-836.

[46]. Shah, M. A., J. B. Hasted, and L. Moore. (1965) "Microwave Absorption by Water Building Materials." *British Journal of Applied Physics*, Vol. 16, 1747-1754.

Curriculum Vitae

Mr. Jason Jon Yoho was born in Fairmont, West Virginia, in 1973. He received his Bachelor of Science degree in Electrical Engineering from Clemson Univeristy, Clemson, South Carolina in 1996. He started his graduate studies in the fall that same year (1996) in Electrical Engineering at Virginia Polytechnic Institute and State University, Blacksburg, Virginia. He worked as a research assistant as well as a teaching assistant during his graduate studies. His areas of interest include radio and microwave measurement systems, networks, and microelectronics.